Viscoelastic-Viscoplastic Model to Predict Creep in a Random Chopped Mat Thermoplastic Composite

by

Jonathan Mui

A thesis
presented to the University of Waterloo
in fulfillment of the
thesis requirement for the degree of
Master of Applied Science
in
Mechanical Engineering

Waterloo, Ontario, Canada, 2008

DECLARATION

I hereby declare that I am the sole author of this thesis. This is a true copy of the thesis, including any required final revisions, as accepted by my examiners.

I understand that my thesis may be made electronically available to the public.

ABSTRACT

Random glass-mat thermoplastic (GMT) composites are widely used in automotive applications due to their mechanical properties and relatively low processing cost. However, there is an inherent issue with these materials in that the thermoplastic matrices exhibit viscoelastic behaviour. In order for manufacturers to have confidence in their products, it is important to be able to predict the long-term behaviour of these materials.

In this work, chopped glass fibre mat reinforced polypropylene was studied over a stress range of 5 -50 MPa at room temperature. An upper limit of 50 MPa was used because experiments at 60 MPa resulted in a high percentage of failed specimens. Through short-term creep (30 minutes) experiments, a material variability of ±18% was determined. Using statistics, the short-term test data also indicated that the material was only slightly nonlinear above 45 MPa. Since the nonlinearity was within the margin of experimental scatter, a linear viscoelastic model was used.

One day creep experiments indicated the presence of viscoplastic damage accumulation in the composite, which was verified using *in-situ* microscopy. The creep deformation in this GMT material has been modeled using a viscoelastic-viscoplastic model. To verify the model at the limit stress level of 50 MPa, two separate creep tests of 33 day duration were conducted. The test results agreed well with the model.

The temperature effects and applicability of time-temperature superposition (TTS) principle on the chopped fibre composite have been investigated over a temperature range of 25°C to 90°C. A stress range of 20 MPa to 40 MPa was studied at each temperature level and it was found that the increase in creep compliance with temperature is similar for all stress levels. However, the variation in the creep compliance values increased by 3 to 7% on average at higher temperatures. Parametric studies conducted suggest that the failure modes for chopped fibre composite become matrix dominated at temperatures higher than the secondary glass transition of 60°C. Through the development of a master curve based on 20 MPa data and comparisons to long-term verification experiments at

20MPa and 50 MPa at room temperature, it was shown that TTS is applicable to the composite.

Short-term tests indicated that the material response of chopped fibre mat composites is far too random to be meaningfully quantified and this is further exacerbated at higher temperatures. Simply, the long-term creep behavior of these materials is not sufficiently repeatable to consider the use of a complex viscoelastic-viscoplastic model and therefore there is no practical reason to pursue development of such a model for the short fibre composite.

From 1 day creep tests at various temperatures, it was seen that temperature appears to increase plastic strain in the material exponentially at each stress level. By comparing the results from these tests to micrographs of the material, it showed that above the secondary glass transition, 60°C, bulk deformation of the matrix phase in the composite is dominant due to matrix softening. Deformation of the matrix phase accelerates fibre-matrix debonding and therefore the progressive failure process. It suggests then that bulk plastic deformation of the matrix phase is a major contributor to residual strains measured in this work.

Overall, there is strong evidence from this extensive experimental program that even for materials with inherently high property scatter, it is possible to identify the effects of nonlinearities arising from external factors such as stress and temperature using short-term creep tests on single specimens. It is, however, more difficult to develop an accurate generalized long-term model that can account for stress and temperature conditions because of the wild experimental scatter.

ACKNOWLEDGEMENTS

TABLE OF CONTENTS

LIST OF TABLES

LIST OF FIGURES

1.0 INTRODUCTION

1.1 Glass-Mat Thermoplastic (GMT) Composites

In recent years, there has been increasing use of fibre-reinforced plastic composites to manufacture semi-structural parts for the automotive industry [1, 2]. The use of these materials, particularly glass-mat thermoplastic (GMT) composites, has advantages over metals including high strength-to-weight ratio, corrosion resistance, relatively low processing costs, and good impact strength [1]. GMT composites are usually polypropylene matrices reinforced with either chopped or continuous glass fibre mats. The mat structure itself plays an important role in the mechanical behaviour of the material. Although E-glass is typically used, the fibre length and manner in which they are integrated into the polypropylene matrix can vary; glass fibres that are woven together, unidirectional, or randomly oriented and dispersed can all exhibit drastically different properties. The usual fibre content of these materials is between 20-50% by weight.

GMT composites are usually supplied to manufacturers in the form of semi-finished sheets that are later compression moulded into finished products. A typical compression moulding process for the fabrication of GMT components is shown schematically in Figure 1.1.
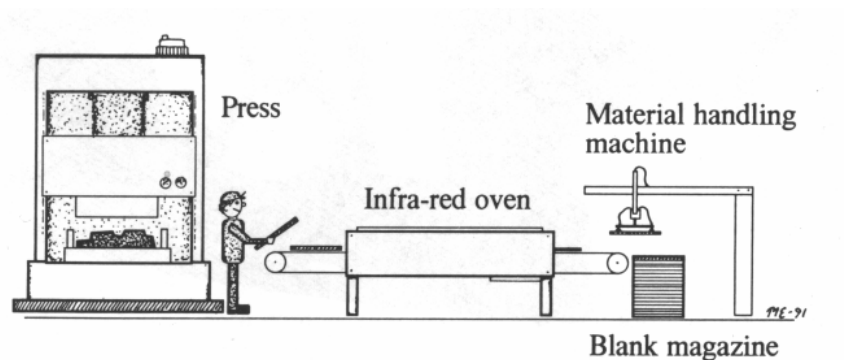
Figure 1.1: Schematic diagram of typical GMT compression moulding process. [1]

Blanks are first cut from semi-finished sheets supplied to the manufacturers and fed through an oven. After passing through the oven, the charges are often placed manually into a heated mould where sufficient pressure is applied to cause the charge to flow and create the desired component.

GMT composites can be used to form parts with complex geometries quickly and are used to create a variety of semi-structural automotive components such as [3]:

- seat back structures
- battery trays
- tail gates
- front-ends
- under-body shields

1.2   Motivation and Objectives of Research

Although there are many benefits to using GMT composite materials, there are a number of challenges with their long-term use due to the inherent viscoelastic (time- and temperature-dependent) response of thermoplastic polymers and the presence of voids which is a characteristic of random mat materials. In order for manufacturers to have confidence in their finished products, they need to know how the material durability will be affected by various factors including:

- Time-dependent behaviour
- Susceptibility to environmental factors such as temperature
- Possible aging effects
- Possible crystallinity effects and degradation
- Large variability in properties (due to flow, fibre distribution, fibre structure, and processing parameters)

The current work is part of a wider experimental program aimed at characterizing and modeling creep response in GMT composites. Creep is a time-dependent phenomenon expressed in terms of deformation of the material over time due to a constant applied load. The main objective is to develop a constitutive model that can reasonably predict the long-term creep behaviour of a random chopped mat composite under various thermal and mechanical load conditions. The range of conditions is similar to those in automotive service. While a number of mathematical expressions can be used to describe creep, the resulting semi-empirical model in this work will be in a form that will allow future implementation into finite element code.

1.3   Scope of Research Work

This work will focus on a commercially available GMT material that is supplied by Quadrant Plastic Composites. The composite material identified as D100 F40 F1 consists of untreated, randomly oriented chopped glass fibre mat in a polypropylene matrix.

To develop a semi-empirical model for the random chopped fibre glass mat reinforced polypropylene, the scope of work will consist of the following tasks:

- creep experiments at many combinations of stress and temperature levels
- determination of linear and non-linear viscoelastic regions
- determination of viscoplastic behaviour (if found)
- determination of temperature effects
- determination of appropriate method for long-term creep predictions
- development of a constitutive model from creep data
- verification of the developed model

It is noted that the characterization of physical and tensile properties for this material have already been completed by other investigators in our research group. In addition, a number of possible effects such as physical ageing, changes in crystallinity, and material

3

degradation on creep behaviour have also been previously investigated by others. The results that are relevant to the current work have been summarized wherever appropriate.

1.4 Thesis Structure

Chapter 2 of this thesis provides background information and a literature review that covers topics such as viscoelastic behaviour, linear and nonlinear viscoelastic models, developments in viscoplastic research, modeling of long-term time-dependent behaviour, and scatter in random GMT materials. Chapter 3 provides details on the material, specimen preparation, equipment, and experimental program used in this study. Chapter 4 contains the experimental results and findings from the creep tests conducted at room temperature, as well as the short-term constitutive model development for the material using this data. The fifth chapter of this thesis contains the results from and discussion on creep tests conducted at various temperatures. An attempt is made in this chapter to incorporate the temperature effects into the short-term model developed in Chapter 4. The final chapter of this thesis contains the conclusions of this research work.

2.0 REVIEW OF LITERATURE

2.1 Linear Viscoelasticity

Polymeric materials can exhibit a wide range of mechanical behaviours from that of an elastic solid to that of a viscous liquid depending on loading and environmental conditions. Due to this combination of behaviours, polymers are usually referred to as viscoelastic, or time and temperature-dependent. The mechanism responsible for this behaviour in polymeric materials operating above their glass transition temperature, T_g, is the sliding and relative moment of molecular chains in the material. As a result of this behaviour, polymeric materials can exhibit the phenomenon known as creep; following an initial, instantaneous linear elastic response the material continues to accumulate strain over time, even when the applied load is held constant. Figure 2.1 shows the loading and typical creep strain response to illustrate this concept.
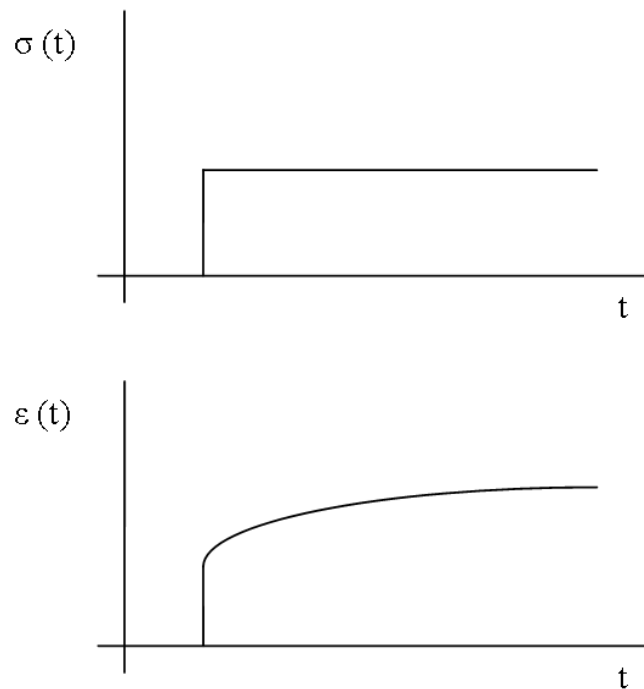
Figure 2.1: Typical creep behaviour.

There are several stages of creep development that occur within a material, eventually leading to final failure of the material known as creep rupture. Figure 2.2 illustrates these three stages of creep behaviour.
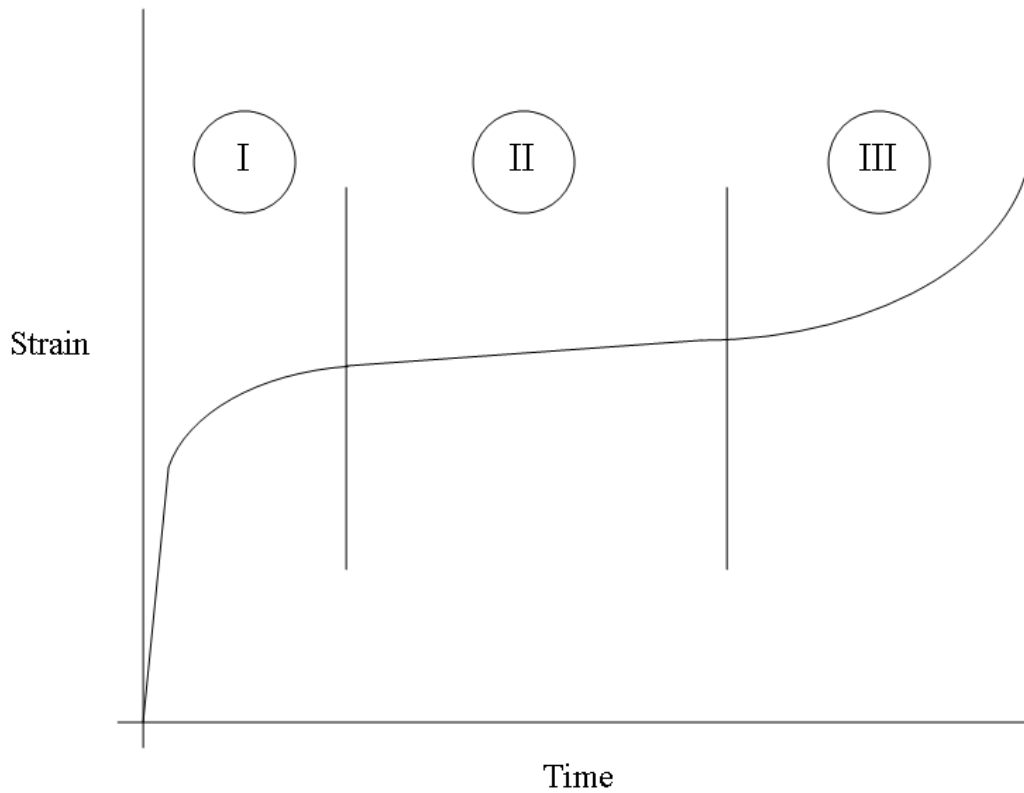
Figure 2.2: Various stages of creep behaviour.

During primary creep, stage I, the material experiences a rapid strain rate, eventually slowing to a relatively constant value, stage II. This constant strain rate behaviour is known as the secondary creep region. Tertiary creep occurs when the creep rate increases exponentially, leading to final failure in the material.

For a viscoelastic material, the creep strain response to a constant applied stress is given by:

$$\varepsilon(t) = D(t)\sigma \tag{1}$$

where $D(t)$ is the creep compliance function, $\varepsilon(t)$ is the total creep strain, and σ is the constant applied stress.

Understanding the creep behaviour of a material is important in design and manufacturing as this can lead to dimensional instability of the end product, as well as failure at applied constant stresses that are significantly lower than the ultimate tensile strength.

Another phenomenon that results from time-dependent material behaviour is stress relaxation, where the stress in the material will decrease over time while subjected to a constant strain. Figure 2.3 illustrates the typical strain and stress response of a material undergoing stress relaxation.
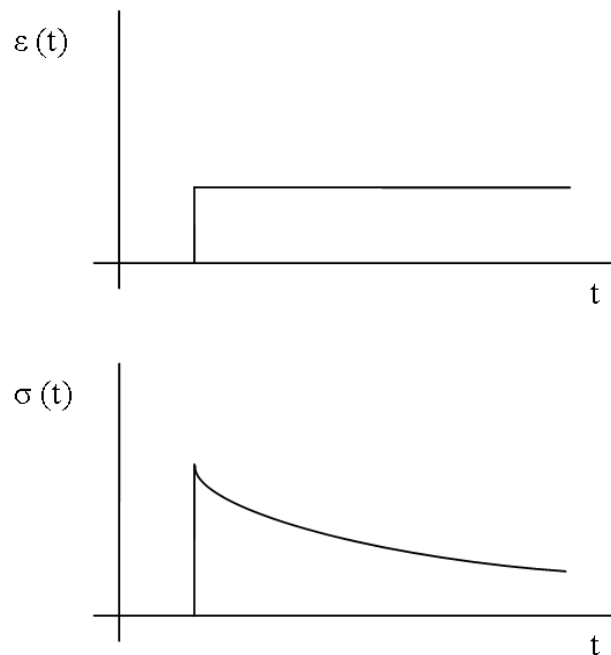
Figure 2.3: Typical stress relaxation behaviour.

While many researchers have studied the relaxation behaviour of GMT and other composite materials, the current study focuses mainly on creep as this is the expected mode of failure in the anticipated application.

2.1.1   Mechanical Models

Mechanical models have been created to better visualize the stress and strain relationship in viscoelastic materials. These models use springs and dashpots to represent the dual nature of the behaviour.

One of the basic mechanical models is the Maxwell model, which is represented by a spring and dashpot in series as shown in Figure 2.4.
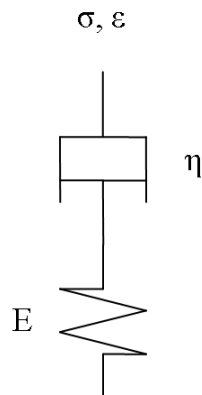
Figure 2.4: Schematic diagram for the Maxwell model.

The linear elastic behaviour of a solid is represented by the spring and is typically governed by Hooke's Law:

$$\sigma = E\varepsilon \tag{2}$$

where σ is the stress, E is the elastic modulus, and ε is the strain in the material. The viscous behaviour of simple fluids represented in the model by the dashpot obeys Newton's Law of Viscosity:

$$\sigma = \eta \frac{d\varepsilon}{dt} \tag{3}$$

8

where η is the material property known as viscosity.

The stress and strain equations representing the two components in this system are combined to give the following equation for viscoelastic behaviour:

$$\frac{d\varepsilon}{dt} = \frac{1}{E}\frac{d\sigma}{dt} + \frac{\sigma}{\eta}$$

(4)

A problem with this particular approach is that it fails to properly represent the complexity of creep behaviour [4].

Another mechanical model is the Voigt model, which uses a spring and dashpot in parallel as shown in Figure 2.5.
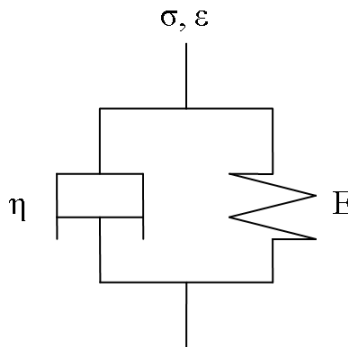
Figure 2.5: Schematic diagram for the Voigt model.

By combining the stress and strain equations of the spring and dashpot, this model results in an equation of the following form:

$$\sigma = E\varepsilon + \eta\frac{d\varepsilon}{dt}$$

(5)

While this model provides a more reasonable representation of creep behaviour, it does not represent the stress-relaxation behaviour adequately [4]. More realistic

9

representations of viscoelastic behaviour can be developed using these simple mechanical elements by combining many Maxwell elements in parallel, many Voigt elements in series, or even a combination of Maxwell and Voigt elements.

2.1.2 Boltzmann Superposition Principle

One of the fundamental mathematical representations used in the modeling of linear viscoelastic behaviour is derived from the Boltzmann superposition principle. This principle states that the creep strain in a given material is related to its loading history, and that strains due to multiple load steps are summative and independent

From the Boltzmann superposition principle, total creep strain of a material due to multiple loading is [4]:

$$\varepsilon(t) = D(t - \tau_1)\sigma_1 + D(t - \tau_2)\sigma_2 + ... \tag{6}$$

where τ_1, τ_2, etc. are the times at which the stresses σ_1, σ_2, etc. are applied. Figure 2.6 (a) shows the total creep strain in response to a 2-step loading, illustrating that the total strain response is simply the sum of the individual responses to each load.
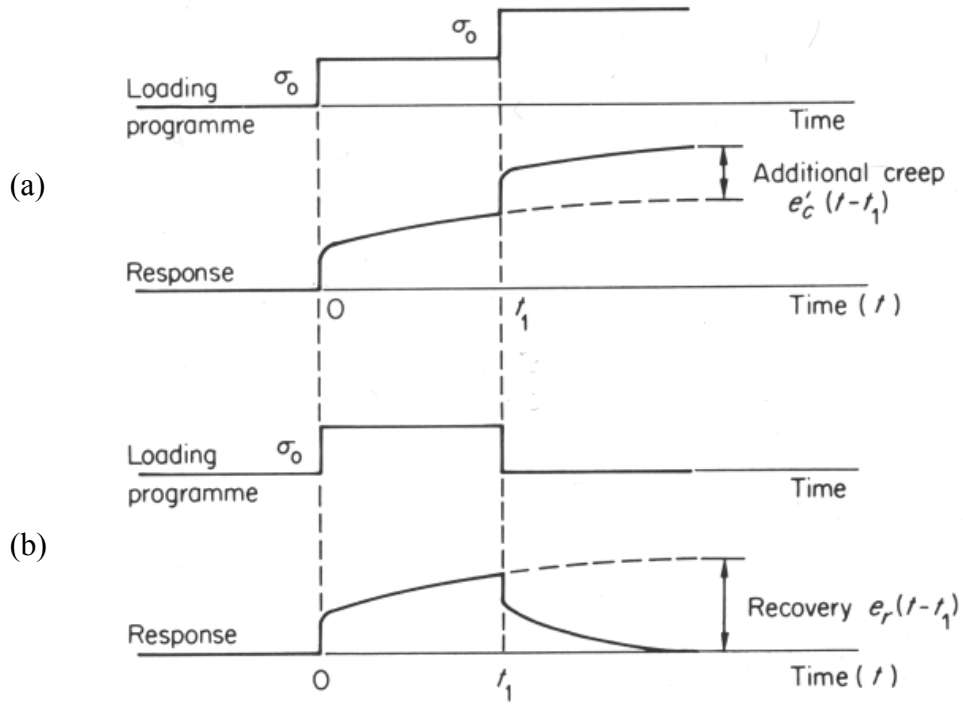
Figure 2.6: Creep response to (a) two-step loading and (b) recovery based on Boltzmann superposition. [4]

An interesting result of this principle is illustrated in Figure 2.6 (b). The recovery (removal of applied load) response in a linear viscoelastic material can simply be modeled by the superposition of a negative load of equal magnitude, applied at the time of recovery.

The Boltzmann superposition principle can be generalized into the following form, known as the hereditary integral representation of linear viscoelastic behaviour:

$$\varepsilon(t) = D_0\sigma + \int_0^t \Delta D(t-\tau)\frac{d\sigma}{d\tau}\,d\tau \tag{7}$$

where D_0 is the instantaneous creep compliance, $\Delta D(t)$ is the transient creep compliance, σ is the applied stress, and τ is a variable introduced into the integral in order to account for the stress history of the material.

11

Similarly, the principle can be used for stress relaxation data, resulting in an analogous relation:

$$\sigma(t) = E_0 \varepsilon + \int_0^t \Delta E(t - \tau) \frac{d\varepsilon}{d\tau} d\tau \qquad (8)$$

where E_0 and ΔE are components of the stress-relaxation modulus. Equations (7) and (8) are sometimes referred to as linear viscoelastic material functions and are interrelated mathematically [5]. Therefore, if the linear viscoelastic material behaviour is known under creep loading, the stress relaxation behaviour can also be determined without the need to conduct additional experimentation and vice versa.

2.1.3 Creep Compliance Function

It can be seen from the hereditary integral representation of linear viscoelastic behaviour found in equation (7), that the creep compliance can be separated into an instantaneous component, D_0, and a time-dependent component, $\Delta D(t)$. The transient creep compliance function, $\Delta D(t)$, is often given the form of a Power law or a Prony series in viscoelastic modeling. The Power law form of this function is as follows:

$$\Delta D(t) = D_1 t^n \qquad (9)$$

The benefit of this function is that it is mathematically simple and has been found to provide an adequate prediction of short-term creep behaviour. It has been successfully applied to a variety of materials which include GMT composites, high-density polyethylene, pure polypropylene, carbon-epoxy composites, and flax-polypropylene composites [6-11].

A Prony series expansion would result in a transient creep compliance function and hereditary integral equation of the following forms:

$$\Delta D(t) = \sum_{i=1}^{N} D_i \left(1 - e^{-t/\tau_i} \right) \tag{10}$$

$$\varepsilon(t) = D_0 \sigma + \sum_{i=1}^{N} D_i \sigma \left(1 - e^{-t/\tau_i} \right) \tag{11}$$

Even though the use of both Power Law and Prony series are common in creep modeling, the use of Prony series is dominant when finite element methods are involved [12-14]. One of the main reasons for this is that a linear combination of exponential terms such as the Prony series can be used to eliminate storage problems in iterative numerical integration [13, 14]. Also, it is sometimes necessarily to interconvert linear viscoelastic material functions when employing finite element software. While this interconversion is often mathematically difficult, involving convolution integrals, there have been methods developed based on Prony series to simplify the solution [5].

Dasappa *et al* [15], studied the creep behaviour of a continuous fibre GMT composite. In the study, a comparison is made between the Power law and Prony series expansion forms of the creep compliance function and it was concluded that the latter provides more accurate long-term predictions of creep strains.

2.1.4 Linear Viscoelastic Behaviour

In order for a material to be considered linear viscoelastic, it must meet the following criteria:

- the Boltzmann Superposition Principle is applicable
- creep compliance is stress independent

13

Isochronous creep and recovery tests at varying stress levels are often conducted to determine the linear viscoelastic region of a material. In order to test whether or not the superposition principle is applicable, a model of the creep compliance can be created and used to predict the recovery behaviour. If the predictions based on this application of the principle are accurate, then this condition for linear viscoelasticity is satisfied.

Stress independence of creep compliance can be verified by selecting discreet time points and examining the creep response curves from various stress levels at these times. The compliance value can be calculated for each stress level and compared by simply rearranging equation (1) to isolate for $D(t)$. If the compliance values are equal, then this condition for linear viscoelasticity is met. Another method to test this condition is simply to examine the stress and strain values at the selected time point. The resulting strains should scale linearly, or be proportional to the applied stress.

2.2 Nonlinear Viscoelasticity

If any of the conditions for linear viscoelasticity are no longer satisfied, the viscoelastic behaviour is considered to be nonlinear. The degree of nonlinearity can be influenced by factors such as applied stress level, strain rate, and temperature [16].

In a recent study, the effects of time and temperature on the stress at which a thermoset resin starts to exhibit nonlinear viscoelastic behaviour were examined [17]. Through a series of 12 hour creep experiments at various stress levels and temperatures, it was shown that the stress at which the viscoelastic behaviour could be considered linear decreased significantly with increasing temperature. The linear-nonlinear viscoelastic stress threshold dependence on temperature is important to note as the point where linear viscoelastic behaviour ends and nonlinear behaviour begins needs to be determined before models can be developed.

2.2.1　Schapery Model

One of the most widely accepted models for nonlinear viscoelastic behaviour was developed by Schapery. In [18], a constitutive equation based on irreversible thermodynamics of the following form was developed to predict viscoelastic creep strains:

$$\varepsilon(t) = g_0 D_0 \sigma + g_1 \int_{0^-}^{t} \Delta D(\Psi - \Psi') \frac{dg_2\sigma}{d\tau} d\tau \qquad (12)$$

where D_0 and $\Delta D(\Psi)$ are the instantaneous and transient linear viscoelastic creep compliance, and Ψ is the reduced-time which is defined by:

$$\Psi = \int_{0}^{t} \frac{dt'}{a_\sigma[\sigma(t')]} \quad (a_\sigma > 0) \qquad (13)$$

and

$$\Psi' = \Psi(\tau) = \int_{0}^{\tau} \frac{dt'}{a_\sigma[\sigma(t')]} \qquad (14)$$

The factors g_0, g_1, g_2 and a_σ in the model are all stress dependent nonlinearity parameters. It can be noted that when these parameters are all equal to 1, this equation reduces to the hereditary integral representation of a linear viscoelastic material. The nonlinearity parameters g_0, g_1, g_2 are associated with higher order dependence of Gibb's free energy on the applied stress, while a_σ is a result of higher order effects in both entropy production and free energy [18]. While these parameters result from fundamental energy principles and have thermodynamic significance as outlined above, their placement in the constitutive equation gives an indication of how these parameters might influence the physical response of the material.

The g_0 term indicates the nonlinearity in the instantaneous elastic compliance due to varying stress and temperature, and can therefore be a measure of the stiffness of the

material. Factor g_1 has a similar interpretation but acts on the transient creep compliance, and g_2 shows the nonlinearity effects of loading rate. The parameter a_σ is a time shift factor that is both stress and temperature dependent [19].

The Schapery model has been successfully applied to model the nonlinear viscoelastic behaviour of many different materials over the past several decades [5, 7, 8, 10, 11, 15, 20-22]. In addition, different parameter estimation methods have been developed and modifications have been made to the original model to extend its application.

2.2.2 Parameter Estimation

To determine the parameters, a graphical method is described in [18]. If the applied stress σ is constant, then the $dg_2\sigma/d\tau$ term in equation (12) is equal to 0 except at $\tau = 0$. This reduces the equation to the following form:

$$\varepsilon(t) = [g_0 D_0 + g_1 g_2 \Delta D(\frac{t}{a_\sigma})]\sigma \tag{15}$$

where the nonlinear creep compliance can now be defined as:

$$D_n(t) = \frac{\varepsilon(t)}{\sigma} = g_0 D_0 + g_1 g_2 \Delta D(\frac{t}{a_\sigma}) \tag{16}$$

Equation (16) can be manipulated to isolate the transient portion of the nonlinear creep compliance, after which the logarithm of both sides can be taken resulting in an equation of the following form:

$$\log(D_n(t) - g_0 D_0) = \log(g_1 g_2) + \log \Delta D(\frac{t}{a_\sigma}) \tag{17}$$

16

If the transient nonlinear creep compliance data from experiments is plotted against time on a log-log scale, the data collected at multiple stress levels can be shifted vertically and horizontally to superpose onto a reference curve at a stress in the linear viscoelastic region to form a "master curve". These vertical and horizontal shifts determined graphically correspond to log (g_1g_2) and log a_σ respectively. Separate values of g_1 and g_2 cannot be determined from this procedure alone. It should be noted that in the case where the curves resemble straight lines this graphical technique will not yield unique values of g_1g_2 and a_σ [18]. This limitation is seen in [23], where the model and parameter estimation method are applied to a unidirectional, glass fibre-epoxy composite using a Power law to represent the transient linear viscoelastic creep compliance. The authors studied the effects of fibre orientation and provided detailed procedures for determining the nonlinearity parameters in the Schapery model, showing that this graphical method only yields a combination of g_1g_2/a_σ^n from the log-log plot of creep data. It was concluded that both creep and recovery data are necessary to fully define the nonlinearity parameters.

By first examining equation (12) for the case of a 2-step loading, where a constant stress, σ_c, is applied over the time domain $0 < t < t_r$ after which a new stress, σ_r, is applied over $t_r < t < t_f$, the equation yields the following form after taking into account the stress history and recognizing that $dg_2\sigma/d\tau$ is equal to 0 except at $\tau = 0$ and $\tau = t_r$:

For $t_r < t < t_f$,

$$\varepsilon(t) = g_0^r D_0 \sigma_r + g_1^r [g_2{}^c \sigma_c \Delta D(\Psi) + (g_2^r \sigma_r - g_2{}^c \sigma_c \Delta D(\frac{t-t_r}{a_\sigma^r})] \qquad (18)$$

where

$$\Psi = \frac{t_r}{a_\sigma^c} + \frac{t-t_r}{a_\sigma^r} \qquad (19)$$

During recovery, σ_r in equation (18) can be taken to equal 0. This substitution according to [18] results in a recovery strain during $t > t_r$ given by:

$$\varepsilon_r(t) = [\Delta D(\frac{t_r}{a_\sigma} + t - t_r) - \Delta D(t - t_r)]g_2\sigma \tag{20}$$

The logarithm can be taken of both sides in equation (20), and by setting a reference recovery strain in the linear viscoelastic region, the recovery curves from other stress levels can be shifted graphically to superpose onto a master curve. The amount of horizontal and vertical shift allow a_σ and g_2 to be determined.

With the advancement of technology, the use of computers to curve fit theoretical equations to experimental data using the least-squares method has become an alternative to the graphical methods proposed originally for determining the model parameters. In [8], a function is defined based on equations (15) and (20) to describe the recovery strain response of the material:

$$\varepsilon_R(t) = \varepsilon(t_r) - \varepsilon_r(t) \tag{21}$$

By curve fitting this function to experimental data from different applied stresses and evaluating the various terms in the linear viscoelastic region (nonlinearity terms equal 1), Lai and Bakker were able to determine the creep compliance function parameters as well as the stress dependence of g_0, g_1, g_2, and a_σ.

Zaoutsos *et al* developed an analytical method of estimating g_0 and g_1 values in [10], and eventually used the developed method with equation (20) to estimate values for g_2 and a_σ [19]. Based on their work, the stress dependence of g_0 can be determined by examining the differences in instantaneous compliance values between the linear and nonlinear viscoelastic regions, and values of g_1 can be estimated using:

$$g_1 = \frac{\Delta\varepsilon_{trans} - \varepsilon_{plastic}}{\Delta\varepsilon_{trans} - \Delta\varepsilon_{inst} - \varepsilon_{plastic}} \tag{22}$$

where $\Delta\varepsilon_{trans}$ is the transient strain accumulated during creep, $\varepsilon_{plastic}$ is any plastic strains developed in the material during creep, and $\Delta\varepsilon_{inst}$ is the difference in response during instantaneous loading and unloading. The benefit of this approach is that the values required in estimating both g_0 and g_1 are easily obtainable from the experimental data. With the values of g_1 and equation (20), curve fits can be performed using the recovery data to determine a_σ and finally g_2.

2.2.3 Other Nonlinear Models

In a recent paper by Kolařík and Pegoretti [24], a Boltzmann-like superposition principle is developed that is applicable to nonlinear viscoelastic behaviour. A three-step creep experimental procedure was used, applying free-volume theory to isotactic polypropylene and several polypropylene blends. By examining each step input individually and accounting for interaction effects between successive loads, the authors were able to develop a superposition principle similar to that of Boltzmann that could predict nonlinear viscoelastic behaviour reasonably.

Although the Schapery model for nonlinear viscoelastic behaviour is the most common in literature, there has also been notable research based on the Drozdov and Kalamkarov micromechanical model for nonlinear viscoelastic behaviour in noncrosslinked polymers. In [25], a series of adaptive springs are used to model the chemical links between polymer chains, a concept first introduced by Green and Tobolsky [26]. These springs are categorized into two types: ones that brake due to external forces, and ones that replace one another as old springs collapse. Chemical kinetics is used in the model to describe each type of spring, and nonlinear behaviour results from the rate dependence of these processes on applied stress level. The model is verified using polypropylene fibres, and found to agree well with the predicted values

Drozdov continued to develop the nonlinear model [27] based on a network of adaptive springs and was able to include thermal and physical aging effects. These effects were introduced into the model by considering the temperature and entropy dependence of the breakage and reformation rates of springs [28, 29]. The constitutive equations were developed using the laws of thermodynamics. More recently, Drozdov and Gupta developed a nonlinear viscoelastic-viscoplastic model for injection moulded isotactic polypropylene. Viscoplasticity was considered in the model as a result of damage and slip in the lamellae of the crystalline phase, as well as slipping between chains in the amorphous phase of the material [30]. The model developed was found to be in fair agreement with experimental data.

2.3 Viscoplasticity

Strains in the material induced by creep loading are not always fully recovered, even after sufficiently long periods of time. This unrecovered, or viscoplastic strain in polymeric composites is usually attributed to matrix cracks, fibre-matrix debonding and matrix plasticity [31]. Damage in GMT composites has been investigated by many researchers over the last two decades [3, 32-35].

Ericson and Berglund studied deformation and fracture differences between chopped fibre and continuous bundled fibre composites over a range of fibre weight content. Scanning electron microscope (SEM) micrographs showed poor fibre-matrix adhesion and more extensive fibre pull-out in the chopped fibre material compared to the continuous bundled fibres [3].

Hugo *et al* investigated the effects of fibre content and temperature on creep and creep damage in a short glass fibre GMT composite by measuring the rate of steady-state creep and examining SEM micrographs. The researchers found that above 60°C, the creep and

creep damage at higher temperatures was accelerated with increasing fibre content due to induced crazing [32].

Lindhagen and Berglund studied the damage mechanisms between short and continuous glass fibre composites through tensile testing, and discovered that the major points of damage in the materials were transversely oriented fibres to the loading direction [33].

Ségard *et al* studied the damage mechanisms in treated and untreated short glass fibre composites through acoustic emission and SEM micrographs. Damage mechanisms identified in the study were microcracks of the matrix, fracture of the fibre-matrix interface, fibre pull-out, and fibre fracture [34]. The data collected was used to model creep damage accumulation with the Kirsch-Pluvinage model.

Law studied the deformation mechanisms during creep of the chopped fibre GMT composite used in this study by conducting micro-tensile tests under a microscope with image capturing capability. Law found that even at low stress levels the development of transverse cracks in the matrix material was evident, and with increasing stress fibre-matrix debonding was also observed in the material [35].

Much research in recent years has concentrated on more complex and comprehensive modeling, realizing that a simple viscoelastic model is not always sufficient for prediction the creep behaviour. In these viscoelastic-viscoplastic models, the total creep strain is often treated as the sum of a viscoelastic component and a viscoplastic component:

$$\varepsilon(t) = \varepsilon_{ve}(t) + \varepsilon_{vp}(t) \qquad (23)$$

Xiao *et al* included viscoplastic terms in their model of creep behaviour in carbon fibre reinforced PEEK by separating the damage into an instantaneous deformation and a time-dependent accumulation [36]. A viscoplastic term was also introduced in the work by Papanicolaou *et al* on modeling a carbon-epoxy composite with the Schapery model [10, 19]. However, the approach taken to model this damage accumulation was not specified.

Nordin and Varna investigated the stress and time dependence of viscoplastic strains in paper fibre composite through an extensive experimental program involving creep and recovery of specimens at the same stress level for different durations of time, and isochronous tests at varying stress levels [37].

2.3.1 Zapas-Crissman Model

One of the most common mathematical models for creep damage was developed by Zapas and Crissman, which uses a functional that is related to the stress history of the material, as given in equation (28) [38]:

$$\varepsilon_{vp}(t) = \phi(\int_0^t g(\sigma(\tau))d\tau) \tag{24}$$

where $\Phi(\ )$ is a functional based on stress history and $\sigma(\tau)$ is the applied stress at time τ.

For single step creep at a constant applied stress σ:

$$\varepsilon_{vp}(t) = \phi(g(\sigma)t) \tag{25}$$

Zapas and Crissman found that the simplest form of the functional could be represented by:

$$\phi(g(\sigma)t) = (g(\sigma)t)^n \tag{26}$$

where n is a constant and values of $g(\sigma)$ can be determined through recovery data. The function $g(\sigma)$ was found to follow the form of a Power law quite well.

Tuttle *et al* modeled graphite/bismaleimide composites under cyclic thermo-mechanical loading by using the nonlinear Schapery model combined with the Zapas-Crissman

model [20]. A Prony series was used to represent the transient creep compliance, and the $g(\sigma)$ function in the Zapas-Crissman model was assumed to be a simple power law of the form:

$$g(\sigma) = B(\sigma^m) \tag{27}$$

where B and m are both empirical constants. The resulting viscoplastic model was therefore given the form:

$$\varepsilon_{vp} = (B\sigma^m t)^n = A(\sigma^m t)^n \tag{28}$$

It was found that the model developed could predict cyclic loadings under isothermal conditions well, but when attempting to apply the model to high temperature behaviour significant ageing effects were discovered in the material.

Ségard *et al* also used a combination of the nonlinear Schapery model with the Zapas-Crissman model to study behavioural differences between treated and untreated glass fibres in an injection moulded composite [7]. A Power law was used to represent the transient creep compliance, and the same form of the Zapas-Crissman model as Tuttle *et al* was used. It was found in this study that both viscoelastic and viscoplastic strains are greater in the material with untreated fibres.

Marklund *et al* modeled the nonlinear viscoelastic-viscoplastic behaviour of flax/polypropylene composites also by using the Schapery model and the exact same form for viscoplastic development as Tuttle and Ségard [11]. The difference between a Power law and Prony series form of the transient creep compliance was investigated, and it was found that a reasonable viscoelastic-viscoplastic model could not be obtained using the power law at high stresses unless the exponent was stress dependent.

23

2.3.2   Lai and Bakker Model

Lai and Bakker developed a model for viscoplasticity in [8] and introduced the concept of effective time to address loading history. If plastic strains due to multiple step loadings are cumulative and functions of stress and time, then:

$$\Delta \varepsilon_{vp}^{i} = \varepsilon_{pl}(\sigma_i, t'_i + \Delta t_i) - \varepsilon_{pl}(\sigma_i, t'_i) \tag{29}$$

where $\Delta \varepsilon_{vp}$ is the incremental plastic strain induced by step load i, σ_i is the current applied stress, Δt_i is the duration of the current applied load, and t'_i is the effective time. t'_i is equal to the time required by the current applied stress to generate the same amount of plastic strain in the material already present at the moment of loading due to any previous load steps. The total plastic strain would simply be a sum of all the $\Delta \varepsilon_{vp}$, leading to an integral form:

$$\varepsilon_{vp}(t) = \int_{0}^{t} \frac{d\varepsilon_{pl}[\sigma(\tau), t'(\tau)]}{d\tau} d\tau \tag{30}$$

Lai and Bakker found that the plastic strain function could be represented by:

$$\varepsilon_{pl} = \sigma D_{pl}(\sigma) t^{m(\sigma)} \tag{31}$$

where D_{pl} and m are stress dependent parameters

2.3.3   Schapery Model

Schapery also developed a viscoplastic constitutive equation, but one based on thermodynamic principles [39, 40]. In [39], a detailed formulation based on Gibbs free energy in relation to internal state variables that account for viscoelastic, viscoplastic, and high-energy structural changes within the material is given. The model developed was

24

shown to account for a large number of thermally activated phenomena in polymers such as physical ageing, and was further generalized in [40].

2.4 Temperature Effects and Long-Term Prediction

Peretz and Weitsman studied viscoelastic behaviour of an adhesive under various stresses over a temperature range of 30-60°C [21, 41]. Creep and recovery experiments were conducted and modeled using a Power law creep compliance function and the Schapery model. In order to include temperature effects into the original model, Peretz and Weitsman used the following constitutive equation:

$$\varepsilon(t) = g_0 D_0 \sigma + D_1 g_1 \int_0^t [\Psi(t) - \Psi(\tau)]^n \frac{dg_2\sigma}{d\tau} d\tau + \alpha\Delta T \tag{32}$$

where D_0, D_1, and n are constants defining the linear viscoelastic creep compliance at room temperature, α is the coefficient of thermal expansion, and ΔT is the temperature difference with respect to the reference temperature of 30°C. To incorporate temperature effects into the nonlinearity parameters a, g_0, g_1, and g_2, they were defined in the study as a product of a stress dependent term and a temperature dependent term:

$$a(\sigma,T) = \bar{a}(\sigma)\hat{a}(T) \tag{33}$$

$$g_i(\sigma,T) = \bar{g}_i(\sigma)\hat{g}_i(T) \quad \text{for } i = 0, 1, \text{ or } 2 \tag{34}$$

These stress dependent and temperature dependent functions were determined at the reference temperature and at 10 MPa (a stress level in the linear viscoelastic region) respectively. This means that $\bar{a}$ and $\bar{g}_i$ (i = 0, 1, or 2) characterize the nonlinear isothermal behaviour, while $\hat{a}$ and $\hat{g}_i$ (i = 0, 1, or 2) help define the complete linear thermoviscoelastic response of the material. A least-squares fitting routine was used on the creep and recovery data collected at various stress and temperature states, resulting in a final model that provided satisfactory predictions. However, it was noted that the

developed model is only applicable within the duration of the experiments conducted and should no be used for term creep strain predictions.

More recently, Tuttle *et al* incorporated temperature effects into the nonlinear viscoelastic-viscoplastic model developed in [31]. To account for changes in behaviour due to temperature the nonlinearity parameter, *a*, in the Schapery model was assumed to be both stress and temperature dependent using the same form as Peretz and Weitsman shown by equation (33). For temperature effects on the elastic compliance, only g_0 was chosen to be both stress and temperature dependent, being defined as:

$$g_0(\sigma,T) = g_0(\sigma) + g_0(T) \tag{35}$$

Thermal effects on viscoplastic development were introduced by letting parameters in the Zapas-Crissman model be temperature dependent. From equation (28), the parameters *B* and *m* were arbitrarily chosen to be temperature dependent, but stress independent. The final model developed agreed well with verification test data.

2.4.1   Accelerated Characterization

Long-term prediction of GMT and other materials has been studied in depth over the past decades. While there is great value in determining a long-term model for viscoelastic behaviour in the magnitude of years, it is impractical to conduct multiple experiments of this length in order to collect the necessary experimental data. Fortunately, there are established principles from which long-term viscoelastic behaviour of materials can be characterized using short-term experimental data. The underlying theory behind these methods is based on research conducted by Leaderman, finding that linear viscoelastic behaviour at high temperatures can be related through time shift factors to long-term creep behaviour at lower temperature creep [42, 43]. This allows several shorter duration creep tests to be conducted at varying temperatures and horizontally shifted together

along the log time scale in order to form a master curve which predicts the long-term behaviour of the material.

2.4.2 Time-Temperature Superposition Principle (TTSP)

Time-temperature superposition (TTS) only applies to the linear viscoelastic region and only when the shape of creep curves at adjacent temperature levels match. Williams, Landel, and Ferry were major contributors to this principle and developed a mathematical approach to finding these time shift factors, a_T, for stress relaxation of amorphous polymers [44]. The equation that was initially developed by these researchers is known as the WLF equation:

$$\log(a_T) = \frac{-c_1(T - T_{ref})}{(c_2 + T - T_{ref})} \qquad (36)$$

where c_1 and c_2 are empirical constants, and T_{ref} is an arbitrary reference temperature (all temperatures are measure in Kelvin).

This equation was found to apply to a wide variety of amorphous polymers over the temperature range of $(T_{ref} - 50°) < T < (T_{ref} + 50°)$. In [44], the shift factors were also related to concepts with more physical significance such as the activation energy ΔH_η required for stress relaxation though the following equation:

$$\Delta H_\eta = R \frac{d[\ln(a_T)]}{d(1/T)} = \frac{2.303 R c_1 c_2 T^2}{(c_2 + T - T_{ref})^2} \qquad (37)$$

However, it was stated that this particular function to determine ΔH_η is inadequate as it does not take into account the molecular structure of the polymeric material [45]. Williams, Landel and Ferry also related a_T values to free volume theory in their study. When the reference temperature was chosen to be the glass transition temperature, it was

shown that the shift factors were dependent on the increase in coefficient of thermal expansion and the fractional free volume.

There has been considerable debate regarding the applicability of TTS to polypropylene. Struik extensively studied the effects of physical ageing (stiffening of the material over time) and applicability of TTS to semi-crystalline polymers [46-49]. In the study, the glass transition temperature, T_g, was assumed to be a distribution with lower bound T_g^L, and upper bound T_g^U. The temperature range studied was divided into 4 regions: $T < T_g^L$, $T \sim T_g^L$, $T_g^L < T < T_g^U$, and $T > T_g^U$. In region 3, significant ageing effects were found and TTS was determined not to be applicable in the materials studied. However, the superposition principle was possible in the other regions, as shown in Figure 2.7.
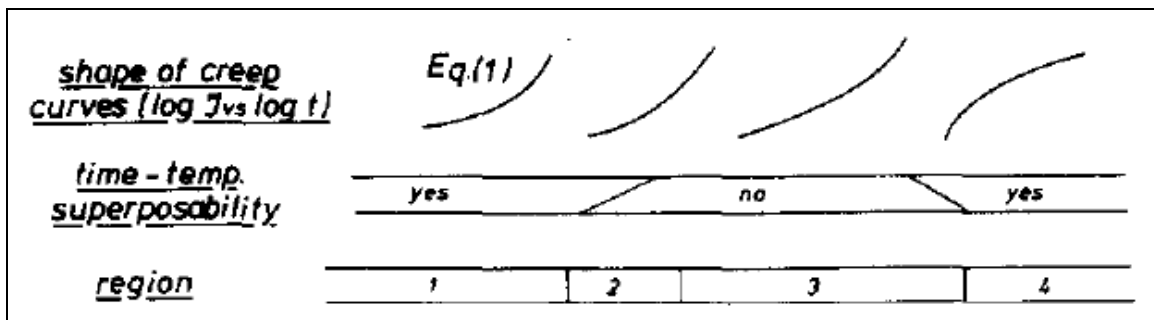
Figure 2.7: Temperature regions where TTS can be applied. [46]

Within region 3, increasing temperature caused the amorphous phase to become rubbery, which effectively softened the material causing the creep curve to flatten out at higher temperatures as shown in Figure 2.8 [46]. Since the shape of the creep curves belonging to adjacent temperatures did not match up, time shifting the curves together would have resulted in coincidence of curves at a single point as opposed to a smooth extension of the curves.

28
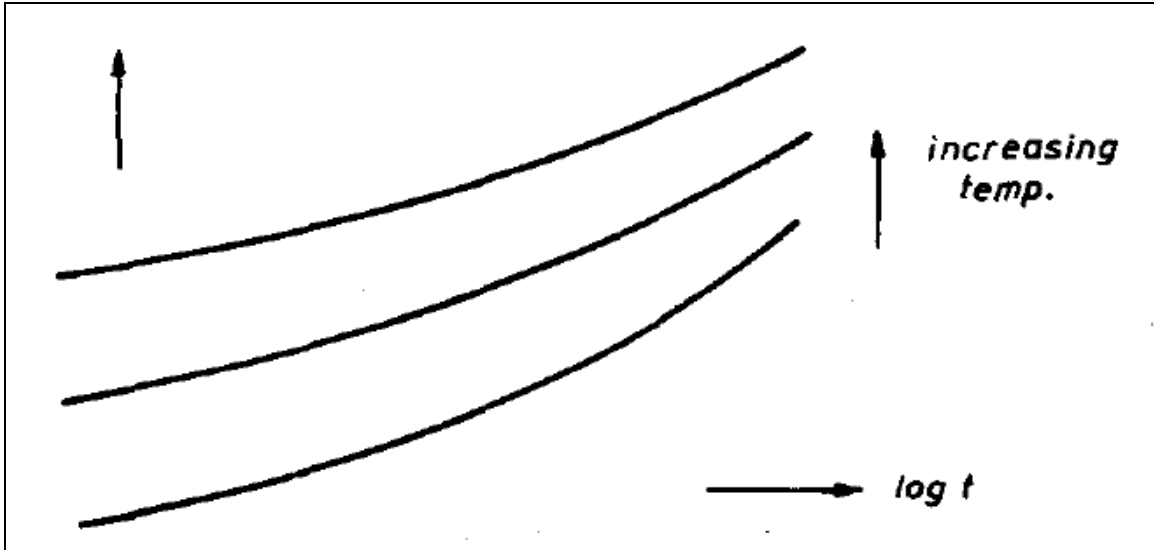
Figure 2.8: Development of creep curves with increasing temperature in region 3. [46]

When ageing effects are present in the material, it has been found that simple TTS for long-term creep prediction is invalid [46-51]. However, modifications can be made to the TTS procedure to incorporate the effects of ageing and accurately predict long-term creep behaviour such as the equivalent time temperature method developed by Barbero and Ford [51].

It has also been shown in open literature that TTS is unable to accurately predict long-term creep behaviour when there is a change in crystallinity in the material over the temperature range of the short-term experiments [52]. Issues such as physical ageing and changes in crystallinity will be addressed later on in this chapter.

In [53], Tshai *et al* applied TTS and the WLF equation to isotactic polypropylene and found that it could accurately model the thermal response of semi-crystalline polypropylene over a temperature range similar to that studied in this work.

2.4.3   Time-Stress Superposition Principle (TSSP)

In the case of non-linear viscoelastic elastic behaviour, a variety of other methods have been developed over the years to aid in long-term predictions. Time-stress superposition is analogous to TTS, and states that the short-term creep behaviour at higher stresses corresponds to longer term creep responses at lower stresses. By conducting experiments at various stresses a time shift factor, a_σ, can be used to create a master curve that describes long-term creep behaviour.

Lai and Bakker used time-stress superposition in order to predict the long-term nonlinear creep and recovery behaviour of high-density polyethylene (HDPE) while taking into consideration physical ageing effects with favourable results [54, 55]. The time shift factors related to applied stress were found to follow the expression:

$$\log(a_\sigma) = \frac{C_1(\sigma - \sigma_{ref})}{C_2 + (\sigma - \sigma_{ref})} \tag{38}$$

where C_1 and C_2 are constants and σ_{ref} is the reference stress level.

This approach to accelerated characterization and long-term creep predictions combined with TTS into a time-temperature-stress superposition principle (TTSSP) was used by Brinson and his colleagues [56-58]. Xiao, Hiel, and Cardon applied this characterization method to carbon fibre reinforced polyether ether ketone (PEEK) and used Schapery's nonlinear viscoelastic model with a general power law to reasonably predict the material behaviour [36, 59].

2.5 Random Glass Mat Thermoplastic Composites and Scatter

Glass mat thermoplastic composites are often supplied to manufacturers in the form of semi-finished charge plates, which are typically fabricated using melt impregnation or slurry deposition [1, 60]. Figure 2.9 shows a schematic of the melt impregnation process.
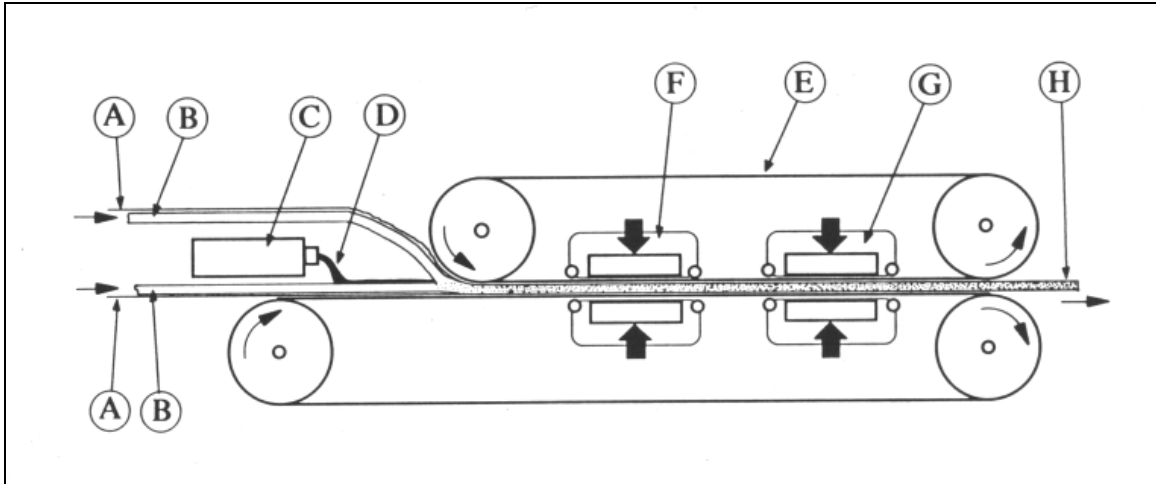
Figure 2.9: Schematic diagram of melt impregnation. (A) thermoplastic film overlays; (B) glass fibre mat; (C) extruder; (D) thermoplastic extrudate; (E) double belt laminator; (F) heating zone; (G) cooling zone; (H) semi-finished sheet product [1]

Glass fibres are first placed randomly on a conveyor, after which needles are passed perpendicularly through the glass fibres in order to cause entanglement through the thickness of the fibres and create a mat structure. The glass mats are then fed along with molten polymer between thin thermoplastic film overlays into a heated press before being cooled and cut to appropriate dimensions

A schematic of the slurry deposition process can be seen in Figure 2.10. In this process for creating semi-finished sheets of GMT composites, the glass fibres are mixed with powdered polymer and water to form slurry. The slurry is then dried and pressed together similar to the melt impregnation process, or can be left to dry and produce a porous laminate, ready for further processing later one by the manufacturer.
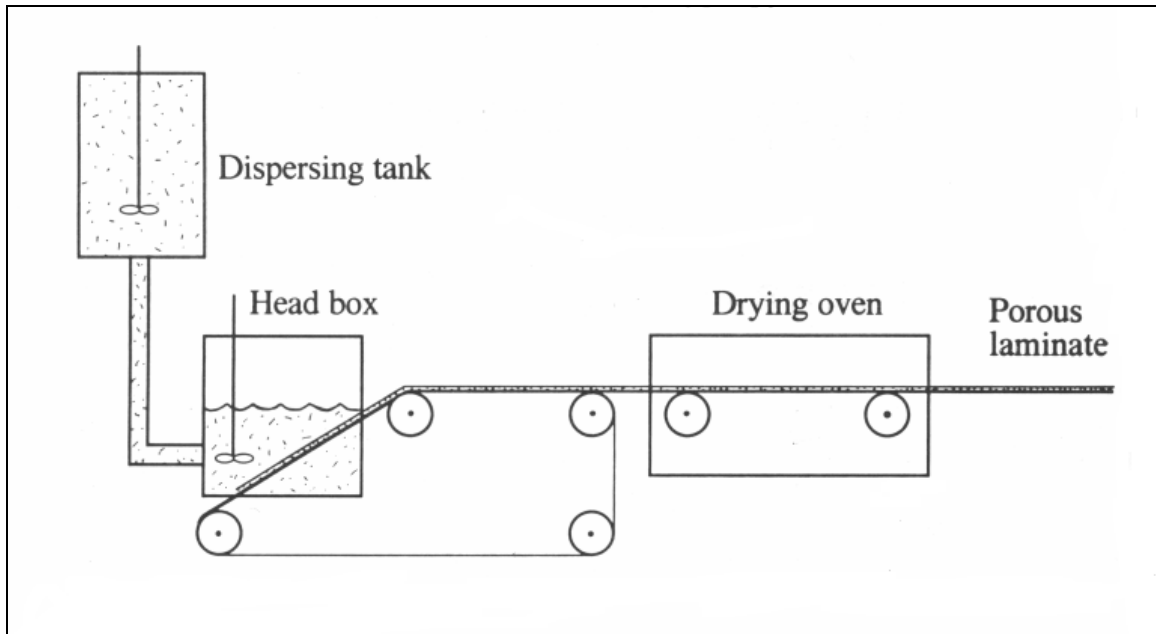
Figure 2.10: Schematic diagram of slurry deposition. [1]

While these are the typical methods to create GMT composites, the processing during manufacturing as well as the fibre content can greatly influence the mechanical properties of the material. It has been shown that the strength of GMT composites increases with fibre content only up to a certain point, after which the strength of the composite drops dramatically [60, 61]. The increased fibre content resulted in higher void content as well as increase localized cracking due to stress concentrations at fibre ends [60].

While the fibre content is often given as a nominal value for GMT composite materials, due to the random placement and distribution of glass fibres when creating the semi-finished sheets as well as any flow which may occur during processing, the localized fibre content can deviate from the stated nominal value. Since fibre content has been shown to change the mechanical properties significantly, this causes higher scatter in material properties during experimentation.

2.5.1 Material Scatter

A major problem in attempting to model this material is the large scatter present in randomly oriented GMT composites. Stokes *et al* published a series of papers on the characterization of tensile strength in a continuous fibre GMT material. From the experiments conducted, it was found that the tensile modulus over a 12.7mm distance on a plaque could vary up to 200%, and the elastic modulus in a 150 x 305mm plaque could vary by 300% [62]. Through extensive investigations into the material behaviour, Stokes and Bushko eventually offered a statistical method by which to characterize this material using a probability density function [63]. The work by Stokes illustrates how large the scatter in GMT material properties can potentially be.

Tomkinson-Walles studied temperature, rate and geometry effects on tensile and flexural properties of four composite systems. It was noted in [64] that scatter is decreased with increased specimen width.

In order to deal with the variability, statistical analysis can be used to help determine the significance (or there lack of) in any observed behaviour. Analysis of Variance (ANOVA) is typically used in such cases, along with proper experimental design to minimize the amount of error in experimental measurements. ANOVA compares mean values while taking into consideration the variability in measurements. The null hypothesis is tested using this technique, which states that the means being compared are not significantly different from each other in terms of statistics and probability. The assumption is that the variance associated with each mean value is the same, and that the individual measurements are normally distributed about the mean values.

2.5.2 Pre-conditioning

It has been shown in previous research that pre-conditioning of specimens can help to produce more repeatable experimental results, reducing scatter by effectively erasing the

long-term memory of the specimen as observed by Gupta and Lahiri in glass fibre reinforced polypropylene [9]. While each composite system may behave differently, similar observations have been made by Peters *et al* in a study of pre-conditioning effects on short glass fibre reinforced epoxy resin [65]. By repeatedly loading and unloading the specimens prior to experimentation at a higher stress level than the tests themselves, Peters *et al* concluded that microcracks were induced in the material, relieving internal stresses in the specimen.

Crissman and Zapas studied the effects of pre-conditioning on ultrahigh-molecular-weight polyethylene (UHMWPE) and made a similar conclusion to Gupta and Lahiri; pre-conditioned specimens exhibit ideal viscoelastic material behaviour [9, 66].

It has been argued by Hiel in [67] that the use of pre-conditioning may cause changes in the basic stress-strain behaviour of the material. Peters *et al* agreed, but found that a stress threshold exists, at least for short glass fibre reinforced epoxy resin, below which the viscoelastic behaviour is insignificantly affected by the induced damage [65]. For glass fibre reinforced polypropylene, it was verified by Dasappa that the induced damage due to pre-conditioning had minimal effect on the viscoelastic behaviour over the stress range of interest in this work [68].

2.6 Previous Studies on Material Behaviour

In [6], a series of tensile and creep experiments were performed along with thermal analysis using Dynamic Mechanical Analysis (DMA) and Differential Scanning Calorimetry (DSC) to characterize the same chopped fibre GMT composites studied in this work.

From mechanical testing, it was concluded that the material can be considered isotropic, and has a total variability based on the creep tests performed of approximately ±18% [6].

A summary of the creep tests results to determine material variability is shown in Table 2.1.

Table 2.1: Summary of creep test data for material variability. [6]

Plaque	Specimen	Instantaneous Compliance	Average for plaque	Compliance at end of creep	Average for plaque
2	0201	164.7	137.8	174.8	144.6
	0202	110.8		114.4	
3	0301	149.1	164.3	159.9	177.0
	0302	179.6		194.1	
5	0501	142.2	127.9	149.4	133.7
	0502	113.6		118.0	
6	0601	132.0	148.3	137.8	155.9
	0602	164.5		174.0	
Mean		144.6	144.6	152.8	152.8
Std Dev		24.8	15.6	28.3	18.5
% RSD		17.2%	10.8%	18.5%	12.1%

Through DMA, it was determined that the glass transition temperature, T_g, for the chopped fibre GMT composite studied in this work is approximately 5°C, and that there exists an alpha star transition, $T_{\alpha*}$, at 61°C [6]. This alpha star transition is associated with slippage between crystal phases in the polymer [69].

It has been mentioned in previous sections that the behaviour of GMT and other composite materials can be affected significantly by physical aging as well as changes in crystallinity, especially when attempting to model long-term viscoelastic behaviour using accelerated characterization. Zhou conducted thermal analysis using DMA and modulated-DSC and could not detect any major physical ageing effects in the material over the temperature range of interest after ageing samples for 10 days [6]. Furthermore,

Law examined the same material for changes in crystallinity using Wide Angle X-ray Scattering (WAXS) and Fourier Transform Infrared Spectroscopy (FTIR). Material degradation was studied using FTIR by examining the oxidation products due to thermal decomposition. Within the temperature range studied in the current work, no changes in crystallinity or material degradation were found [35]. From the conclusions of these investigators, the effects of physical aging, changes in crystallinity, and material degradation were not considered in the development of the constitutive model.

3.0 EXPERIMENTAL DETAILS

3.1 Material

The material used in this study is a randomly oriented chopped fibre glass mat thermoplastic composite known commercially as Quadrant D100-F40-F1, with fibre weight content of 40%. A product data sheet supplied by the manufacturer has been included in Appendix A. The polypropylene matrix is reinforced with a mat structure consisting of untreated glass fibres of varying lengths, ranging from 5 ~ 20 mm [60]. Charge plates of this material were provided by Quadrant Plastic Composites, and compression moulding of charge plates into usable plaques was conducted at Polywheels Manufacturing Ltd in Oakville, Ontario.

The charge plates were pre-heated in an oven with three different temperature zones of 35°C – 40°C, 55°C – 60°C, and 70°C – 75°C. Following the pre-heating, the charge plates were placed into a mould with a cavity temperature maintained at 60°C and a core temperature held at 65°C. A 450 tonne press was actuated for a dwell time of 40 sec to compression mould the charge plates into plaques with approximate dimensions of 390 x 390 x 3.5mm. The total cycle time to create each plaque was approximately 90 seconds, and an "X" was placed in one corner to identify the direction of moulding.

According to standard [70], the specimens for creep testing should have dimensions as outlined in [71] and shown in Figure 3.1.
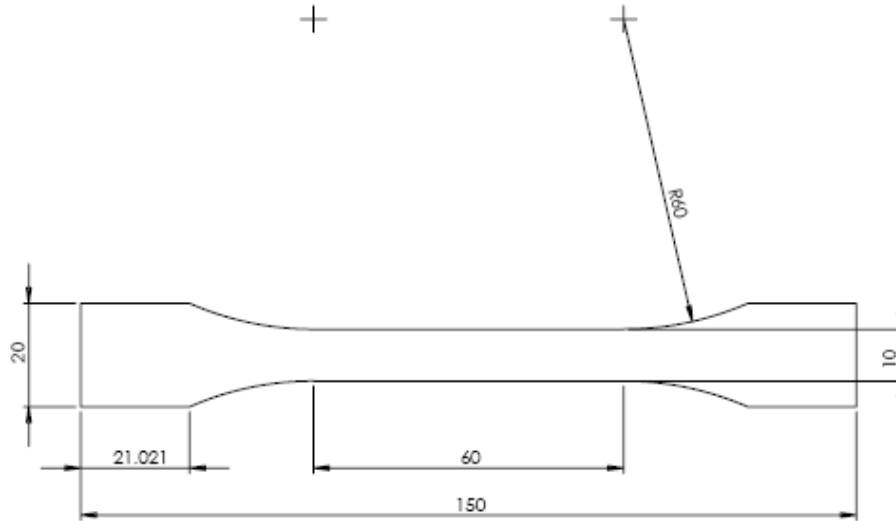
Figure 3.1: ASTM standard creep test specimen dimensions. [6]

However, due to the specific test fixture being used in this study, specimens had to be slightly modified to dimensions shown in Figure 3.2.
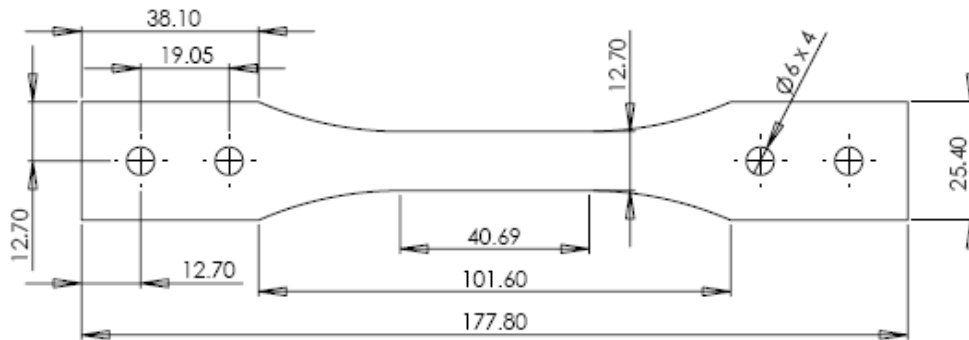
Figure 3.2: Creep test specimen dimensions used in this study. [72]

These specimens were cut from the compression moulded plaques by Baumeier Corp. in Waterloo, Ontario using water jet. All specimens were cut in the same orientation with respect to the "X" made during compression moulding to ensure consistency with moulding direction.

3.2 Equipment

3.2.1 Test Fixture

The creep tests used to characterize the material behaviour were conducted using the test fixtures provided by General Motors based on a design by D. Houston and E. Hagerman specifically for studying creep in polymeric composites [73]. Modifications were made to the original fixture to meet various ASTM testing standards by Dasappa as described in [72]. Figure 3.3 (a) and (b) show the unloaded (recovery) and loaded (creep) positions respectively, of the modified fixture.

(a)   (b)
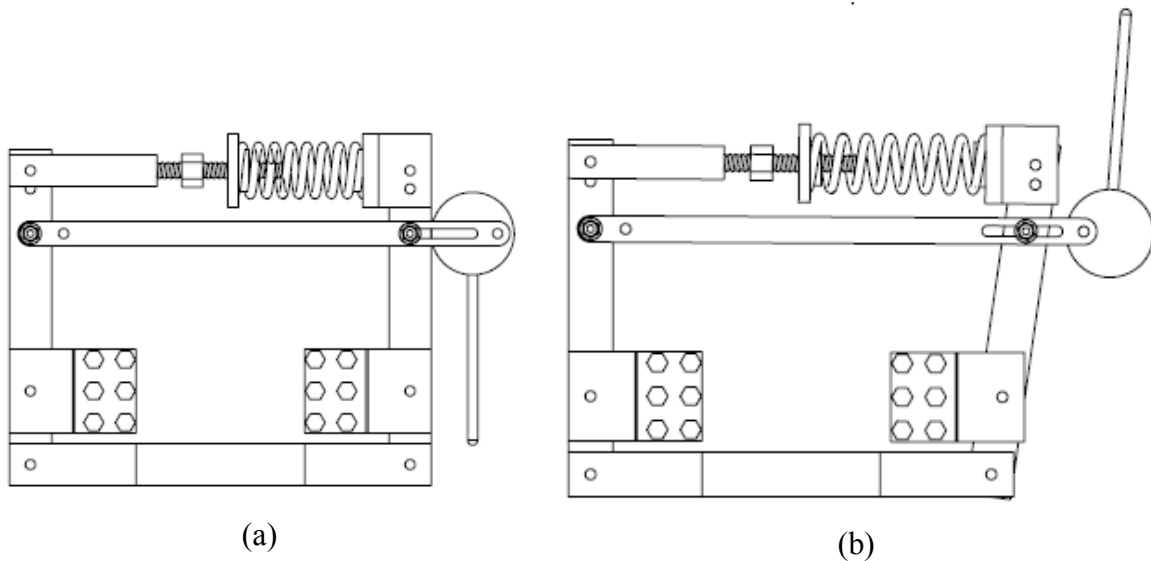
Figure 3.3: (a) Unloaded and (b) loaded positions of modified creep test fixture. [72]

With the new cam assembly and right arm slot modifications as shown in Figures 3.4 and 3.5, the fixture could now be instantaneously loaded and allow for recovery in the specimen.
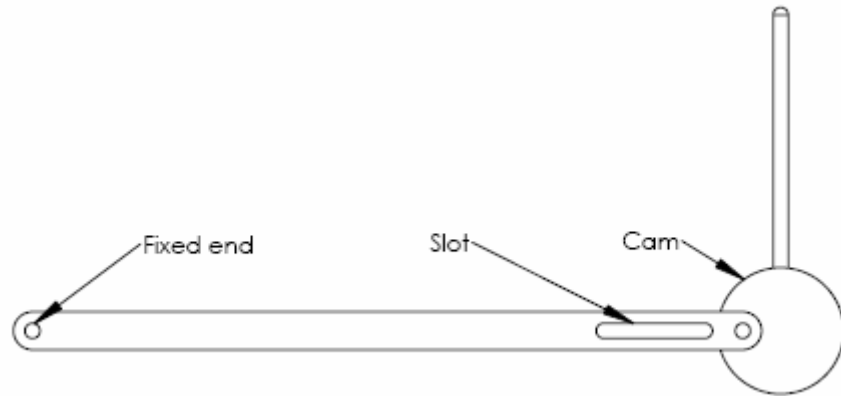
Figure 3.4: Cam attachment of modified test fixture. [72]
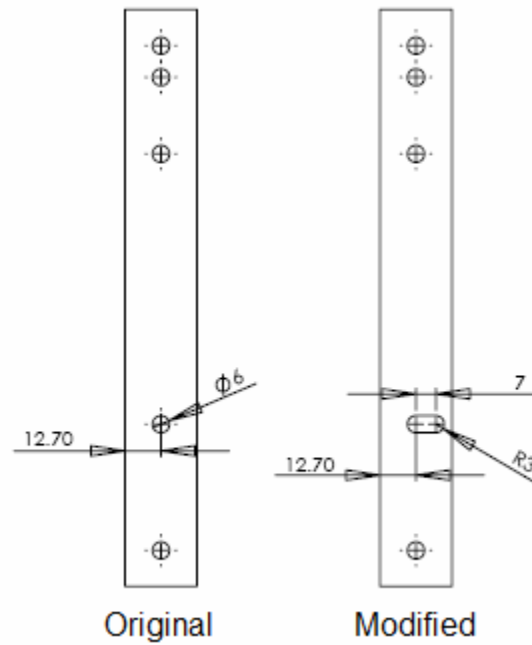
Figure 3.5: Modifications to right arm of test fixture. [72]

A holding plate as indicated in Figure 3.6 was used to hold the specimen in place. The six bolts through each holding plate were hand tightened in the order indicated. Afterwards, the same order was used to apply a 5.4 N·m torque on each bolt with the aid of a torque wrench.
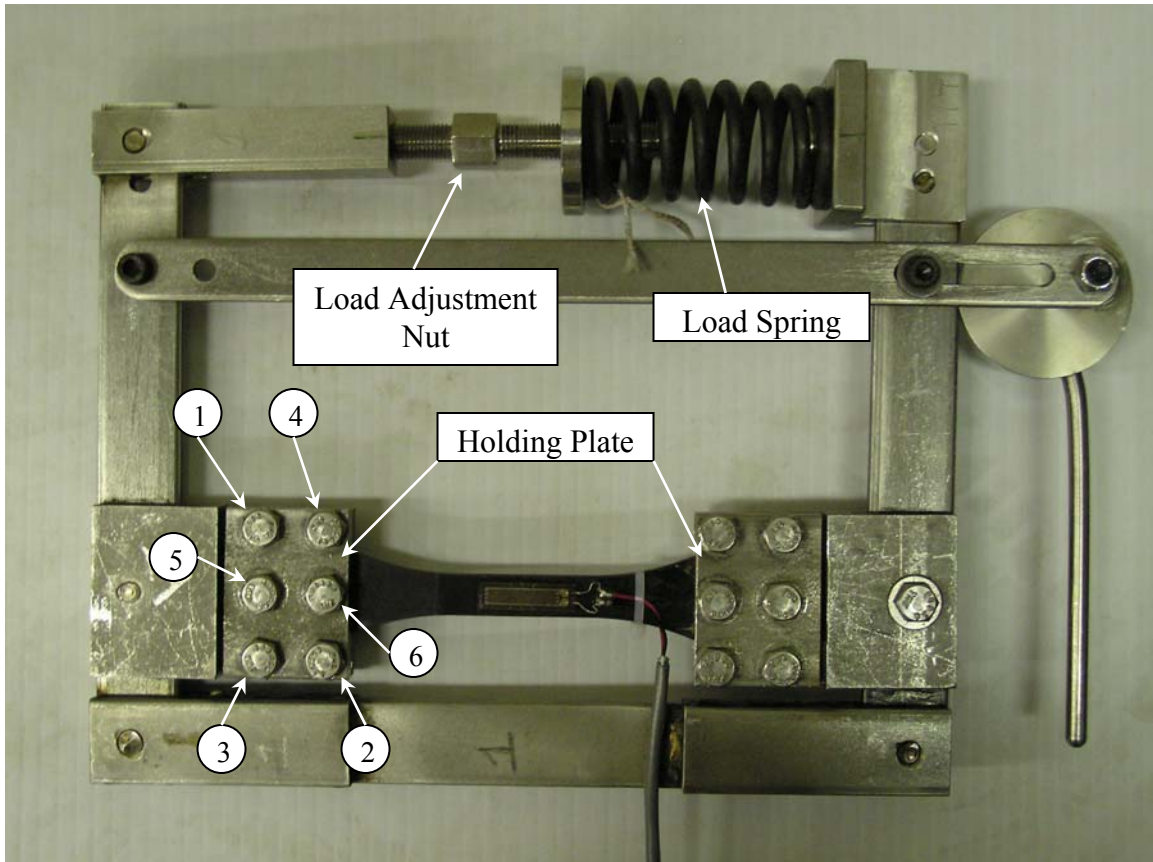
Figure 3.6: Bolt tightening order of creep fixture.

Calibration of the test fixtures was accomplished through the use of a Honeywell Sensotec precision miniature load cell (1000 lb. capacity) with custom attachments and a Micron digital LED display as shown in Figure 3.7. A copy of the load cell specifications can be found in Appendix B. The custom attachments to the load cell as seen in Figure 3.7 allow fastening into the test fixtures, and the digital display shows the current force experienced by the load cell in Newtons.

Figure 3.7: Load cell and digital display used for text fixture calibration.

By adjusting the nut near the load spring in the fixture as shown in Figure 3.6, the applied load could be adjusted until the load cell reading corresponded to the desired testing load. To determine this testing load, three width and three thickness measurements were taken along the gauge of each specimen using a digital Vernier calliper. An average cross sectional area was calculated and using the simple relation:

$$\sigma = \frac{F}{A} \tag{39}$$

the required force to attain the desired applied stress in the material was calculated.

After fastening specimens into the fixtures and calibrating the system, there were usually residual strain readings shown prior to actual creep testing, attributed to slight bending

and misalignment of the specimen. Since this misalignment would be rectified at the beginning of the test (i.e. at the instant of loading the specimen would straighten causing the residual strains to go to 0 before the actual creep strains were recorded), these residual strains were only subtracted from the recovery data as any initial misalignment or bending in the specimens was assumed to return once the load was removed.

3.2.2   Strain Gauges

Kyowa KFG-5-120-C1-11 120 Ω strain gauges were mounted on all specimens prior to testing to record strain data, with the exception of specimens used in the long-term temperature creep tests. Due to supply issues, TML FLA-30-11 120 Ω strain gauges were mounted on these specimens instead. The specification sheets for both strain gauge types are found in Appendix B.

To mount the strain gauges, the surface of the gauge was first polished using 400 and 500 grit sandpaper. Once a smooth material surface attained, the specimen was cleaned using isopropyl alcohol and then neutralized. Following this polishing process, crosshairs were drawn manually on each specimen at the centre of the gauge length. The specimen was cleaned, neutralized and conditioned before the strain gauges were applied using an epoxy adhesive by Vishay Micro-Measurements. The data sheets for the adhesive and the hardening agent can be found in Appendix B. A weight of 2.5 kg was placed on each specimen during curing as recommended. The epoxy adhesive was allowed to cure for a minimum of 24 hours before testing.

3.2.3   Data Acquisition

The data acquisition software was designed by Zhou using Labview application software [6]. The hardware allows up to 8 channels of simultaneous strain data acquisition, in addition to a separate channel for recording data from a thermocouple placed inside the oven. The software allows the user to define the frequency of data point collection and

43

the acquisition system can be calibrated simply through the input of a user defined coefficient. To determine this value, a strain gauge shunt box with several reference values as shown in Figure 3.8 was connected to each channel prior to testing.

Figure 3.8: Strain gauge shunt box used for data acquisition calibration.

The application was started and the reading in each channel was displayed. The calibration coefficient was calculated so that the acquisition system readings would match the reference values induced by the shunt box.

3.2.4   Oven

The oven used for the experiments was VWR International's VWR Signature model 1680, with internal dimensions of 42 in x 20 in x 30 in (width x depth x height). This high

performance horizontal airflow oven is shown in Figure 3.9 and was manufactured by Sheldon Manufacturing Inc. and has a maximum operating temperature of 260°C. Two sliding metal shelves were used, allowing the oven to hold up to 8 test fixtures simultaneously.

Figure 3.9: Oven used for creep testing.

3.3   Experimental Program

3.3.1   Stress Effects

From a literature review on GMT materials and preliminary tensile tests on the chopped fibre GMT, relatively large scatter in the creep test results was expected. Hence, two separate test schemes were considered to study the effects of stress on the viscoelastic behaviour. First, data from short-term creep tests consisting of 30 minutes creep followed

by 30 min recovery previously collected [6] and second, long-term tests conducted in this study consisting of 1 day creep followed by recovery.

The purpose of the short-term test data was to determine the variability of the material and the linear viscoelastic region. The material variability was tested using specimens from four randomly selected plaques. To determine the linear viscoelastic region, data from short-term tests performed on single specimens was used. The specimens were repeatedly loaded at the various stress levels between 5 and 50 MPa in order to reduce variability due to the material scatter and more easily determine trends in material behaviour. At each stress level, the specimens were loaded for 30 minutes, and then were allowed to recover for 30 minutes. A minimum of four replicates were used in this set of experiments. However, since the same specimens were used in multiple tests, any information regarding possible viscoplastic strain development would be inaccurate, and therefore another set of tests was conducted.

Long-term tests were conducted similarly to the short-term tests - each specimen was strain gauged and subjected to 1 day creep followed by 1 day recovery. A major difference between the two types of testing was that the long-term tests were always conducted on new specimens so that the viscoplastic strain behaviour could be studied. Typically four replicates were used at each stress level. Long-term tests were conducted for the purpose of short-term model development between 20 and 50 MPa, at 10 MPa increments. Experiments were also conducted at 60 MPa, but resulted in tertiary creep behaviour and a high percentage of failed specimens. Therefore, data used in developing a model was limited to below 50 MPa.

3.3.2 Temperature Effects

The objective of this series of tests was to study temperature effects on the chopped fibre composite and to determine the applicability of time-temperature superposition (TTS) principle for predicting long-term creep behaviour.

Mechanical pre-conditioning was conducted prior to the short-term creep tests by loading and unloading the specimens for 30 second intervals, 15 times at 50 MPa and room temperature. Pre-conditioning is a common approach used to attain more repeatable data in materials that have large experimental scatter as explained earlier. This was important as each specimen would be repeatedly loaded over the temperature range between 25°C and 90°C. Typical pre-conditioning data for the chopped fibre composites is shown in Figure 3.10.
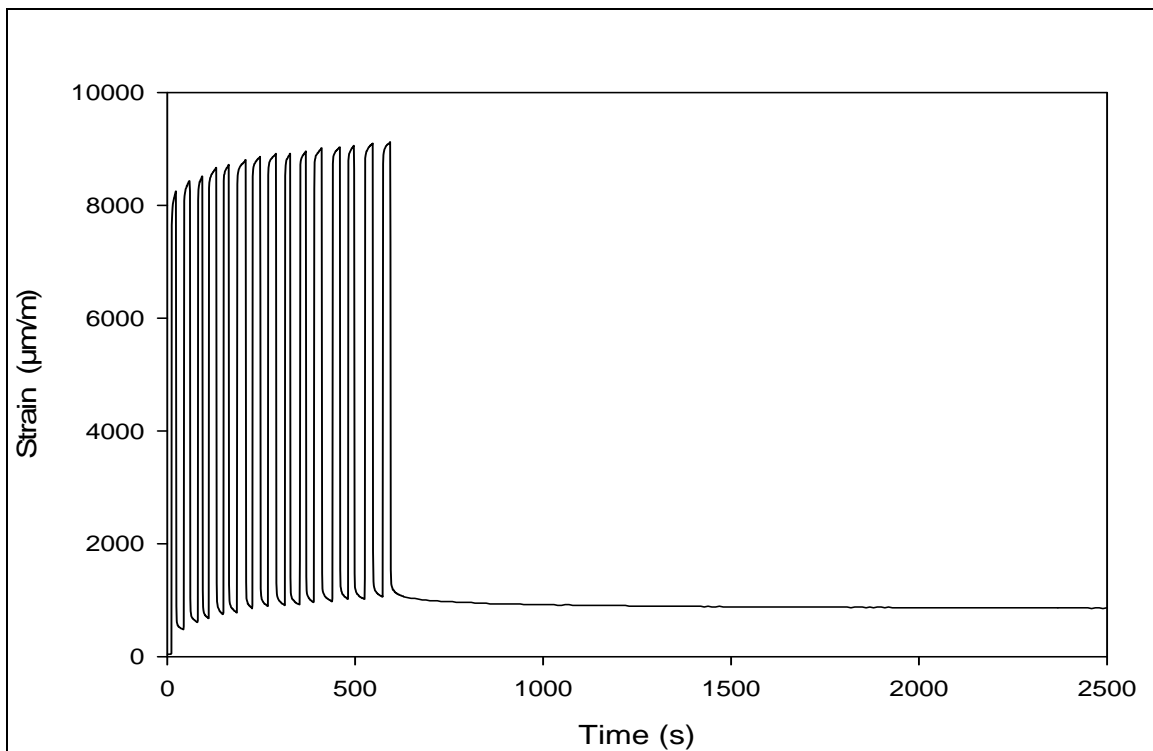
Figure 3.10: Typical pre-conditioning data.

It can be seen from the figure that the material started providing consistent data only after approximately 10 repeated loadings. After pre-conditioning, all specimens were allowed to recover before commencing actual short-term creep tests. The progression of curves seen in the figure shows the accumulation of plastic strains in the material from successive loading.

By repeatedly loading the specimens at 50 MPa, it can be seen in Figure 3.10 that plastic damage was induced in the material as there is a residual strain after pre-conditioning. By conducting the actual tests at lower stress levels, the majority of the viscoplastic damage is assumed to have already occurred, allowing predominantly viscoelastic behaviour to be studied through these short-term temperature tests. The induced viscoplastic damage was found to have minimal effect on the viscoelastic behaviour [68].

Short-term temperature tests were conducted in order to determine the applicability of time-temperature superposition and temperature effects on viscoelastic behaviour. These tests consisted of 30 minutes creep followed by 1 hour recovery, from 25 to 90 °C at 5 ° increments. The oven was allowed to stabilize for 15 minutes at the set temperature before creep testing, and four randomly selected specimens were used per stress level. Each specimen was strain gauged using the method described earlier and tested over the entire temperature range continuously. These short-term tests were conducted at three stress levels, i.e., 20, 30, and 40 MPa.

In order to gain a better understanding of any temperature effects on damage accumulation in the material and collect data for model development, a series of long-term temperature experiments were also conducted. Specimens were strain gauged and allowed to creep for 1 day before recovery. These tests were also conducted at 20, 30, and 40 MPa. For each stress level, four replicates were used at each temperature level tested (40, 60, and 80 °C).

4.0 RESULTS AND DISCUSSION: STRESS EFFECTS

4.1 Short-term Creep Tests

Data collected from short-term creep tests performed on the same specimen at various stress levels was used to determine the region of linear viscoelastic behaviour. Figure 4.1 shows a typical set of creep data for one specimen from the short-term experiments.
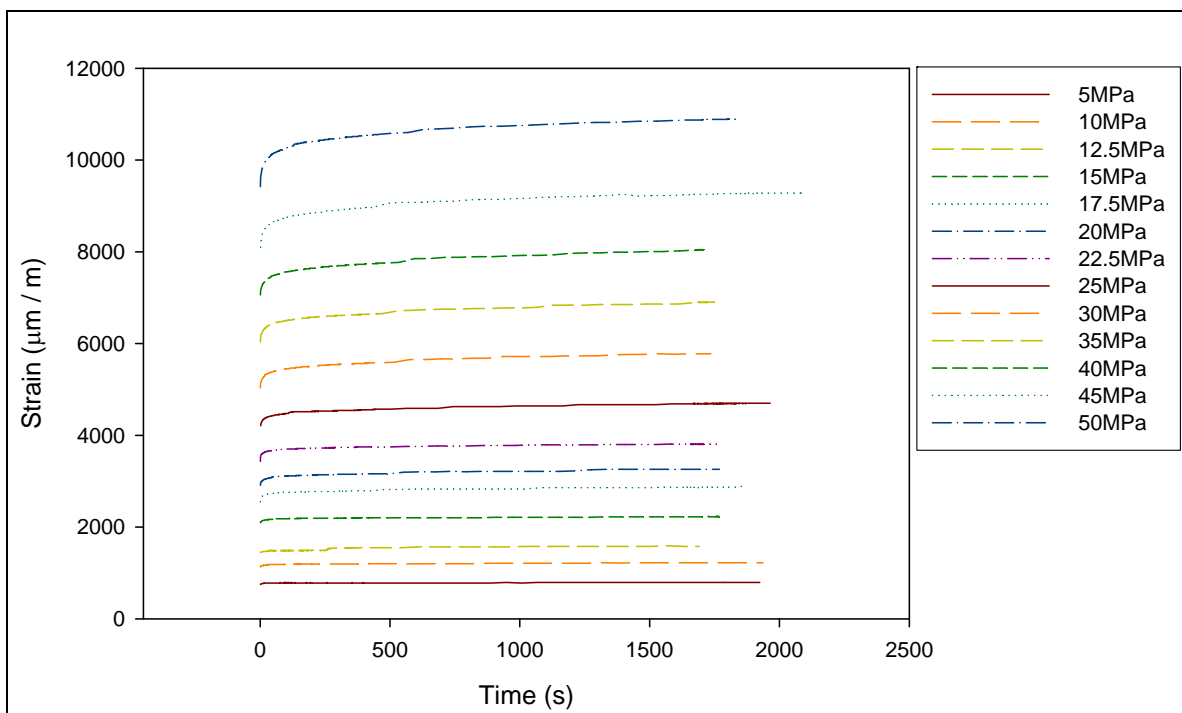
Figure 4.1: Typical short-term creep test data. [6]

Figure 4.2 shows the total creep compliance values after 30 minutes of creep from the short-term experiments at various stress levels, calculated by rearranging equation (1) and isolating the creep compliance into the form:

$$D(t) = \frac{\varepsilon(t)}{\sigma} \tag{40}$$

where *D(t)* are the plotted compliance values in the figure, *ε(t)* are the creep strain values measured from experimentation (at $t = 1800$s for this particular case), and *σ* is the applied stress.
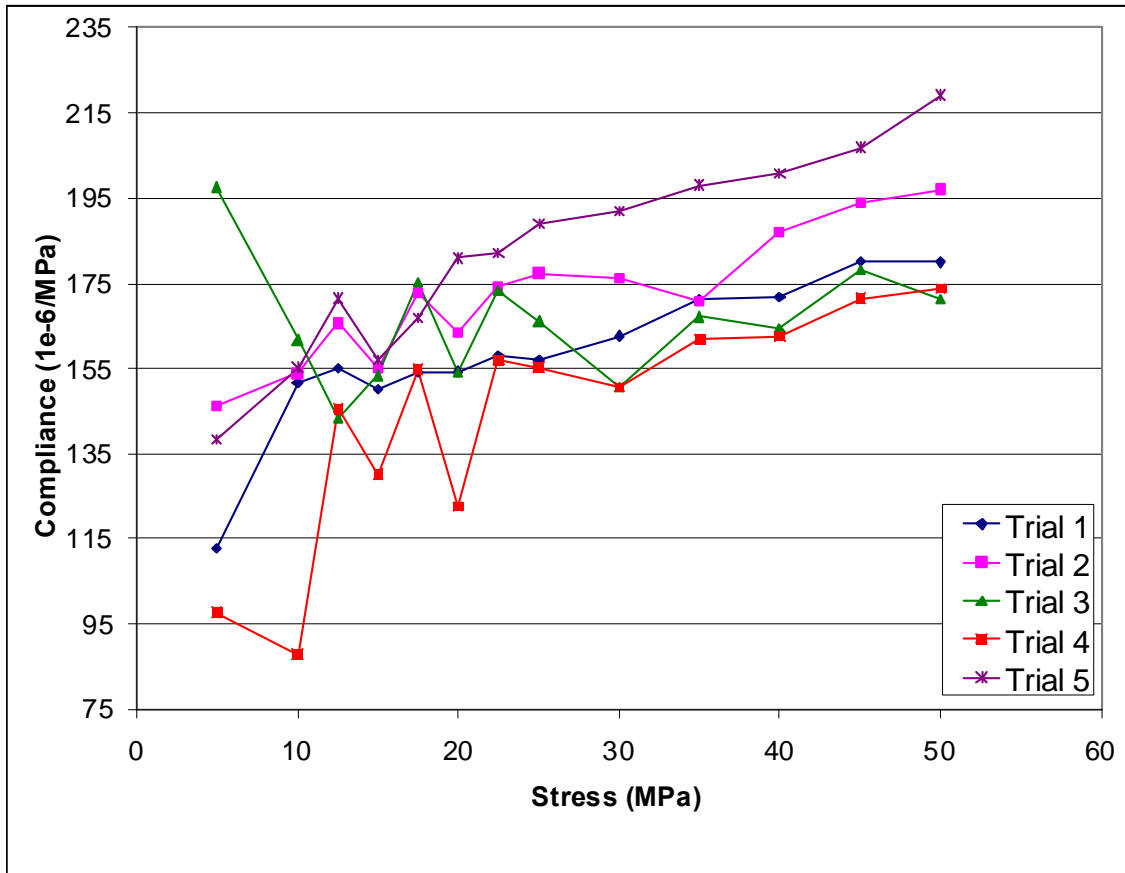
Figure 4.2: Total creep compliance after 30 minutes creep.

It is important to note the large scatter in test results at 10 MPa and below, which is attributed to limitations of the creep test fixture. Due to the rigidity as well as frictional forces between the various components of the fixture, larger loads are required to overcome these forces and provide more accurate data. Initial inspection of the calculated creep compliance values for individual trials between 20 MPa and 40 MPa show a slight increase in creep compliance with stress. As mentioned earlier in section 2.1 regarding conditions for linear viscoelastic behaviour, this slight increase indicates possible nonlinear viscoelastic behaviour in the material.

4.2 Long-term Creep Tests

Figure 4.3 shows the creep strains after 1 day creep from experiments at the various stress levels. Any outliers and anomalous data lying outside of two standard deviations have been removed. The variability in long-term creep experiments was found to be approximately ±19% with outliers, which is similar to the ±18% material variability determined through short-term tests. Creep data which was close to two standard deviations or more from the average compliance value calculated for each stress level were considered outliers, since the probability of lying outside of two standard deviations is less than 5%. After the removal of outliers and anomalous data, the variability was recalculated to be roughly ±7.6% from the data collected. This remaining data was used for analysis and modeling of the material behaviour.
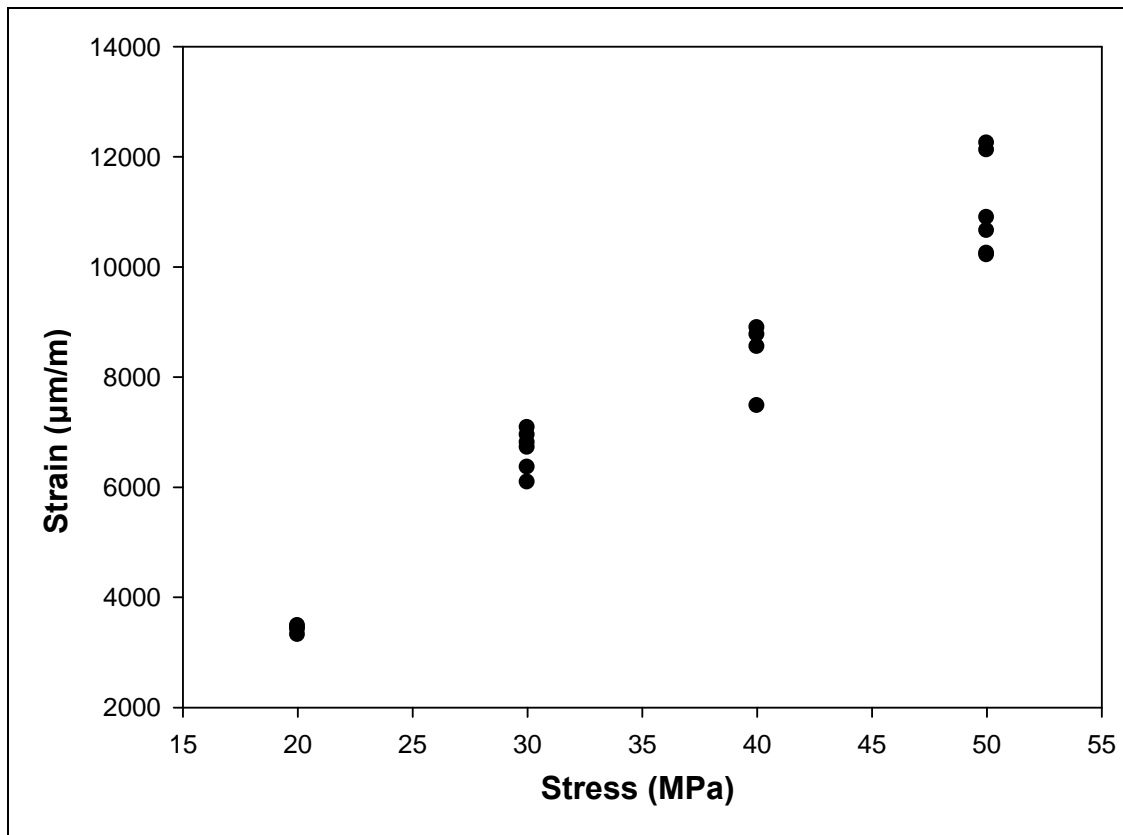
Figure 4.3: Total creep strains after 1 day creep.

For data reduction and consistency in evaluating material scatter, MATLAB was used to calculate average representative curves at each stress level from the creep and recovery data. Figure 4.4 shows the average creep-recovery curves obtained at each stress level, where each curve was calculated using at least four replicates. By observing the recovery portion of each average curve, it can be seen that the response of the material begins to plateau towards a non-zero strain value after 1 day of recovery. The fact that the creep strains are not fully recovered indicates the presence of permanent viscoplastic strains in the composite material even at 20 MPa. An analysis of the material on the microscopic level to confirm the viscoplastic strains is not within the scope of this particular research, however, the work of Law [35] provides support for this argument. In [35], Law conducted creep experiments on micro tensile specimens under a microscope with image capturing capabilities.
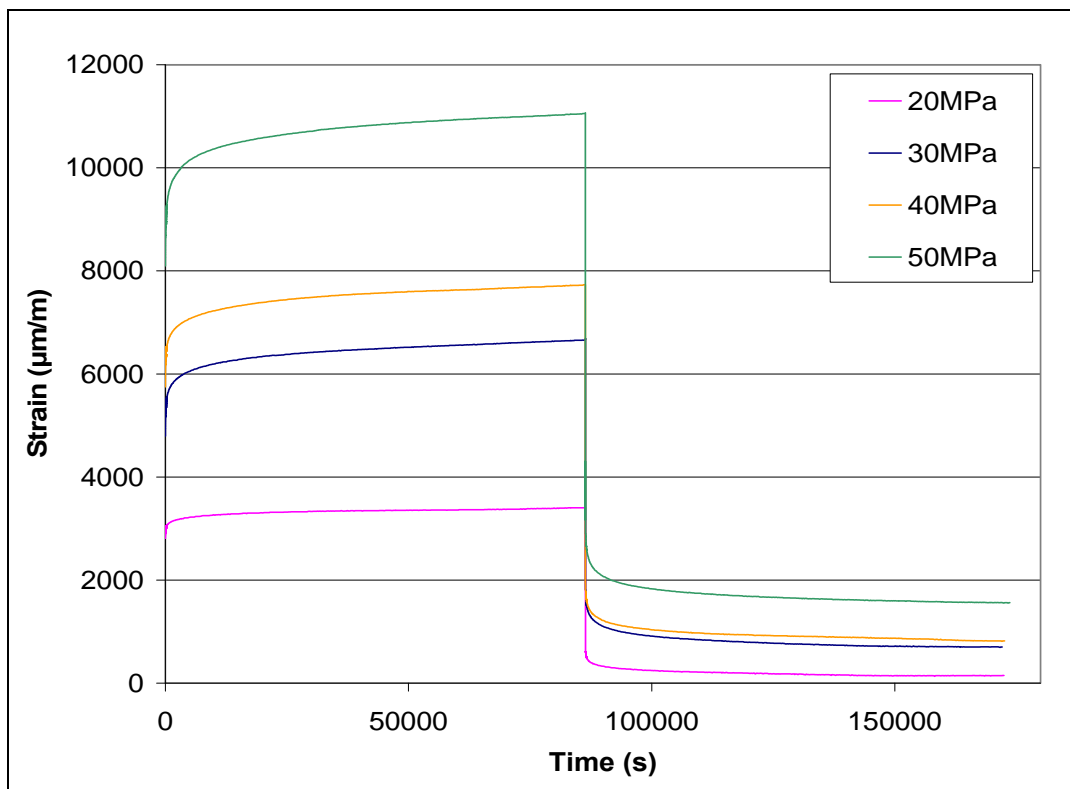
Figure 4.4: Average creep curves at various stress levels from long-term experiments.

As seen in the micrographs obtained from [35] of the random chopped fibre GMT composite in Figures 4.5 and 4.6, the surface of the specimens at room temperature before and after loading at 23 MPa and 47 MPa (which correspond to about 33 % and 67% of the ultimate tensile strength of the material respectively) exhibit increasing amounts of damage with stress. In the figures, the load is applied in the direction indicated by the arrows. The development of transverse cracks initiating at the fibre-matrix interface is evident at 23 MPa as shown in Figure 4.5 (b), while both transverse cracks and fibre-matrix debonding can be observed at 47 MPa as shown in Figure 4.6 (b).
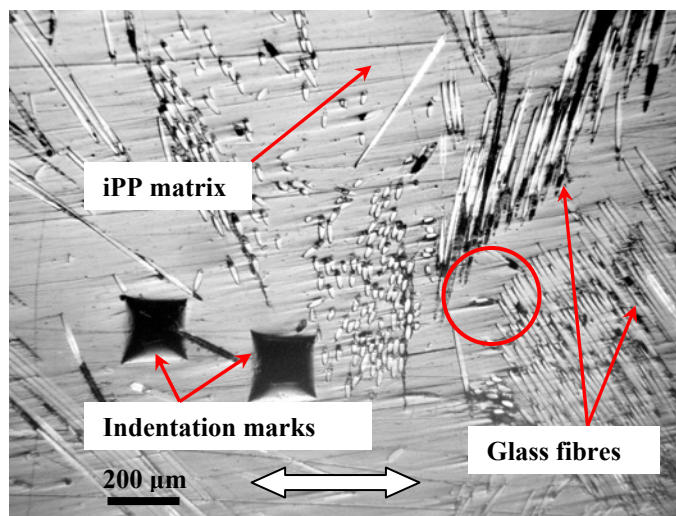
(a)
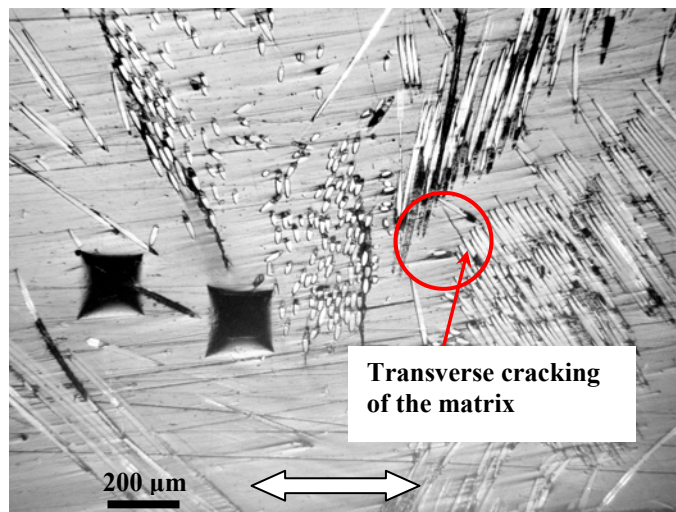
(b)

Figure 4.5: Image of micro-tensile specimen (a) before creep and (b) after 1 day creep at 33% of room temperature ultimate tensile strength (23 MPa). [35]

(a)

Fibre-matrix debonding

**Cracking of
the matrix**
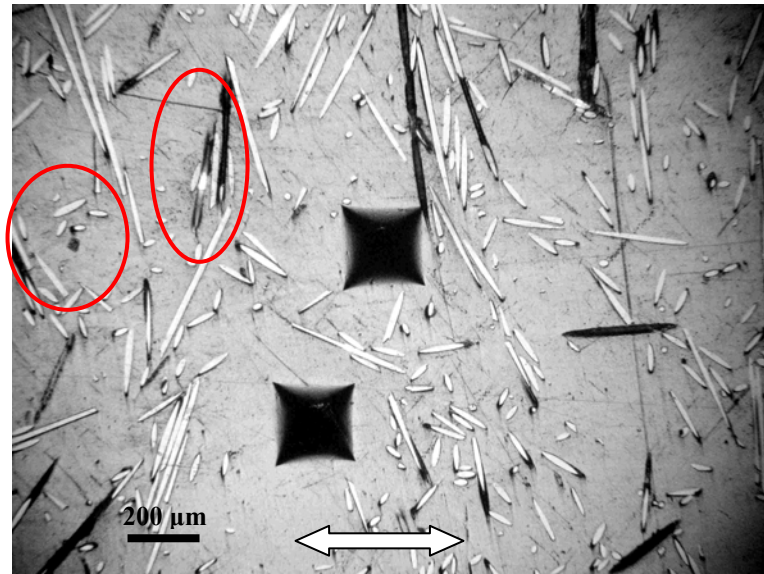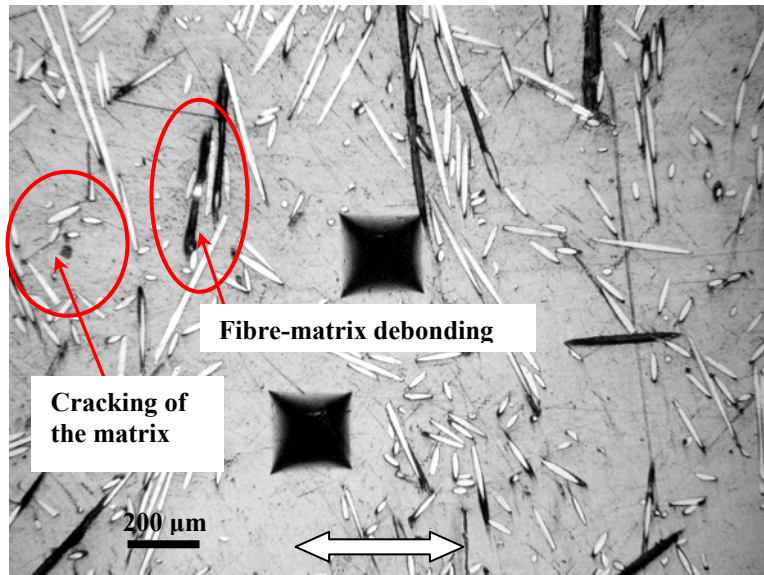
(b)

**Figure 4.6: Image of micro-tensile specimen (a) before creep and (b) after 1 day creep at
67% of room temperature ultimate tensile strength (47 MPa). [35]**

The un-recovered strains at the end of 1 day recovery are assumed to be reasonable
estimates of the plastic strain in the material. The average un-recovered strains at the
four stress levels are plotted in Figure 4.7, showing an increase in these strains with
stress. The amount of viscoplastic strain appears to be quite significant as compared to

the creep strains, indicating that a viscoelastic-viscoplastic (rather than a viscoelastic) model is required to properly predict the material behaviour.
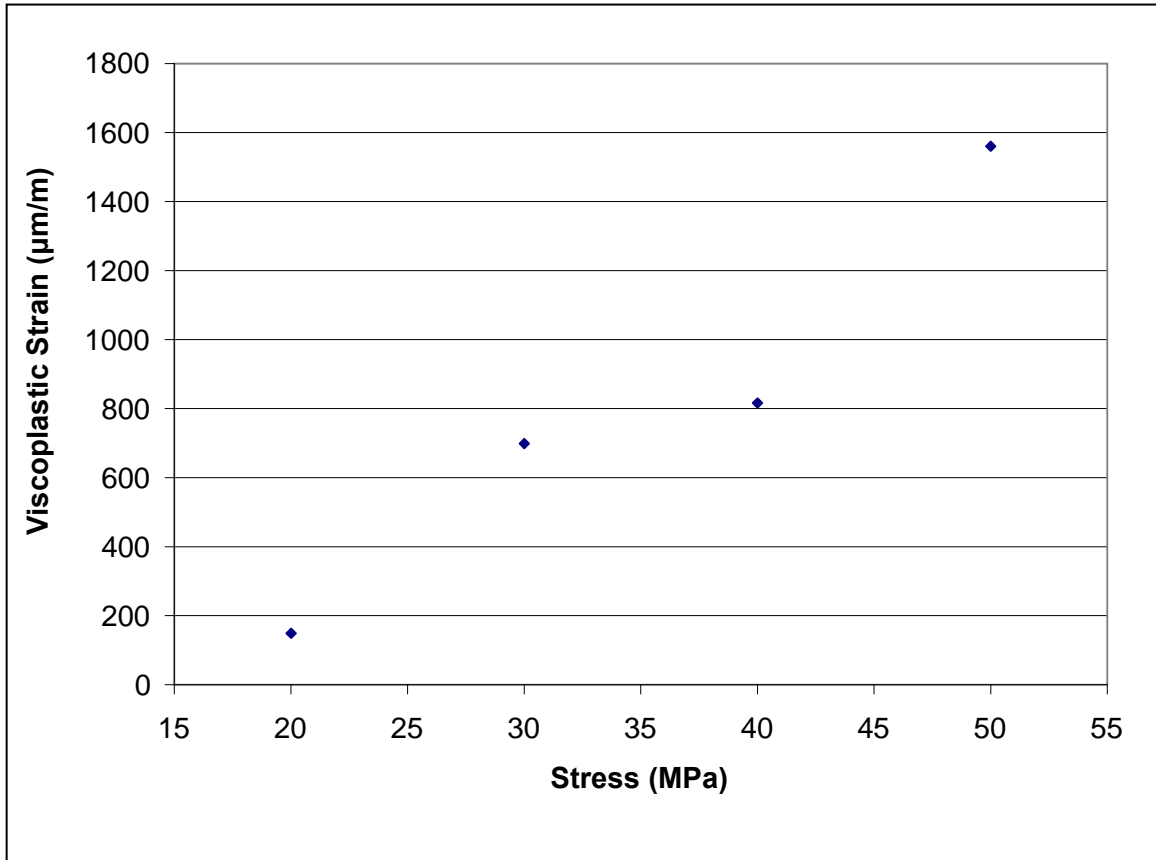
Figure 4.7: Residual plastic strains following 1 day creep.

4.3   Linear Viscoelastic Region

As stated earlier in section 2.1.4, a material is only considered linear viscoelastic when the creep compliance is stress independent and the Boltzmann Superposition Principle is applicable. Accordingly, the short-term test data was used to determine the linear viscoelastic region for the material. This was confirmed with the long-term creep test data.

Following the results of long-term creep tests and the confirmation of viscoplastic response in the material, the total creep compliance values shown in Figure 4.2 were assumed to contain both viscoelastic and viscoplastic components. In order to isolate the viscoelastic compliance and determine the linear region, the un-recovered strains from the short-term experiments were assumed to be the total viscoplastic strain developed during the 30 minute creep period just prior to recovery. Since the load is removed at the start of recovery, t_r in Figure 4.8, no additional plastic strains can accumulate in the material past t_r and the recovery behaviour is therefore predominantly viscoelastic in nature.

The residual strains (indicated by $\varepsilon_{vp}(t_r)$ in the figure below) can then simply be subtracted from experimental creep strain values at t_r to estimate the viscoelastic component at this particular time point as illustrated in Figure 4.8. The benefit of choosing the time at the end of creep to compare compliance values is that the viscoelastic and viscoplastic components can easily be separated without the need to know precisely how the viscoplastic strain develops with time.
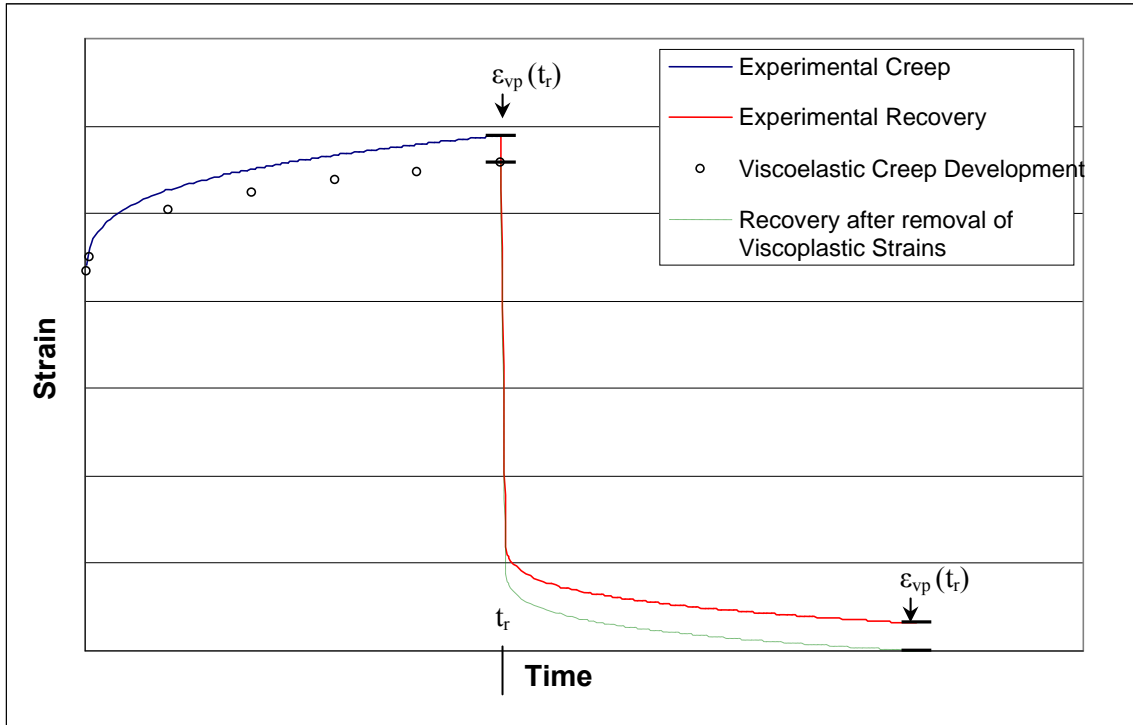
Figure 4.8: Schematic of creep data treatment to determine linear region.

Figures 4.9 and 4.10 show the average viscoelastic compliance values after 30 minutes and 1 day of creep at various stress levels after removing the viscoplastic component. As mentioned in section 4.1, due to large variability at 10 MPa and below, only the data above 10 MPa from the short-term creep data can be considered reliable for the analysis. It is evident that the variations in the mean compliance in Figure 4.9 up to 30 MPa do not exhibit any discernable trend, but it appears that there is a more consistent increase in compliance above this stress level which indicates nonlinear behaviour. However, with the large variance of measured values for each stress level, statistical analysis was needed to determine the significance of the observed behaviour.
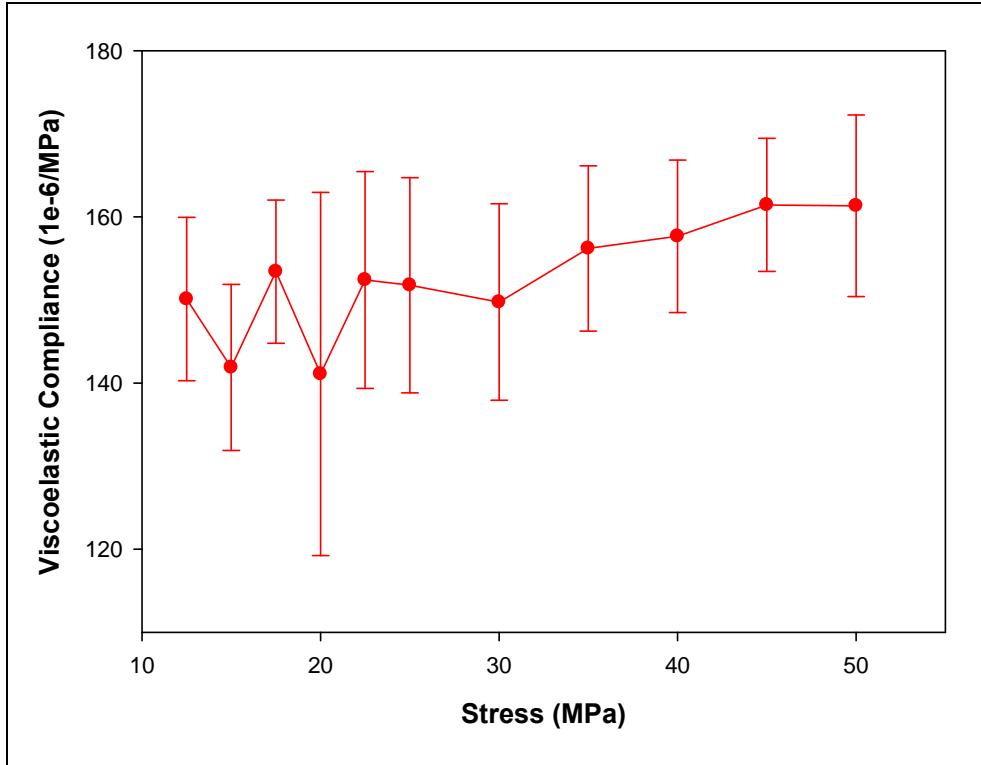
Figure 4.9: Average compliance values after 30 minutes creep.
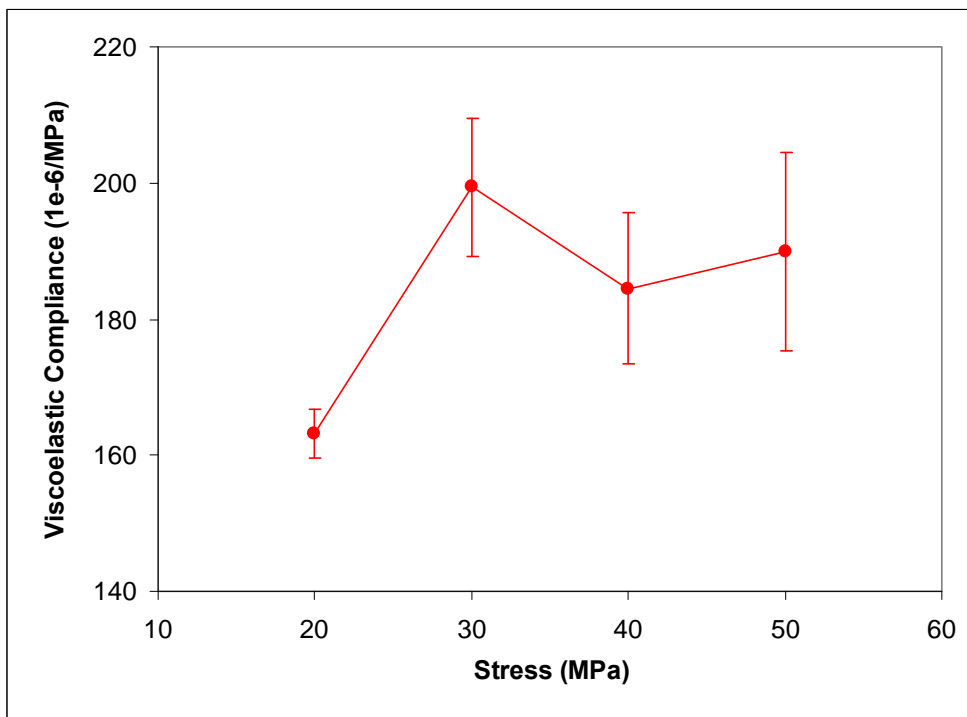
Figure 4.10: Average compliance values after 1 day creep.

Analysis of Variance (ANOVA) and the Tukey test for significance produced a *p*-value of 0.033, where *p*-values less than 0.05 indicate statistically significant differences in treatment means. The results from statistical analysis on short-term test data indicated that there is nonlinearity above 45 MPa. To gain a better idea of the level of nonlinearity in the material, ANOVA was also conducted on the long-term test data. An examination of the confidence intervals and individual treatment group tests showed that the nonlinearity was only marginal. This suggests that the creep compliance values over the stress range of interest (between 20 and 50 MPa) are practically the same after taking into account the randomness of the material. Since the creep compliance values can be considered the same over the stress range studied, the condition of stress independent creep compliance required for linear viscoelastic behaviour can be considered to have been met. The ANOVA results can be found in Appendix C.

The applicability of Boltzmann Superposition Principle is, however, slightly more difficult to assess. Referring to equation (23), the total creep strains ($\varepsilon(t)$) measured from the experiments is a sum of the viscoelastic ($\varepsilon_{ve}(t)$) and the viscoplastic strains ($\varepsilon_{vp}(t)$). It has to be noted that only the total strain and the plastic strain at the end of recovery can be determined experimentally by isochronous creep-recovery experiments. This implies that the viscoelastic and viscoplastic strains as functions of time given in equation (23) are not experimentally separable since they accumulate simultaneously upon loading. Without being able to separate the two strains from the creep data collected, it is not possible to fit a model to the viscoelastic portion and apply the principle to compare the predicted and experimental recovery values. However, several approaches to overcome this problem are available in the open literature.

It is possible to experimentally determine the development of viscoplastic strains (as a function of stress and time) by conducting an additional series of laborious creep-recovery experiments on single specimens at each stress level for multiple durations of creep and recovery [37]. Instead of conducting another full set of experiments, a simplified version of the data reduction method developed in [8] for a non-linear

viscoelastic-viscoplastic consititutive model has been used. The method intrinsically applies the superposition principle by using the recovery data to estimate the viscoelastic strain development and is described in more detail in the following sections. By using this approach, the Boltzmann Superposition Principle is assumed to be applicable to the material, and hence both conditions for linear viscoelastic behaviour have been met over the stress range studied.

4.4 Short-term Viscoelastic-Viscoplastic Model Development

The experimental data presented in section 4.2 indicates that a simple viscoelastic model is insufficient to model the chopped fibre GMT composite due to the presence of viscoplastic strains. In order to predict the behaviour of the material under repeated loading at varying magnitudes, it is necessary to account for the plastic deformation developed in the material due to each load step. Without a viscoplastic component in the model to account for damage accumulation, it would be difficult to reasonably predict behaviour in such realistic applications. Therefore, a viscoelastic-viscoplastic constitutive model would be a more accurate representation of creep in these materials.

4.4.1   Data Reduction Method

The first step in developing a linear viscoelastic-viscoplastic constitutive model for the material is to decide the form of the viscoelastic transient creep compliance function. From the literature review conducted, it appears that even though a Power law form of the function is simple and may provide adequate predictions [6-11], a Prony series expansion would provide advantages in terms of possible implementation of the model into finite element [5, 13, 14] as well as more accurate long-term predictions [15]. For these reasons, the viscoelastic transient creep compliance function was chosen to be a Prony series and given the form shown in equation (10). This results in a model for the viscoelastic behaviour of the material given by equation (11).

Since the model is created using the long-term creep-recovery curves, a 5-term Prony series is required in order to span the time domain of the available data, resulting in a linear viscoelastic constitutive equation that has 14 constants. The steps required to obtain these constants is given in this section. To help visualize the data reduction method, a labelled schematic diagram is shown in Figure 4.11.
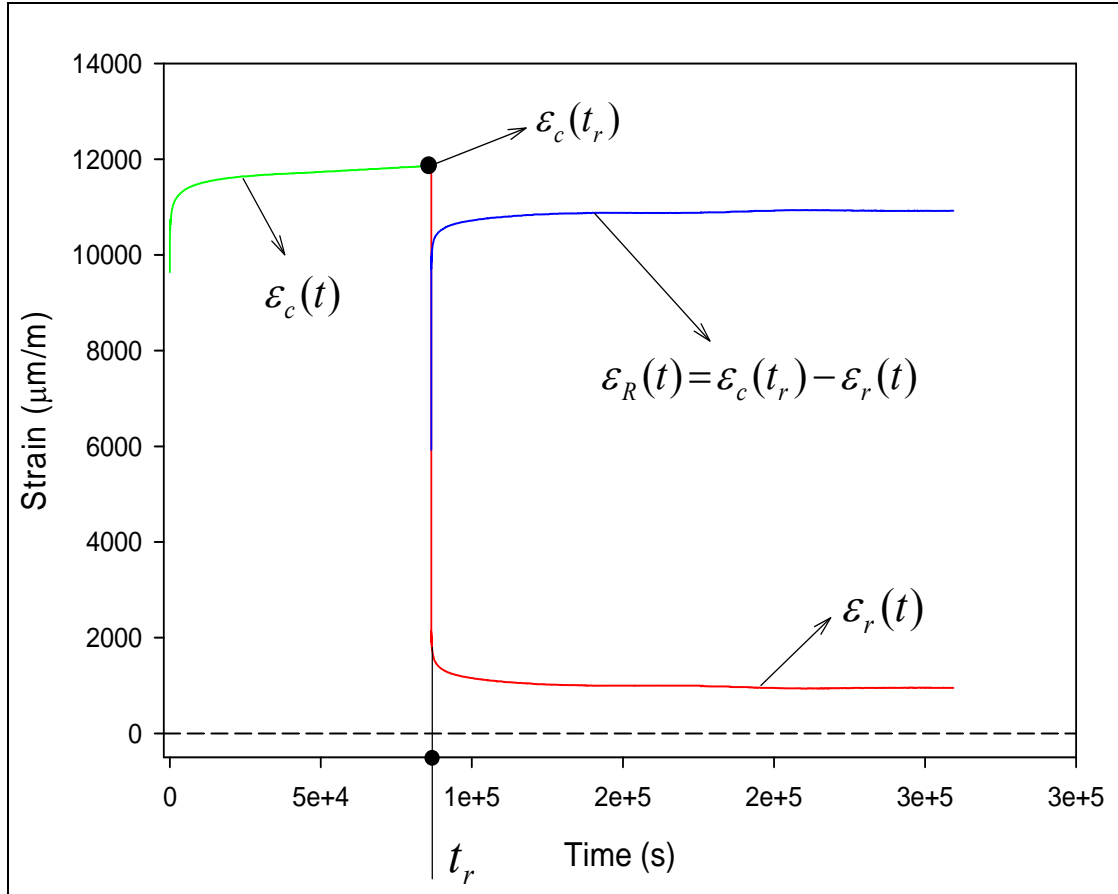
Figure 4.11: Various strain components used in data reduction method. [72]

Beginning from equation (23), during creep the linear viscoelastic-viscoplastic model reduces to:

$$\varepsilon_c(t) = D_0\sigma + \Delta D(t)\sigma + \varepsilon_{vp}(\sigma, t) \tag{41}$$

61

where $\varepsilon_{vp}(\sigma,t)$ represents the viscoplastic strain development which is assumed to be both stress and temperature dependent. During recovery Boltzmann Superposition Principle is applied and the model reduces to:

$$\varepsilon_r(t)=\left[\Delta D(t)-\Delta D(t-t_r)\right]\sigma+\varepsilon_{vp}(\sigma,t_r) \tag{42}$$

where t_r is the time at start of recovery (or end of creep).

Substituting a 5-term Prony series expression into equations (41) and (42), the total creep strains can be written as:

$$\varepsilon_c(t)=D_0\sigma+\sum_{i=1}^{5}D_i\sigma\left(1-e^{-t/\tau_i}\right)+\varepsilon_{vp}(\sigma,t) \tag{43}$$

and the recovery strains are given by:

$$\varepsilon_r(t)=\left(\sum_{i-1}^{5}D_i\sigma\left(1-e^{-t/\tau_i}\right)\right)-\left(\sum_{i=1}^{5}D_i\sigma\left(1-e^{-(t-t_r)/\tau_i}\right)\right)+\varepsilon_{vp}(\sigma,t_r) \tag{44}$$

$$\text{or}\quad \varepsilon_r(t)=\sum_{i-1}^{5}D_i\sigma(e^{-t/\tau_i})\left(e^{(t_r)/\tau_i}-1\right)+\varepsilon_{vp}(\sigma,t_r) \tag{45}$$

Using the strain $\varepsilon_R(t)$ as defined by equation (21), equation (45) can be subtracted from equation (43) evaluated at the end of creep (t_r) to give:

$$\varepsilon_R(t)=D_0\sigma+\sum_{i=1}^{5}D_i\sigma\left(e^{t_r/\tau_i}-1\right)\left(e^{-t_r/\tau_i}-e^{-t/\tau_i}\right) \tag{46}$$

The expression for $\varepsilon_R(t)$ obtained in equation (46) does not contain any viscoplastic terms and can be calculated from the raw experimental data. By fitting the calculated ε_R data to equation (46), R-square values above 0.96 were obtained and D_0 and all the coefficients of the Prony series were estimated. Since the recovery behaviour is reflective of the

viscoelastic behaviour of the material, these constants found from the curve fitting of $\varepsilon_R(t)$ provide a reasonable estimate of parameters in the viscoelastic creep model [8]. Using these parameters and equation (11), an estimate of the viscoelastic creep strains is obtained and the resulting predictions are then subtracted from the experimental total creep strains ($\varepsilon_c(t)$) to isolate the viscoplastic strain development. Due to its simplicity, common use, and reasonable predictive ability [7, 11, 20], the Zapas-Crissman model in equation (28) is used to represent the viscoplastic strain development. This results in a linear viscoelastic-viscoplastic model of the form:

$$\varepsilon_c(t) = D_0\sigma + \sum_{i=1}^{5} D_i\sigma\left(1 - e^{-t/\tau_i}\right) + A(\sigma^m t)^n \tag{47}$$

4.4.2 Viscoelastic Parameter Estimation

It was determined that the material can be practically considered linear viscoelastic, and thus can be modeled using equation (11). Linear viscoelastic behaviour would indicate that D_o and D_i values should be the same at all stress levels; however, there is considerable scatter in the experimental results. In order to estimate these parameters, the average creep curves at the various stress levels were fitted with equation (46). These individual parameters were then averaged to estimate the parameters used in the linear viscoelastic model. To account for the material variability, an associated scatter band was applied to indicate the range in which the material is likely to behave. It was noted in section 4.2 that the variability in the long-term test results was ±7.6% about the mean value for each stress level. A consequence of using a simple linear viscoelastic model and having to take an average of the model parameters from all four stress levels is that the scatter band needs to be increased; not only does it need to encompass the variability in average parameter values at each stress level (~ ±10%), but also the scatter of data used to calculated these averages (±7.6%). As a result, the associated scatter band was determined to be ±17% for the model. This seems reasonable since the scatter in material properties in random GMT composites has sometimes been found to differ as much as

63

300% over a small area [62]. Table 4.1 shows the individual parameter values at each stress level, as well as the average.

Table 4.1: Linear viscoelastic parameters.

Compliance, D_i (1e-6/MPa), and Time Constants, τ_i (s)					
Parameters	**20 MPa**	**30MPa**	**40MPa**	**50MPa**	**Average**
D_0	128.1	150.1	123.7	146.1	137.0
D_1	10.9	11.4	23.5	13.8	14.9
τ_1	10	10	10	10	10
D_2	4.6	8.2	3.3	6.9	5.7
τ_2	100	100	100	100	100
D_3	8.2	12.2	10.9	10.5	10.5
τ_3	1000	1000	1000	1000	1000
D_4	6.5	10.9	6.3	8.1	8.0
τ_4	10000	10000	10000	10000	10000
D_5	15.2	18.3	14.8	13.3	15.4
τ_5	100000	100000	100000	100000	100000

4.4.3   Viscoplastic Parameter Estimation

After isolating the viscoplastic strain from the total creep strain, the data was fitted to equation (28) to determine the viscoplastic parameters. Initially, all parameters in the viscoplastic model were allowed to vary, but from the results parameters *m* and *n* were fairly constant for all stresses and were therefore assumed to be stress independent. The average values of these constants were calculated to be *m* = 4.34 and *n* = 0.087. After making these values stress independent, equation (28) was once again fit to the viscoplastic strain data using the least squares method to find the values of *A* at each stress level. The stress dependent values of *A* were estimated as shown in Figure 4.12.
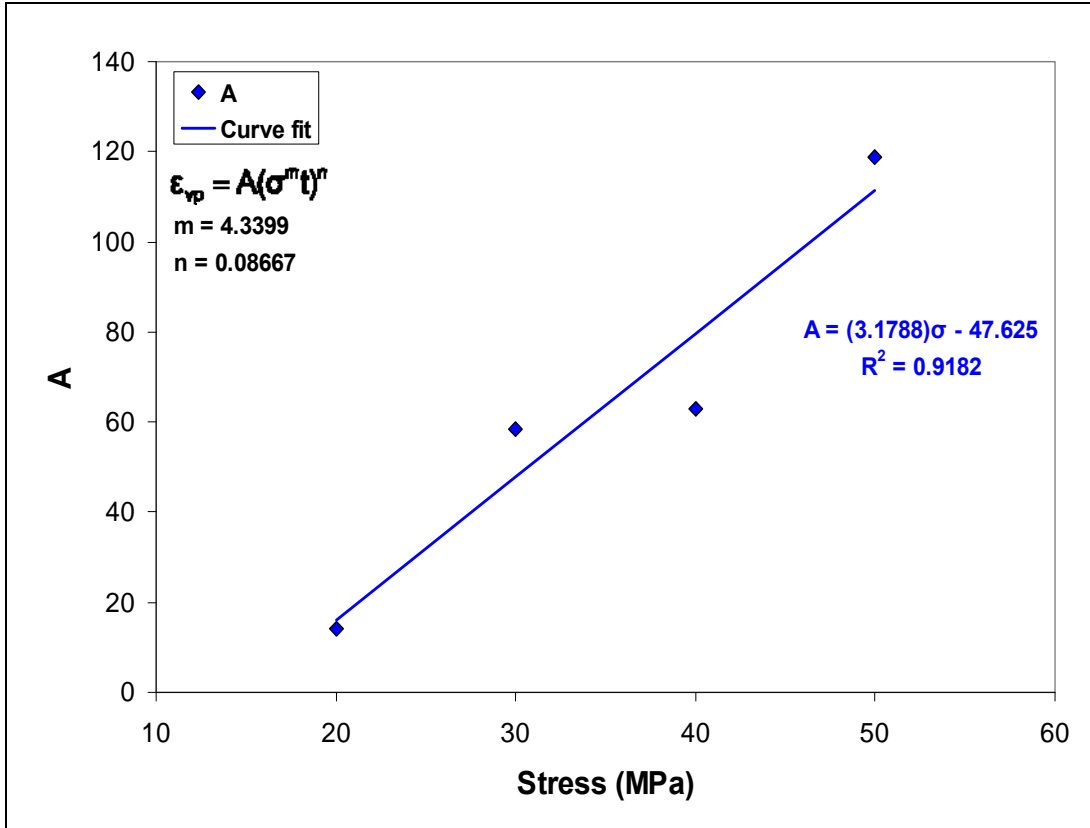
Figure 4.12: Estimated viscoplastic parameters.

The parameter A was found to have a stress dependence over the stress range of 20 to 50 MPa given by:

$$A(\sigma) = 3.18\sigma - 47.63 \qquad\qquad (48)$$

4.4.4 Short-term Model Predictions (without temperature effects)

The predictions based on individual stress level parameters (before averaging) from Table 4.1 can be seen in Figure 4.13. Figure 4.14 compares the model predictions with the experimental values at 50 MPa. The components of the total strains – the instantaneous, viscoelastic and viscoplastic strains are also plotted which shows that the viscoplastic strains are of similar magnitude as that of the viscoelastic strains.
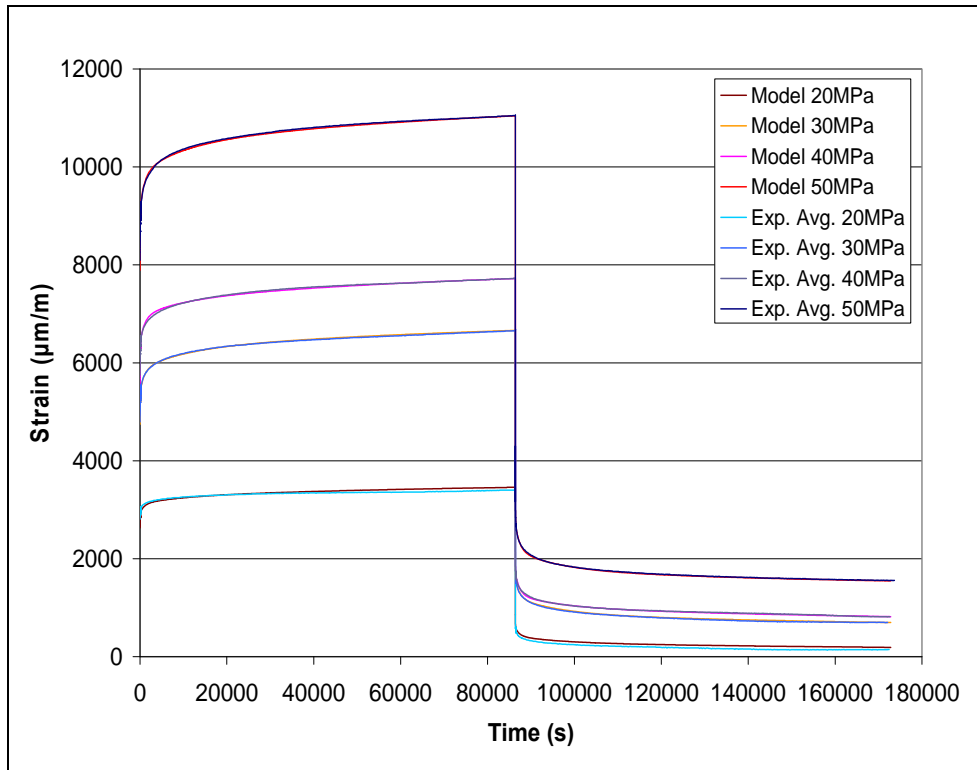
Figure 4.13: Curve fits of average creep data before averaging of parameters.
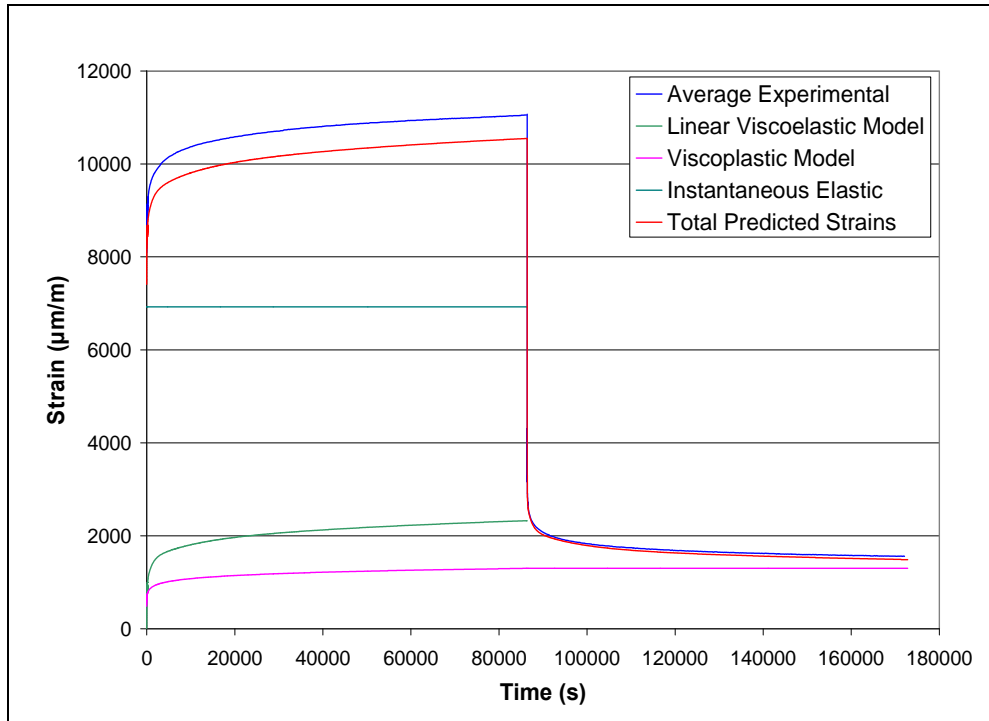
Figure 4.14: Typical model prediction showing both the viscoelastic and viscoplastic strain components at 50 MPa.

66

The final creep and recovery predictions based on the model compared to average experimental curves are shown in Figures 4.15 and 4.16. Figure 4.17 shows a comparison of experimental viscoplastic strains after 1 day creep and estimated strains using the Zapas-Crissman term.
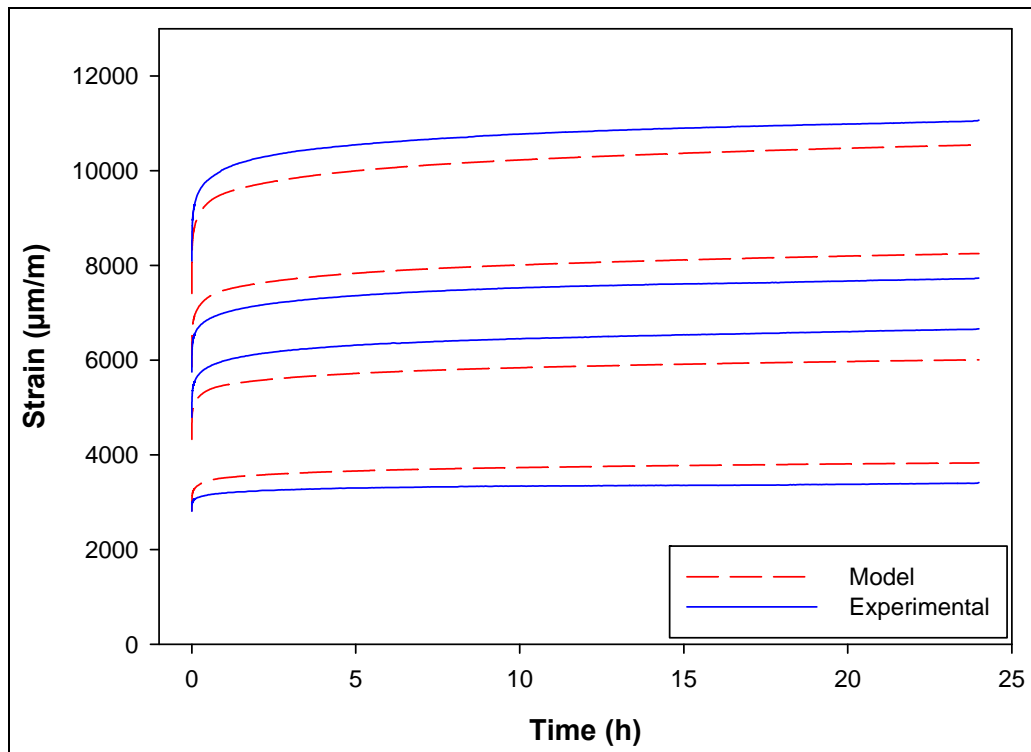
Figure 4.15: Creep predictions based on linear viscoelastic-viscoplastic model.

In Figure 4.10, the creep compliance values for all stress levels studied are shown. Since the material has been modeled as linear viscoelastic, this means that the compliance values at each stress level are theoretically equal, and so the average value was taken of the data collected. In dealing with a random material, the compliance values at each individual stress level were expected to be distributed randomly, both above and below the average value within a certain scatter range. The over predictions in creep strains at some stress levels and under predictions of the strains at others as seen in Figure 4.15 are therefore due to a combination of the randomness of the material and the use of a linear viscoelastic model.
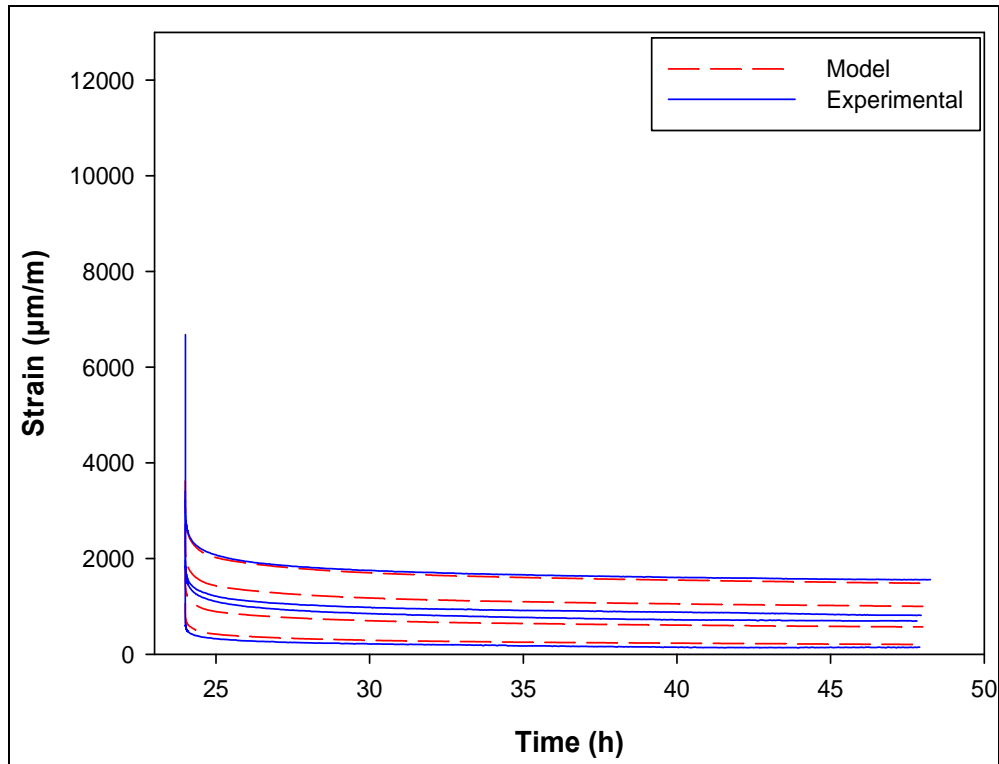
Figure 4.16: Recovery predictions based on linear viscoelastic-viscoplastic model.
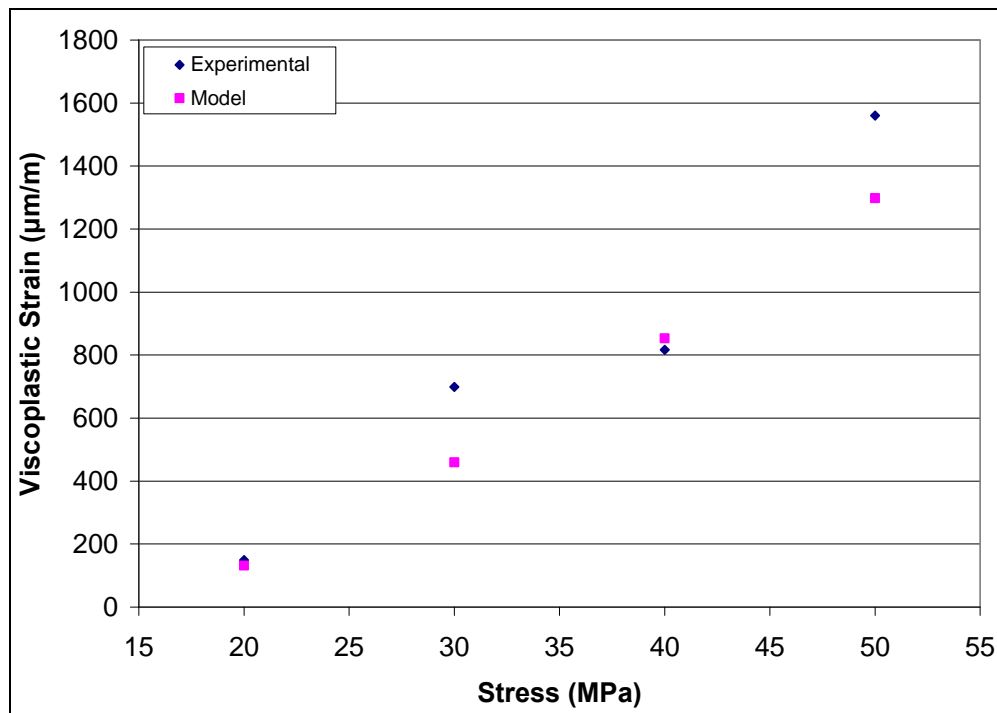
Figure 4.17: Comparison of experimental data and model predictions for viscoplastic strain after 1 day creep.

The predicted compliance after 1 day creep compared to the experimental 1 day creep values can be seen in Figure 4.18. Model predictions agree well with experimental data, considering the scatter found in random GMT materials.
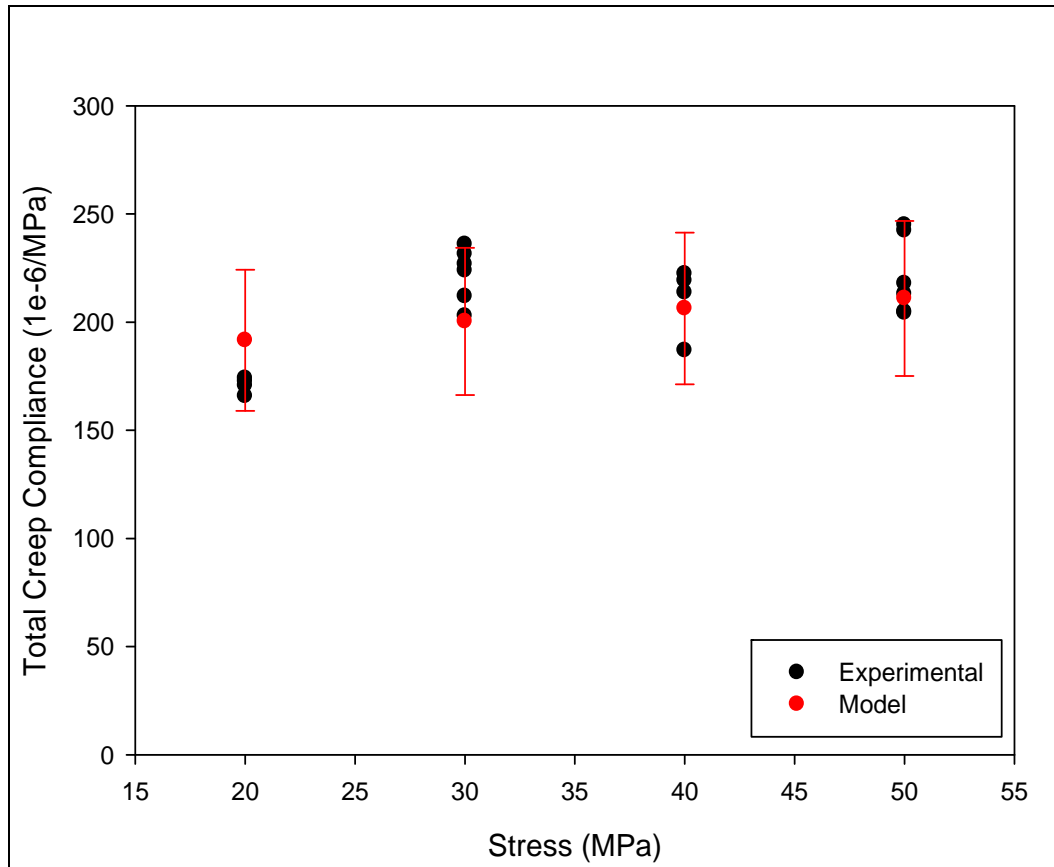
Figure 4.18: Comparison of experimental data and model predictions for creep compliance after 1 day creep.

To test the model, two specimens were loaded at the limit stress level of 50 MPa for 33 days. The raw experimental data is plotted in Figure 4.19 along with the model predictions. Although the second specimen failed shortly after 11 days of creep, the model predictions for the applied stress are very good, that is, they lie within the margins of experimental error for the GMT material.
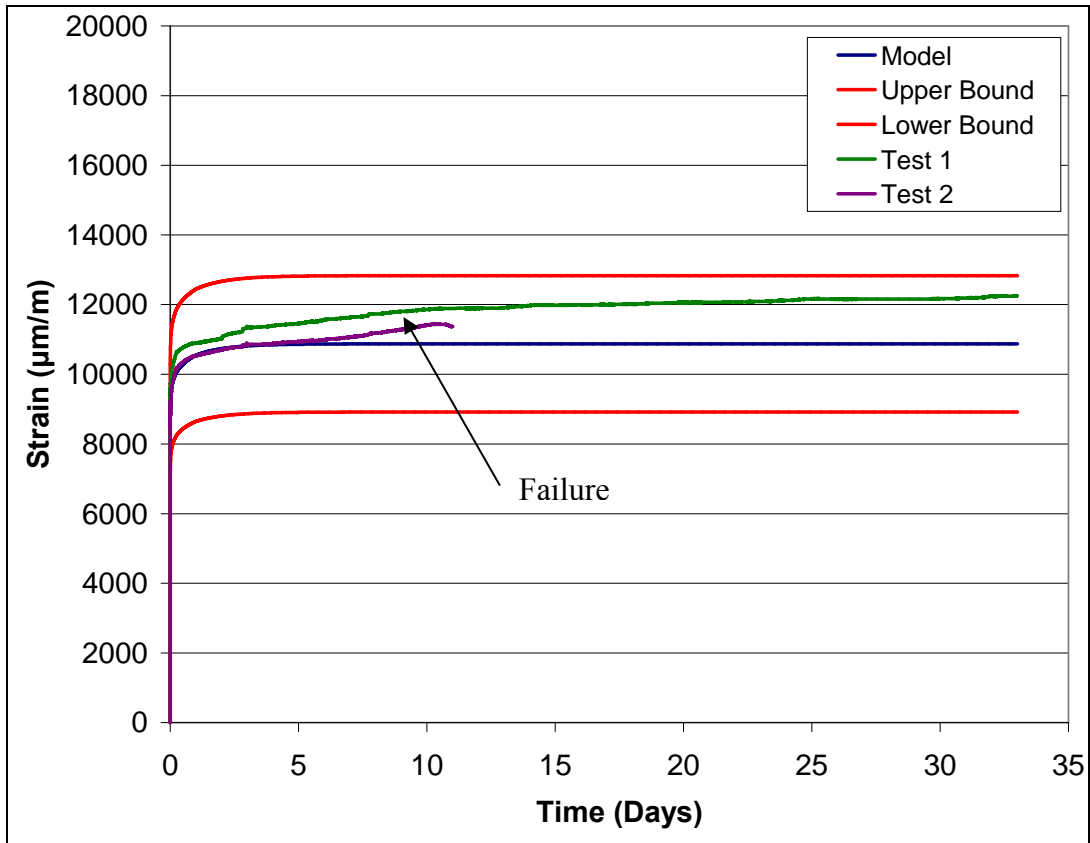
Figure 4.19: Comparison of model and verification test data at 50 MPa.

However, it must be noted that the current model is only valid for a limited time domain that does not extend very far past the time duration of the creep tests conducted. This is clearly shown in Figure 4.19, where the short-term model completely plateaus after approximately 5 days. The reason is that with only 1 day creep data, the maximum number of Prony series terms that could be curve fitted to the data was five. A 5-term Prony series does not contain enough terms to reflect the changes in creep compliance at longer times. In order to obtain a long-term model, much longer experimental creep data is required so that more terms can be introduced into the series.

5.0 RESULTS AND DISCUSSION: TEMPERATURE EFFECTS

5.1 Short-term Creep Tests

The average curves from the four replicates for each combination of stress and temperature were calculated using MATLAB. However, prior to the calculation of average curves, thermal expansion effects were compensated by subtracting the strain due to thermal expansion at elevated temperatures from the data. The strains measured during each incremental temperature increase were assumed to be reasonable estimates because the specimens were allowed to freely expand in the fixture after the modifications outlined in section 3.2.1. The coefficient of thermal expansion of the stainless steel test fixture is also similar to that of the GMT composite in this study, minimizing any effects from the thermal expansion of the fixture itself. During experimentation, one of the specimens at 40 MPa failed at 60°C. Consequently, the viscoelastic compliance analysis at that stress level was only conducted for temperatures up to 55°C. The sets of average creep curves for 20, 30, and 40 MPa are shown in Figures 5.1, 5.2, and 5.3, respectively. Even though the experiments were run continuously over the range of 25 to 90 °C, all curves are shown on the same time scale so that the curves can be more easily compared.
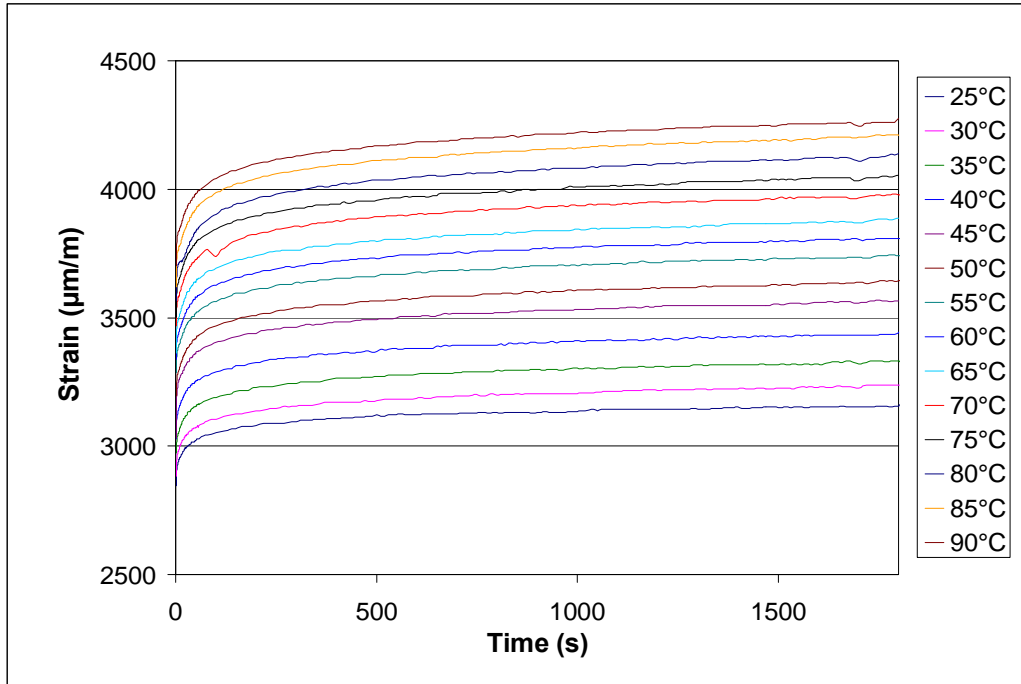
Figure 5.1: Set of average creep curves from temperature tests at 20 MPa.
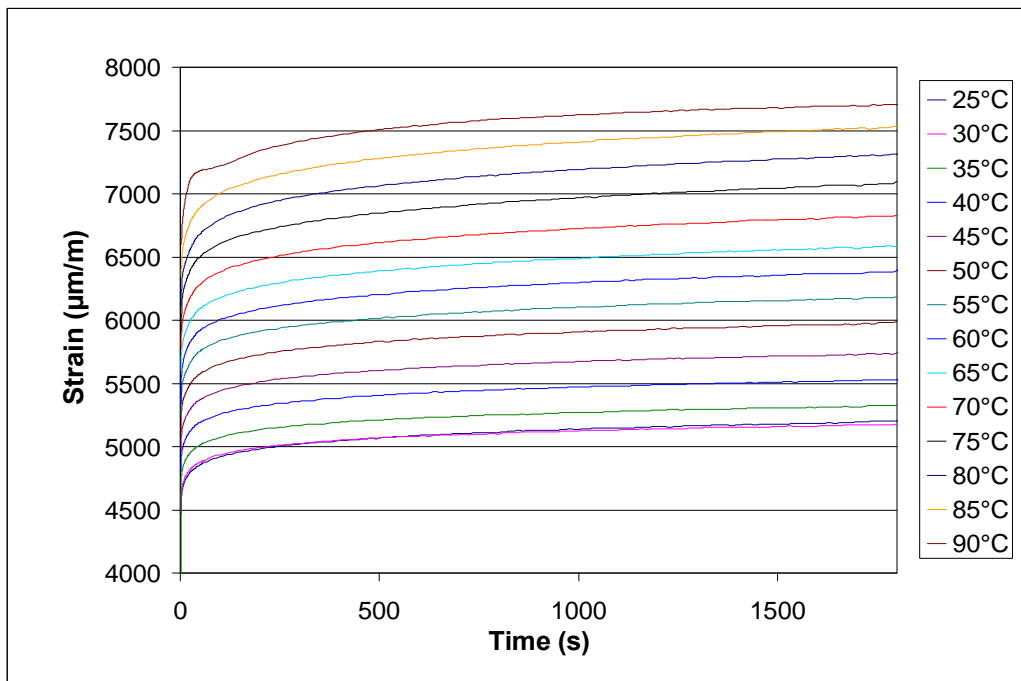
Figure 5.2: Set of average creep curves from temperature tests at 30 MPa.
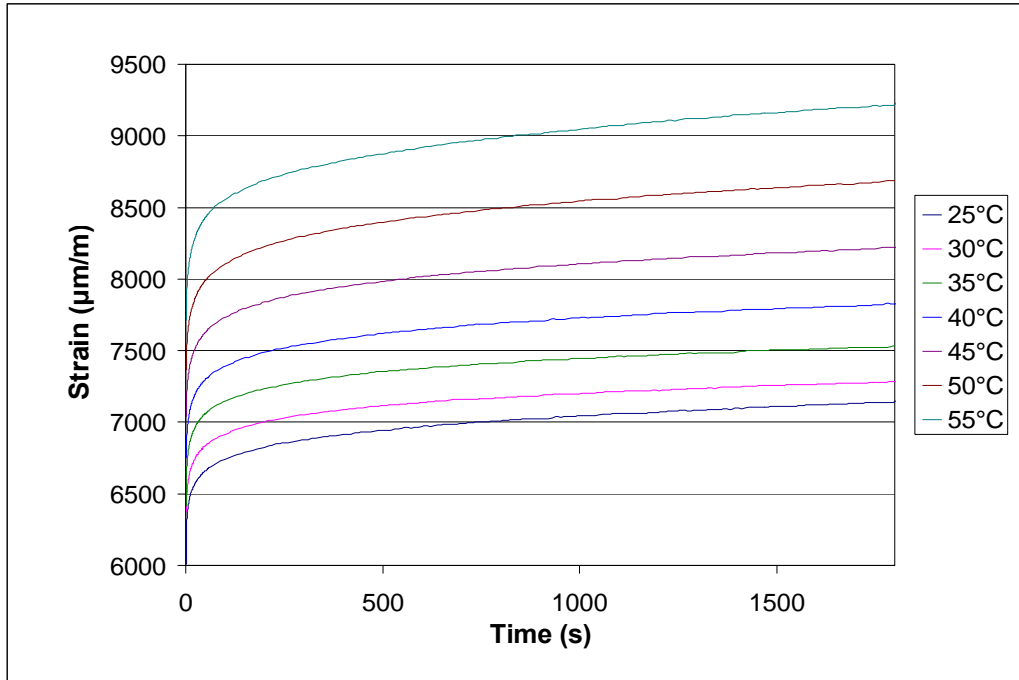
Figure 5.3: Set of average creep curves from temperature tests at 40 MPa.

By comparing the creep strain increases between successive temperature levels for the 20 and 40 MPa data sets, it is clear that temperature does not affect all stresses in the same manner. In Figure 5.1, the increases in creep strain appear to be roughly equal in magnitude with increasing temperature, while Figure 5.3 shows that at 40 MPa the effects of each 5 °C temperature increment accelerate the accumulation of strain in the material. In addition, it is noted that for all stress levels investigated, the magnitude of creep increases with temperature. To further investigate the material behaviour, the average recovery curves for 20, 30, and 40 MPa were calculated and are shown in Figures 5.4 to 5.6.
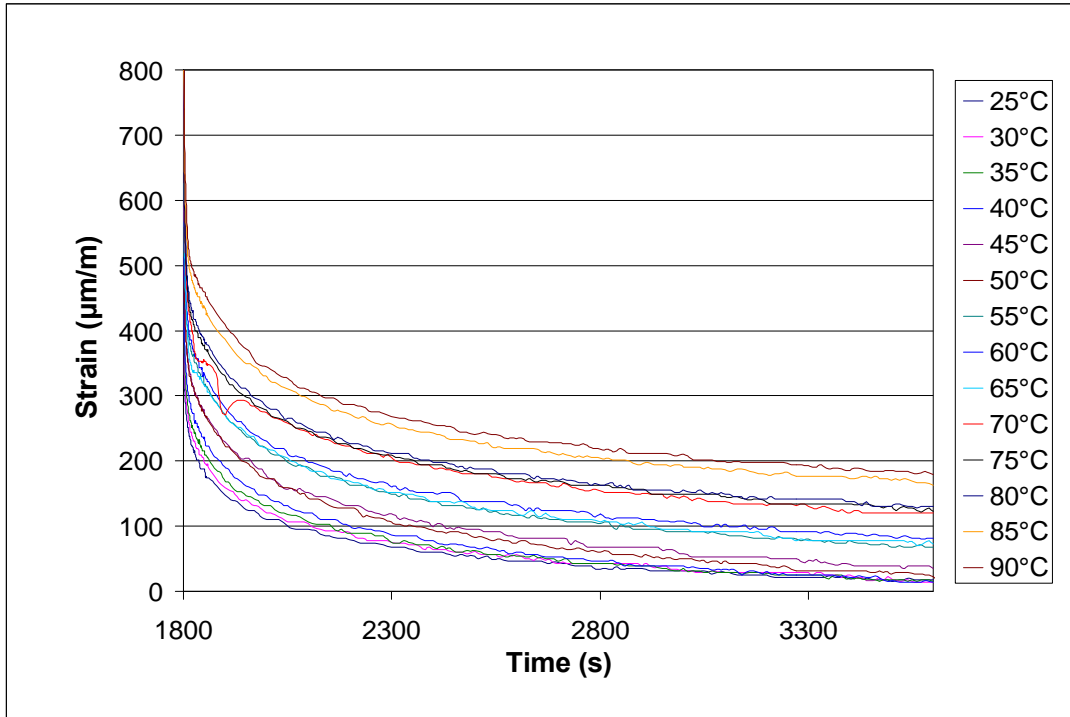
Figure 5.4: Set of average recovery curves from temperature tests at 20 MPa.
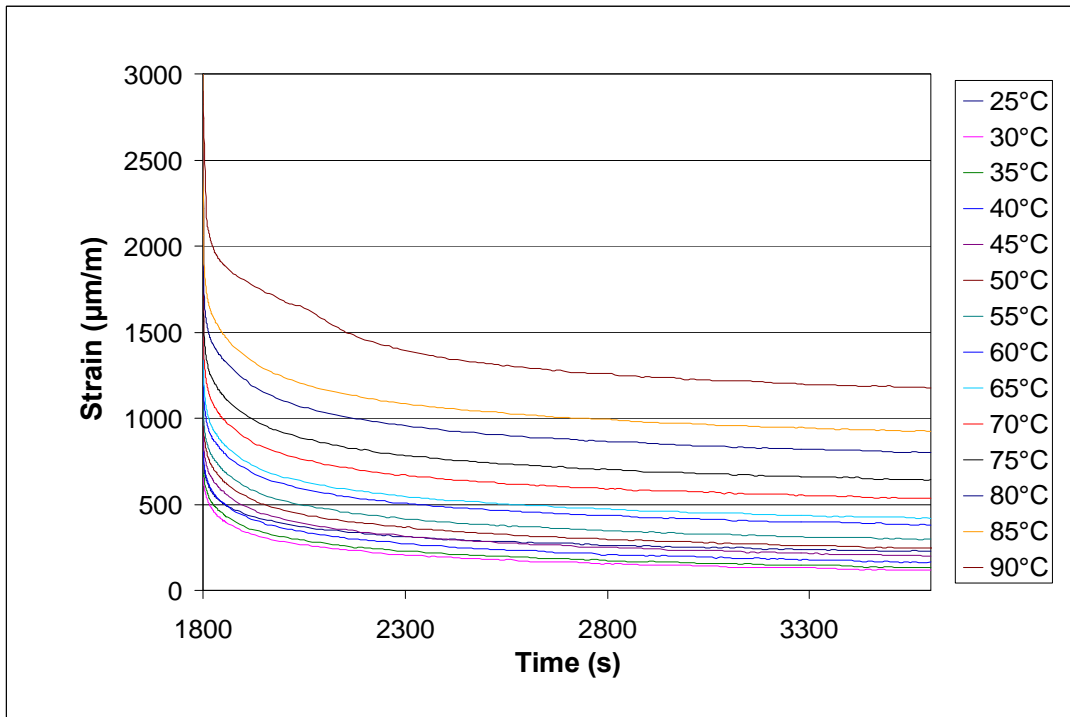
Figure 5.5: Set of average recovery curves from temperature tests at 30 MPa.

74
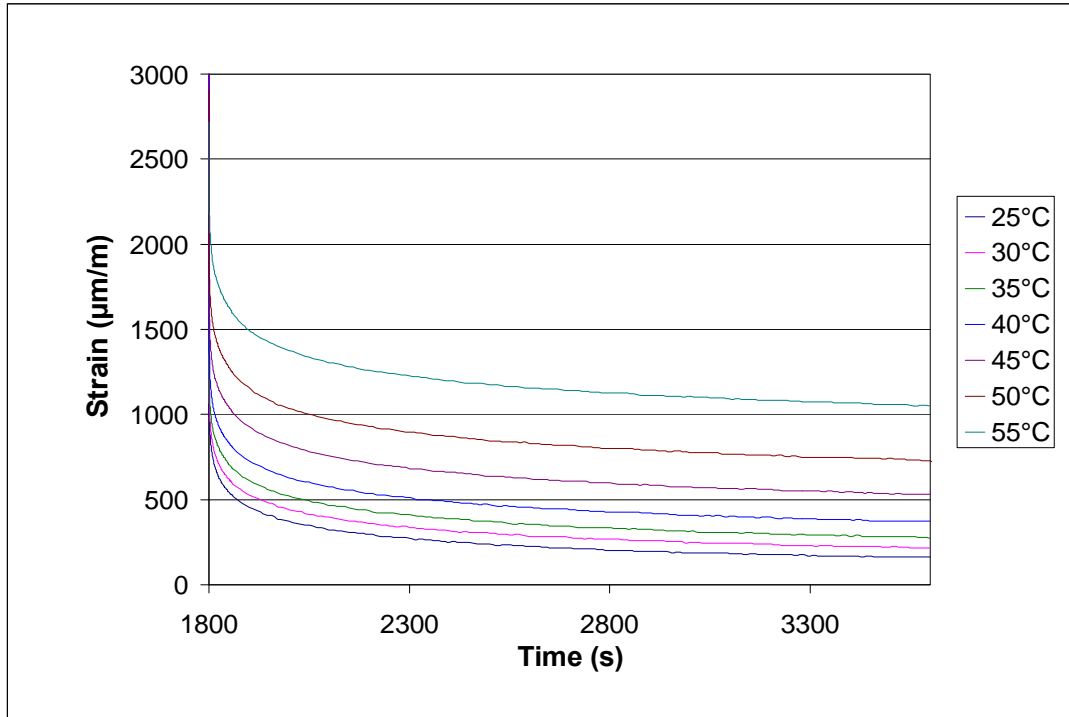
Figure 5.6: Set of average recovery curves from temperature tests at 40 MPa.

From the average recovery curves, it can be noted that even with pre-conditioning at 50 MPa, residual strains still developed, as seen in Figure 5.7. Although the actual numerical values have no physical meaning since the specimens already have induced damage from pre-conditioning, the data does show a clear trend that plastic strains develop as temperature increases. The most important effect of temperature is the exponential increase in plastic strain when the applied stress is increased from 30 MPa to 40 MPa.

To delineate viscoelastic behaviour only, the additional plastic strains are removed from the average curves in Figure 5.8. The average viscoelastic compliances after 30 minutes of creep are displayed as a family of curves. To compare the scatter for each stress level, Figures 5.9 to 5.11 show each curve with error bars. It is evident that compliance values increase with temperature. From the elevated temperature tests, scatter as high as ±21.6% was found, even after the removal of any outliers and anomalous data. Overall, the variation increase with temperature is between 3 and 7%. It is noted that any stress

effects that might appear to be present in Figure 5.8 are not significant when compared to the magnitude of inherent variability in the material, especially at high temperatures.
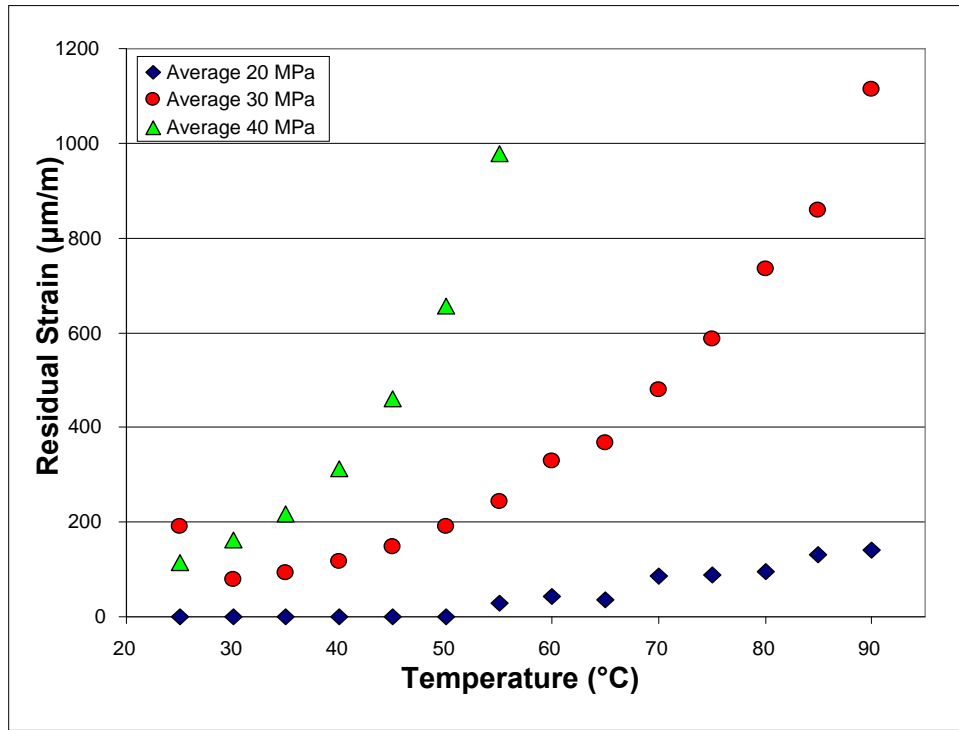
Figure 5.7: Residual strains from average short-term creep tests at various temperatures.
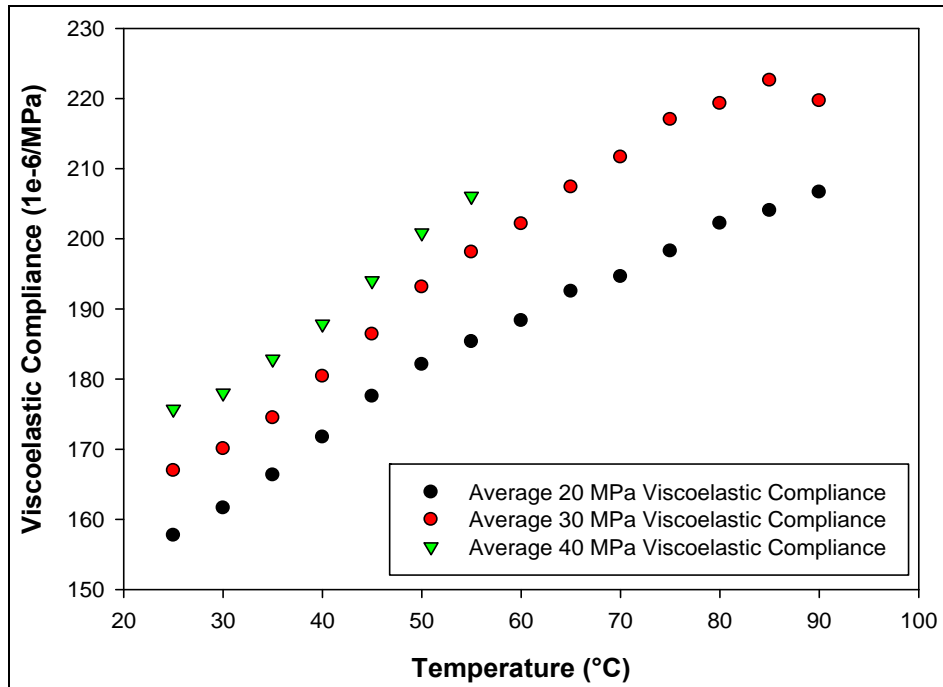
Figure 5.8: Average viscoelastic compliance after 30 minutes creep.
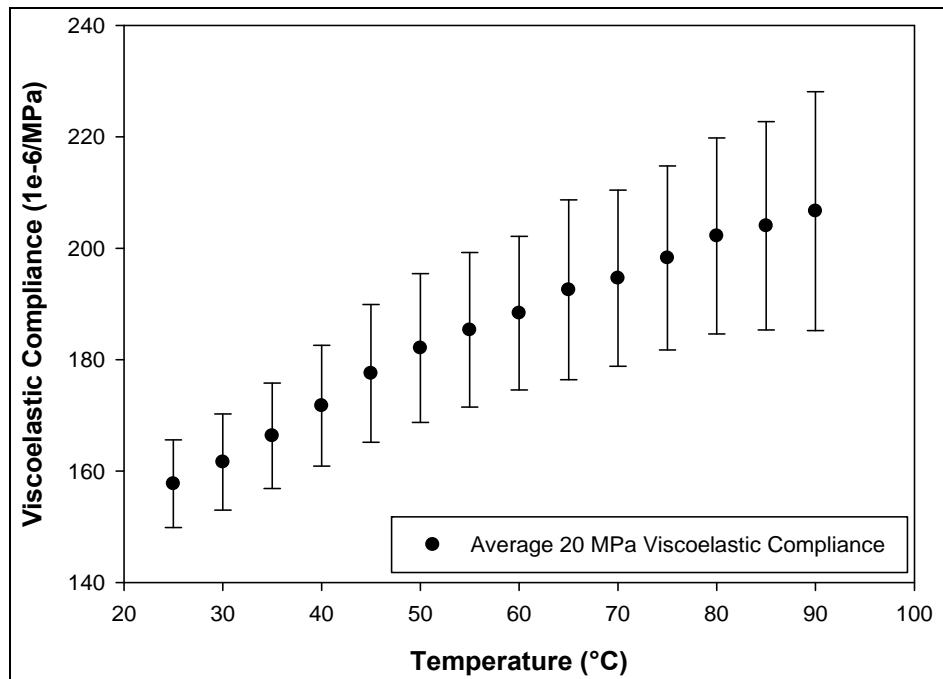
Figure 5.9: Average 20 MPa viscoelastic creep compliance with scatter bars.
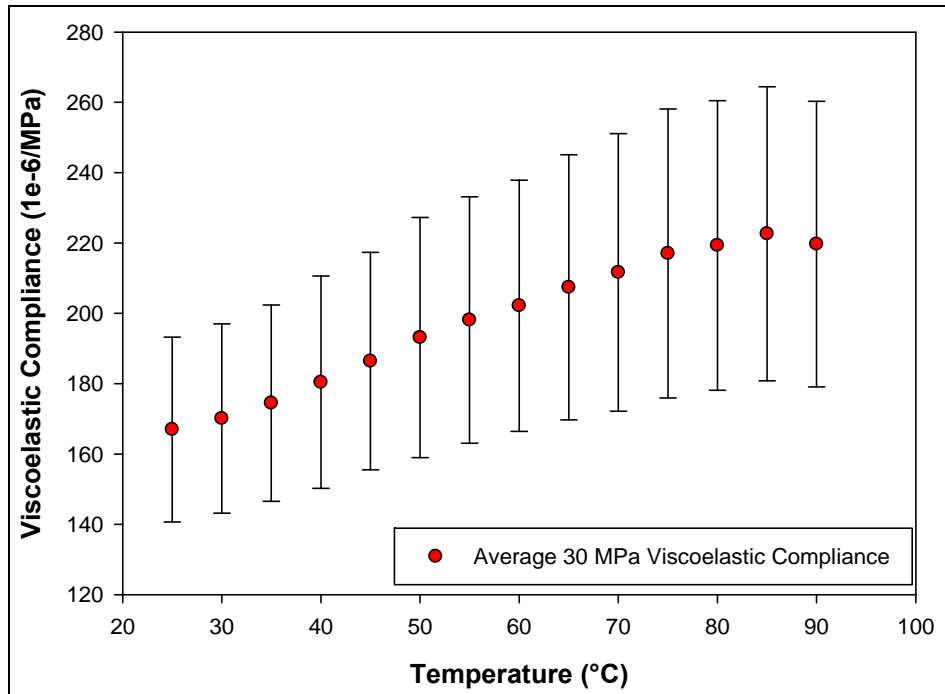
Figure 5.10: Average 30 MPa viscoelastic creep compliance with scatter bars.
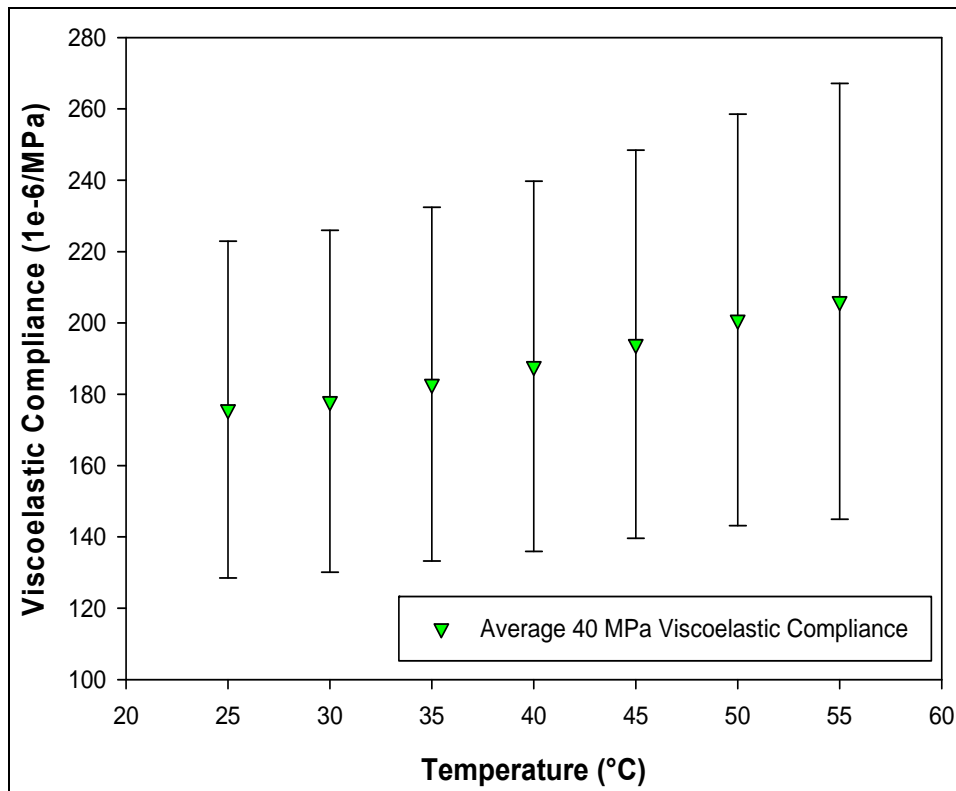
Figure 5.11: Average 40 MPa viscoelastic creep compliance with scatter bars.

To further investigate the effects of temperature, each stress level was analyzed independently. Following the data reduction method described earlier, the viscoelastic creep was modeled using a 3-term Prony series to cover the 30 minutes creep duration of the tests. Two nonlinearity parameters were then introduced into the model as follows:

$$\varepsilon(t) = g_0 D_0 + g_2 \sum_{i=1}^{3} D_i (1 - e^{-t/\tau_i}) \tag{49}$$

These terms resemble the nonlinearity parameters found in the Schapery nonlinear viscoelastic model. The first parameter, g_0, will indicate the relative changes in instantaneous creep compliance, while the second, g_2, will examine the relative changes in transient creep compliance as temperature was increased from 25°C. The D_0 and D_i values at 25°C were used in each case. The creep curves from all successive temperature levels were modeled using equation (49) and the g_0 and g_2 parameters from the least-squares curve fits are plotted in Figures 5.12 and 5.13. It is seen that increasing temperature has the effect of softening the material, as the g_0 values tend to increase for all stress levels indicating that the material is becoming more compliant. While this was to be expected, it is interesting to note the this softening occurs at the same rate for all stress levels until approximately 60°C, at which the behaviour starts to deviate from each other. At the higher stress levels of 30 and 40 MPa, the instantaneous creep compliance actually starts to drop.
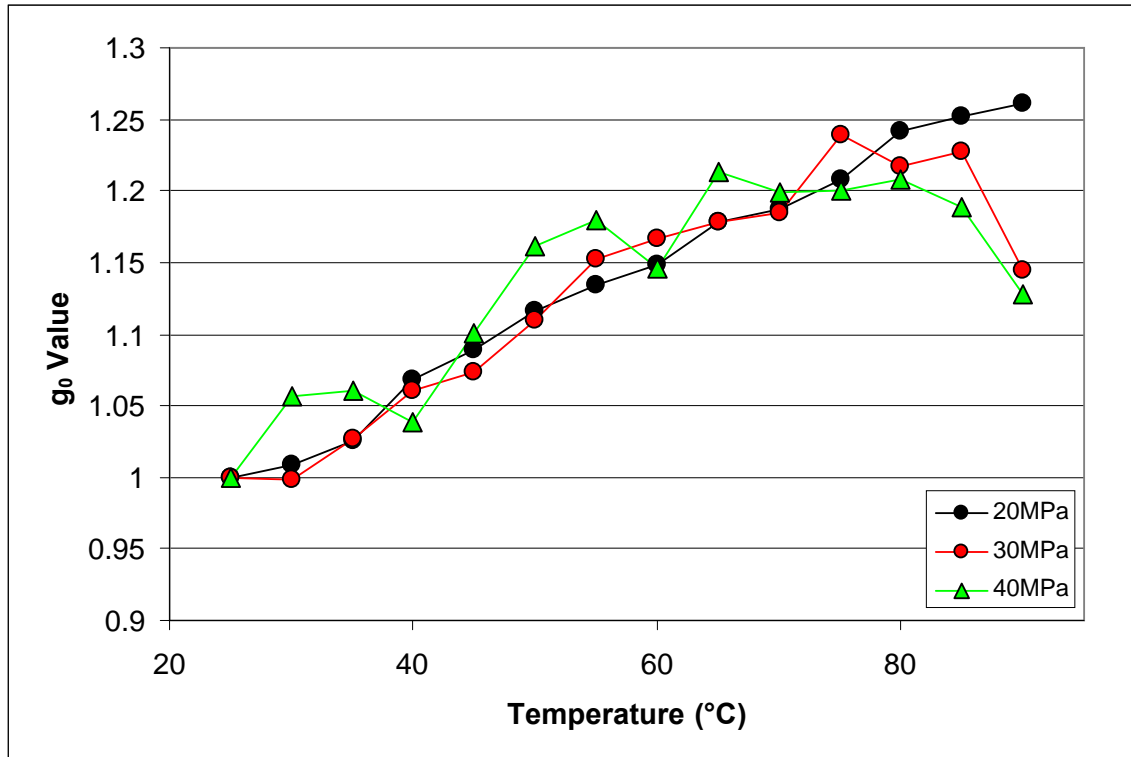
Figure 5.12: The relationship between the g_0 parameter and temperature.

The g_2 values also increase with temperature, indicating that the material creeps more at higher temperatures, which is entirely consistent with observations made earlier. The rate of increase for all stress levels appear similar until approximately 60°C, when the amount of creep increases more rapidly for the 30 and 40 MPa stress levels.
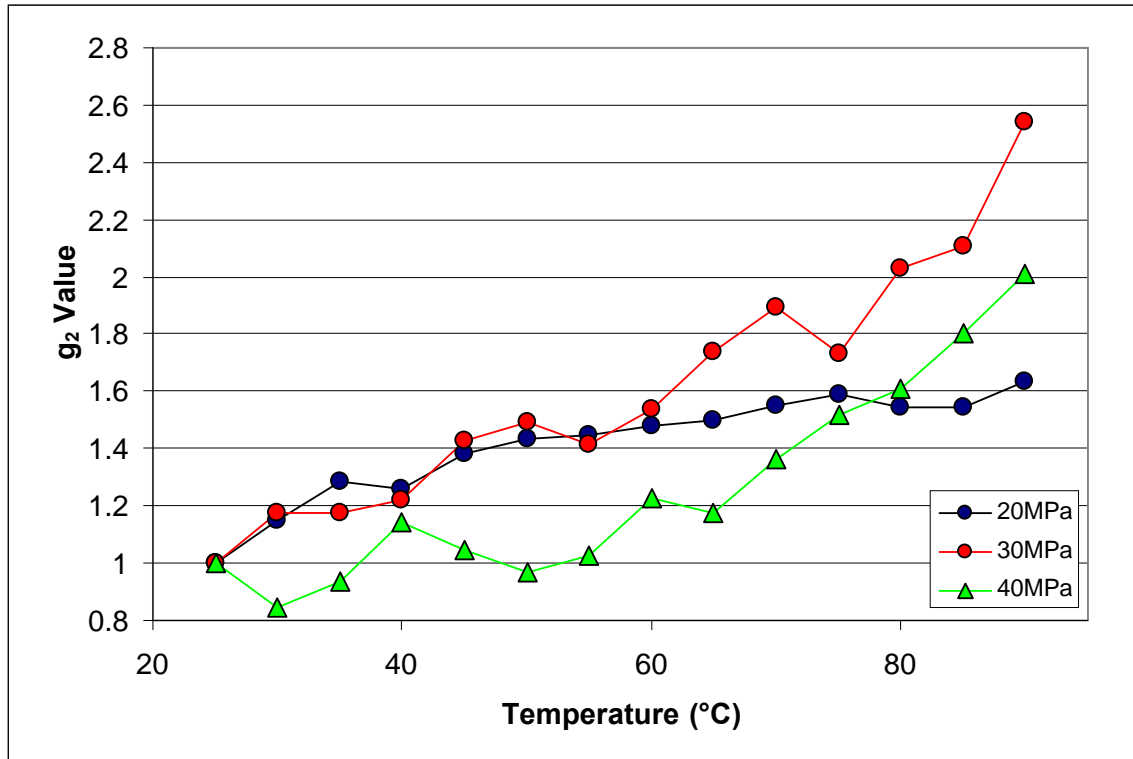
Figure 5.13: The relationship between the g_2 parameter and temperature.

From room temperature test results, the GMT composite can be considered linear viscoelastic at 25 °C. Since g_0 and g_2 behave similarly for all stresses below 60 °C, it suggests that the stress threshold for linear viscoelastic behaviour is maintained and the material is still linear viscoelastic with respect to stress. The deviations between the behaviour of the parameters for the different stress levels above 60 °C indicate possible nonlinear viscoelastic behaviour induced by high temperature.

According to [6], it was found using Dynamic Mechanical Analysis that a secondary glass transition for the polypropylene matrix occurs at 61°C. Interestingly, this transition corresponds with a noticeable change in viscoelastic behaviour, particularly at 30 and 40 MPa stresses. This suggests that creep behaviour of the chopped fibre composite is strongly matrix dominated at temperatures beyond the secondary transition.

5.2   Time-Temperature Superposition

The short-term temperature data was also used to test the applicability of the time-temperature superposition principle for this composite material. To determine the time shift factors and to create the master curve for the material, only the average data set at 20 MPa was used since the response at this stress level is clearly linear viscoelastic. Since TTS only applies to the linear viscoelastic region, the shift factors determined should apply to all other stress levels in the linear range as well.

To create the master curve, the creep data at each temperature level was plotted on a log time scale. The reference temperature of 25°C was used, and beginning with the 30°C creep curve, a time shift of log (a_T) was used to shift the 30°C curve to the right until a portion of the curve superposed and slightly extended the 25°C curve. This extension of the creep curve continued until all the data collected was used, resulting in the master curve found in Figure 5.14.
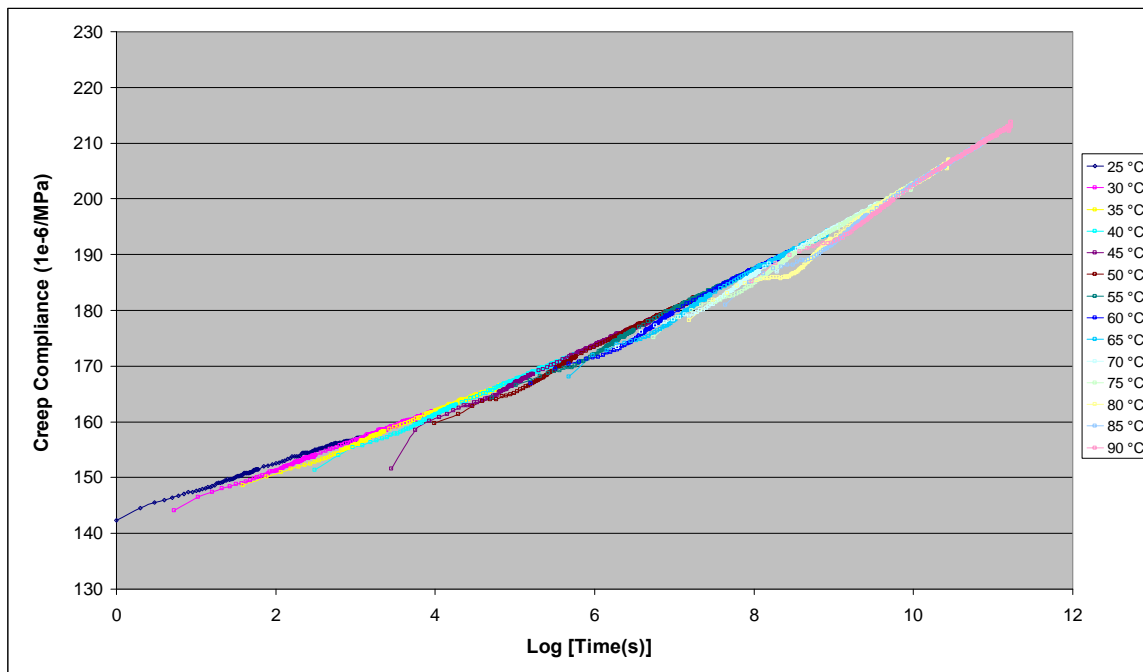
Figure 5.14: Superposed 20 MPa average temperature data.

The common practice is to superimpose only secondary creep data. Accordingly, the initial primary creep portion of the data collected for the entire set was removed. This resulted in a generally smooth curve as shown in Figure 5.15.
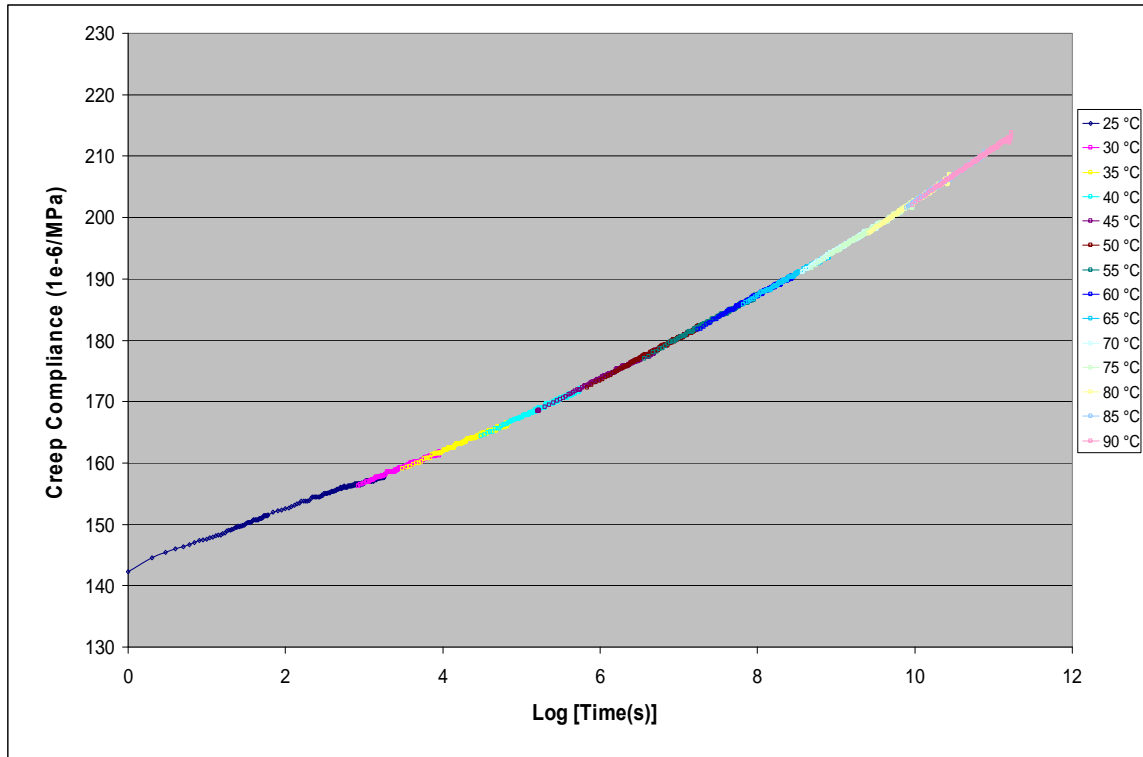
Figure 5.15: Superposed data without primary creep region.

Finally, each segment of the smooth curve from Figure 5.15 was joined together to create the average master curve shown in Figure 5.16.
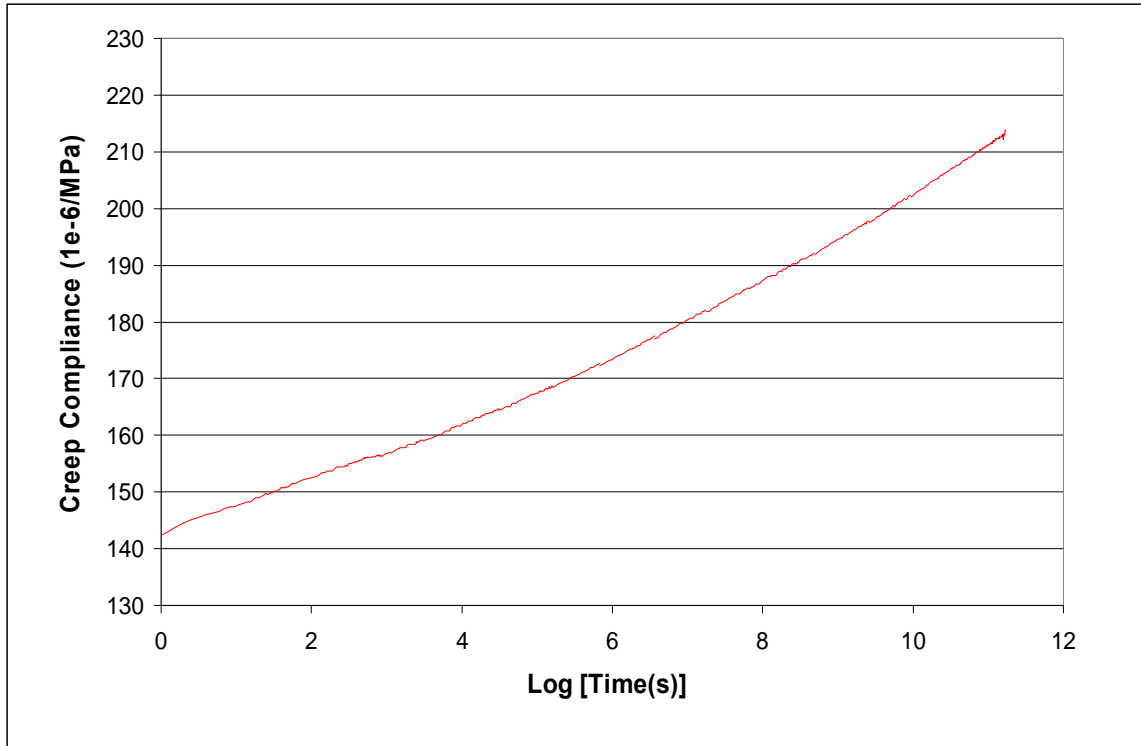
Figure 5.16: Average 20 MPa master curve.

The shift factors used to create the master curve are shown in Table 5.1 and plotted in Figure 5.17.

Table 5.1: Time-Temperature Superposition shift factors.

Relative Temperature (T – 25 °C)	log (a_T)
0°	0.00
5°	0.72
10°	1.59
15°	2.49
20°	3.45
25°	3.99
30°	4.72
35°	5.20
40°	5.68
45°	6.29
50°	6.74
55°	7.19
60°	7.64
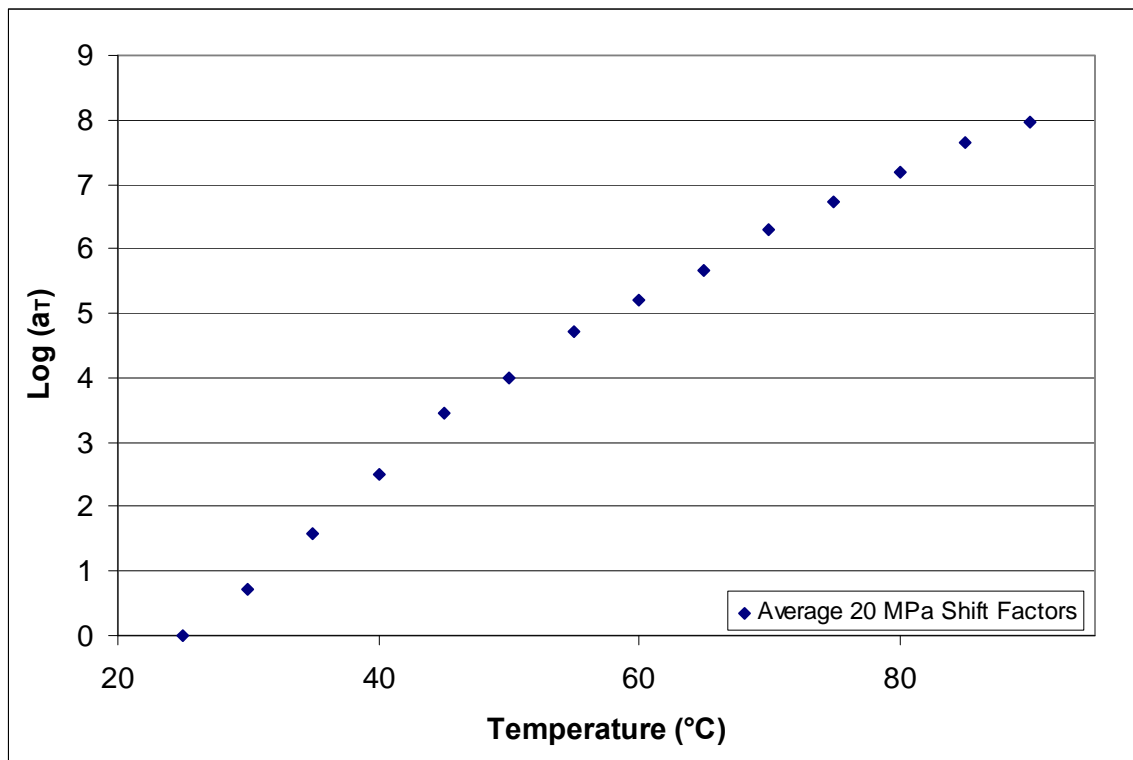
Figure 5.17: Average 20 MPa shift factors.

Conventionally, the $\log(a_T)$ values are taken as negative when the individual creep curves are shifted to the right because a_T values are applied by dividing the time by this factor:

$$t_{equiv.@T_{ref}} = \frac{t_{@T}}{a_T} \quad (50)$$

By taking the logarithm of both sides in equation (50) and applying arithmetic properties of logarithms:

$$\log(t_{equiv.@T_{ref}}) = \log(t_{@T}) - \log(a_T) \quad (51)$$

When creep tests are performed at temperatures above T_{ref}, the data corresponds to the behaviour at T_{ref} further along in time (i.e. the data needs to be shifted to the right in order to superpose onto the creep curve at the reference temperature). From equation (51), it can be seen that in order for this to occur mathematically, $\log(a_T)$ values must be negative when the curves are shifted to the right. Since the $\log(a_T)$ values have been taken as positive in this study, a_T values must be applied as a multiplicative factor instead:

$$t_{equiv.@T_{ref}} = (t_{@T})(a_T) \quad (52)$$

The data from Table 5.1 was curve fitted using a slightly modified equation (36) to account for the sign difference in $\log(a_T)$, resulting in an R-square value above 0.99. Figure 5.18 compares the experimental shift factors and those predicted using the WLF equation. The constants C_1 and C_2 were found to be 22 and 115 respectively.

What is interesting to note in Figure 5.18 is that the $\log(a_T)$ values up to 45 °C increase linearly and slightly deviate from the WLF equation predictions, while the values corresponding to temperatures above 60 °C follow the equation almost exactly with a transitional range between 45 and 60 °C. This clearly indicates a change in the material and is believed to reflect the change from fibre dominated to polymer matrix dominated

behaviour as temperature is increased and more fibre-matrix debonding is occurring in the composite.
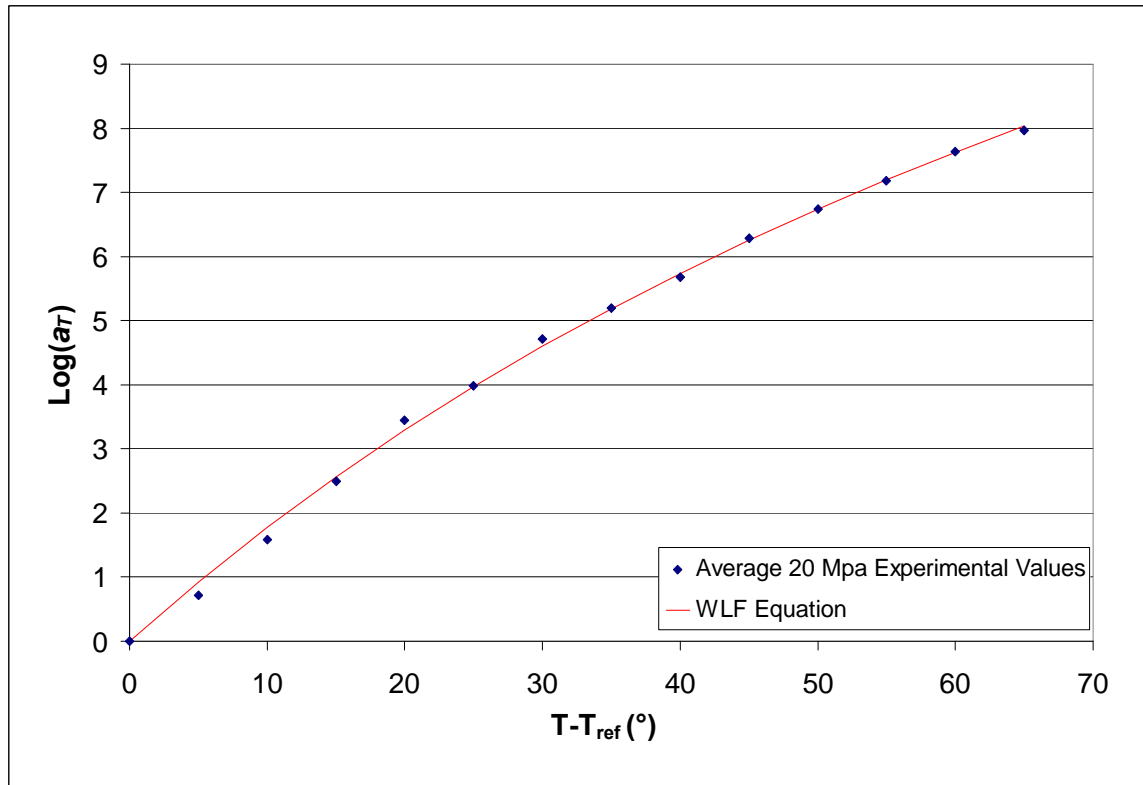
Figure 5.18: Comparison between experimental shift factors and WLF equation predictions.

While it is difficult to find shift factors from creep experiments in open literature to compare the magnitude of values with those of isotactic polypropylene, there is data available similar to the temperature range studied from stress relaxation experiments. In [74] and [75], the shift factors determined from stress relaxation and creep experiments are the same. Therefore, shift factors from other researchers for isotactic polypropylene [53, 76] are compared to the ones obtained for the composite studied in Figure 5.19.
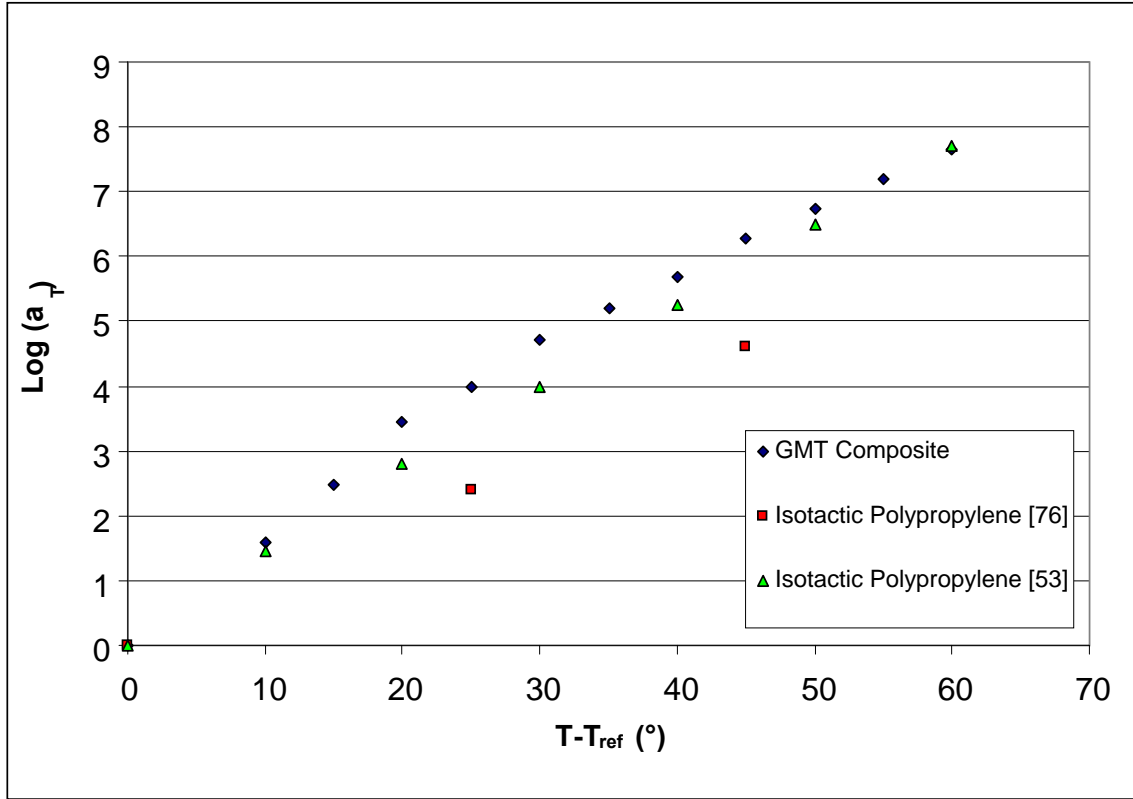
Figure 5.19: Comparison of GMT composite and isotactic polypropylene shift factors.

It can be seen in the figure that the shift factors are comparable to those of isotactic polypropylene. It is difficult to make a direct comparison of values since the specific properties of the polypropylene studied by other researchers differ slightly from those in the GMT composite. However, Figure 5.19 shows that the magnitude of the shift factors obtained are reasonable and have a similar trend. A ratio of the constants, C_1/C_2 from the WLF equation obtained by Tshai *et al* [53] for isotactic polypropylene was 0.11, compared to a ratio of 0.19 obtained from the temperature experiments conducted in this work. Deviations in these values are not surprising as the presence of glass fibre mat reinforcement changes the creep and compliance properties of the material compared to isotactic polypropylene alone.

The procedure for creating master curves was repeated for the individual trials at 20 MPa in order to examine the scatter in the master curves. The resulting curves are compared to the average curve in Figure 5.20.
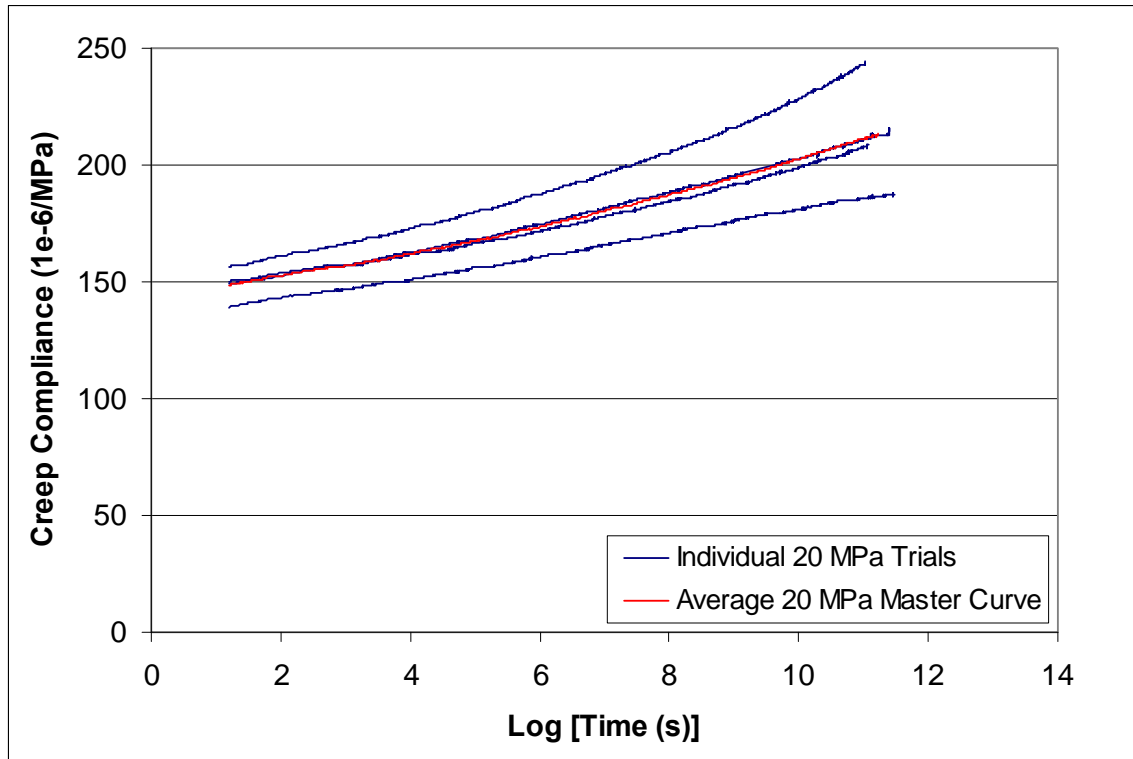
Figure 5.20: Average and experimental 20 MPa master curves.

The average master curves for 30 and 40 MPa data sets are shown in relation to the master curve obtained at 20 MPa in Figure 5.21, and the corresponding shift factors are plotted in Figure 5.22.
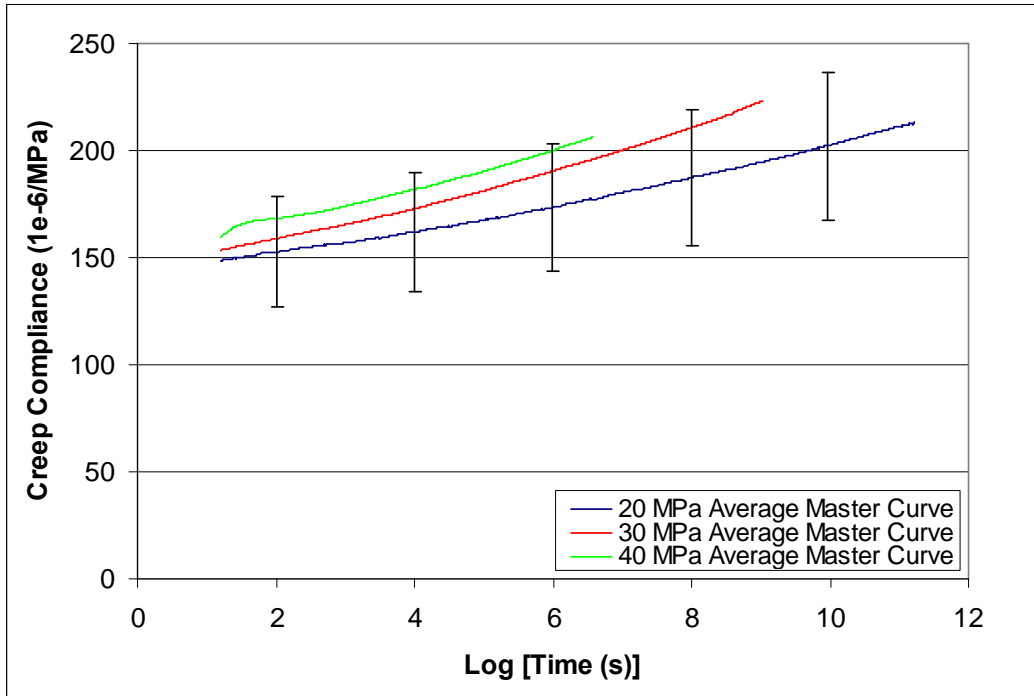
Figure 5.21: Master curves developed from short-term temperature data.
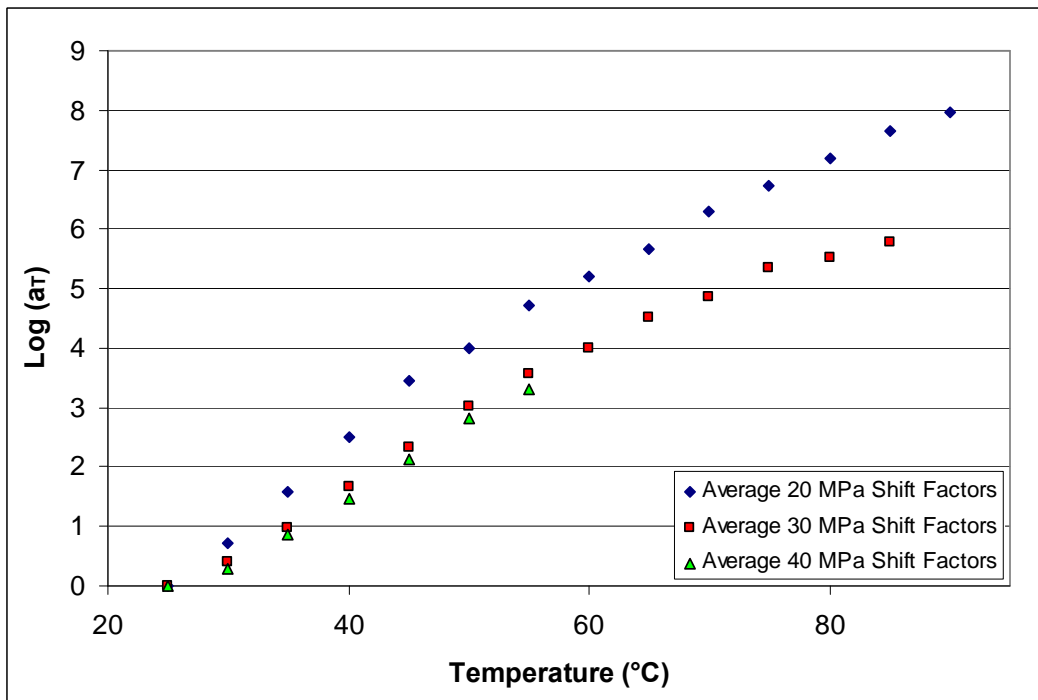
Figure 5.22: Average shift factors at various stress levels.

90

Even though the master curve data set for 40 MPa was about half that for the 20 and 30 MPa tests due to specimen rupture, it can be seen that within the available data range the master curves and shift factors obtained at 30 MPa and 40 MPa are very similar. The fact that they deviate from the 20 MPa data quite significantly may suggest that there is some nonlinearity in the material with respect to stress and temperature, as suggested by the parametric studies on g_0 and g_2 conducted earlier and shown in Figures 5.12 and 5.13. If nonlinearity does indeed exist within the material, then it is very likely that the behaviour was masked by the large material scatter. With the current set of long-term curves, it is not possible to model long-term nonlinear behaviour at high temperatures with any confidence.

If the material is truly linear viscoelastic, then the deviations in the master curves between 20 MPa and the other two stress levels can only be attributed to scatter in the material. A scatter band of ±17% is shown in Figure 5.21. It is noted that the average master curves obtained from 30 and 40 MPa data sets narrowly fit within this scatter band when a linear viscoelastic model is used. To try and apply TTS to all the stress levels and incorporate temperature effects would require an even larger scatter band to include the range of possible material responses seen in the short-term temperature experiments. Even if one could draw such a scatter band, the use of such a master curve as a long-term predictive design tool would be questionable. Clearly, material response of chopped fibre mat composites is far too random to be meaningfully quantified. The problem is further exacerbated at higher temperatures. Simply, the long-term creep behaviour of these materials is not sufficiently repeatable to consider the use of a complex viscoelastic-viscoplastic model with temperature effects. Therefore, it is not practical to pursue development of such a model for this material.

Even though a complex long-term model cannot be developed using the experimental data that can confidently be applied to all stress levels and temperatures studied, it can still be used to demonstrate the applicability of TTS at room temperature in the composite. Assuming the 20 MPa master creep curve is representative of the long-term viscoelastic behaviour at room temperature, an 11-term Prony series can be curve fitted

using least-squares method to cover the entire time domain of the master curve. The time, t, in the model was replaced with $t(a_T)$ to accommodate the shift factors determined from the experimental data, resulting in a long-term constitutive equation as follows:

$$\varepsilon(t) = \sigma[D_0 + \sum_{i=1}^{11} D_i(1 - e^{-t(a_T)/\tau_i})] + A(\sigma^m t)^n \tag{53}$$

The parameter values are shown in Table 5.2.

Table 5.2: Master curve parameters of an 11-term Prony Series.

Parameter	Value	Parameter	Value
D_0	143.5	τ_1	10
D_1	5.4	τ_2	100
D_2	5.1	τ_3	1000
D_3	3.7	τ_4	10000
D_4	5.5	τ_5	100000
D_5	5.5	τ_6	1000000
D_6	6.3	τ_7	10000000
D_7	7.0	τ_8	100000000
D_8	6.8	τ_9	1E+9
D_9	7.4	τ_{10}	1E+10
D_{10}	8.2	τ_{11}	1E+11
D_{11}	10.7	A (for 20 MPa)	16.0
m	4.3	A (for 50 MPa)	111.3
n	0.09		

The viscoplastic term previously developed was added to this model to create a long-term viscoelastic-viscoplastic model. This model was used to predict the total creep strains at 20 MPa and 50 MPa (the total stress range studied previously at room temperature). Figure 5.23 shows comparisons to several 14 day trials at 20 MPa, while Figure 5.24

shows comparisons of the model to a couple 33 day trials at 50 MPa. Both model curves were given a scatter band of ±17%.
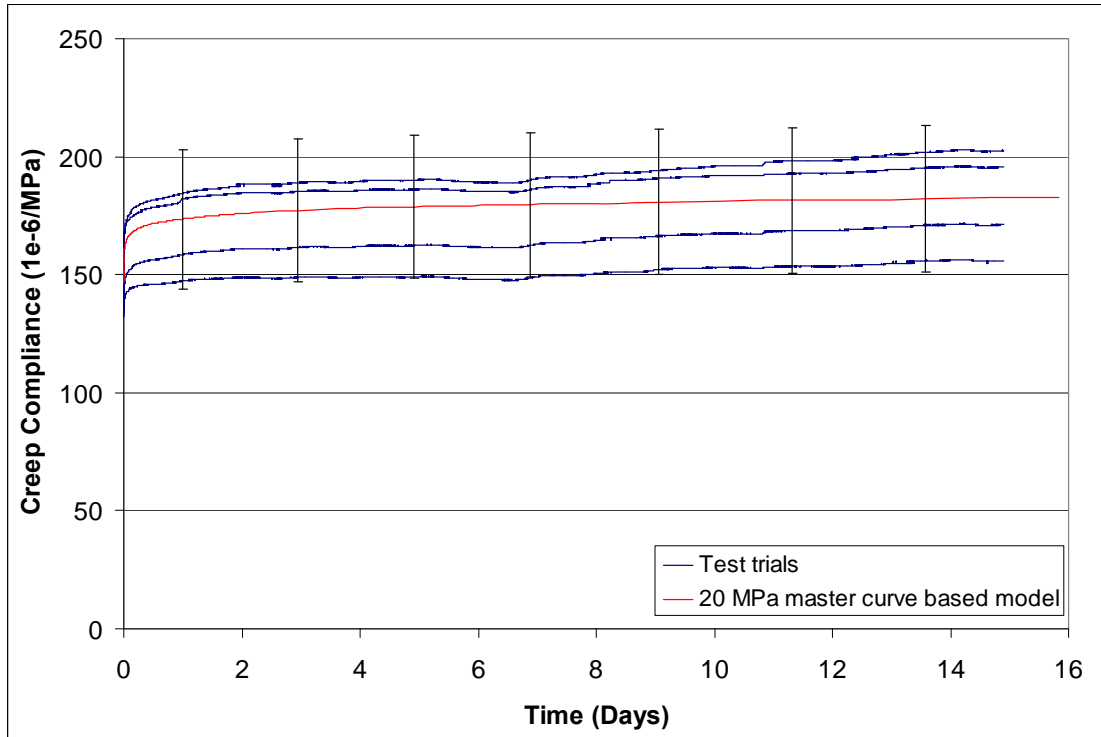
Figure 5.23: Long-term model prediction of 20 MPa data.
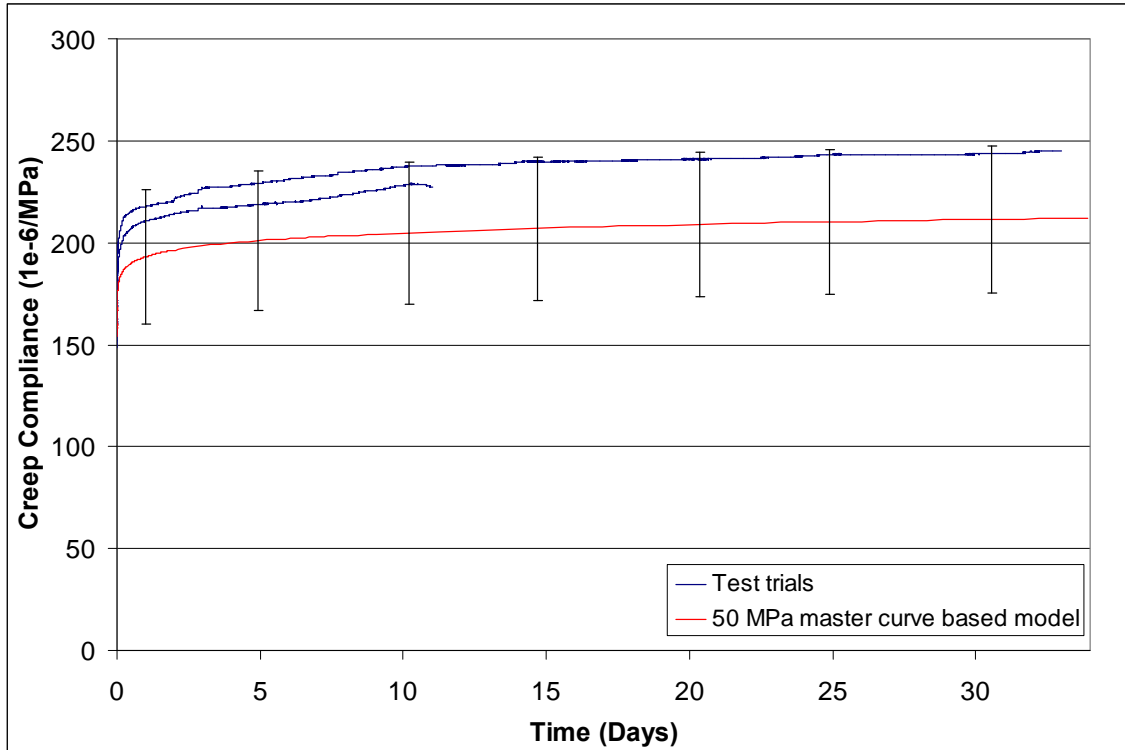
Figure 5.24: Long-term model prediction of 50 MPa data.

It can be seen that TTS is applicable to the chopped glass fibre mat thermoplastic composite studied, based on room temperature verification tests. If Figure 5.24 is compared to Figure 4.19, it can be seen that unlike the earlier model that completely plateaued after several days, a model based on the master curve gives increasing creep compliance values. The model is also verified using a separate set of test trials.

5.3 Long-term Creep Tests

Average curves were also used to study the long-term creep data, similar to the short-term results. The 1 day viscoelastic compliance from the tests is shown in Figure 5.25. No data was collected at 80°C under a 40 MPa load as all 4 specimens tested under these conditions failed prematurely.
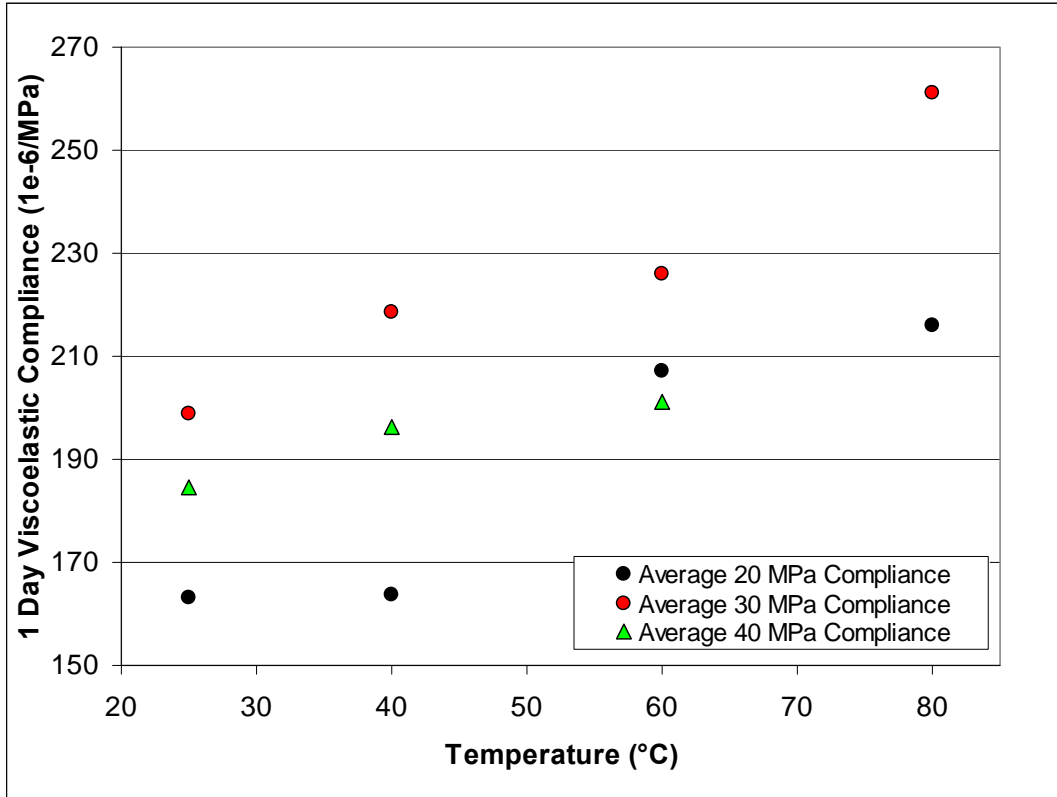
Figure 5.25: 1 day viscoelastic compliance from long-term temperature tests.

The residual strains after 1 day creep are shown in Figures 5.26. The long-term experimental data is consistent with the short-term test data, which should be the case since the damage mechanisms are the same. Temperature appears to increase plastic strain in the material exponentially at each stress level.
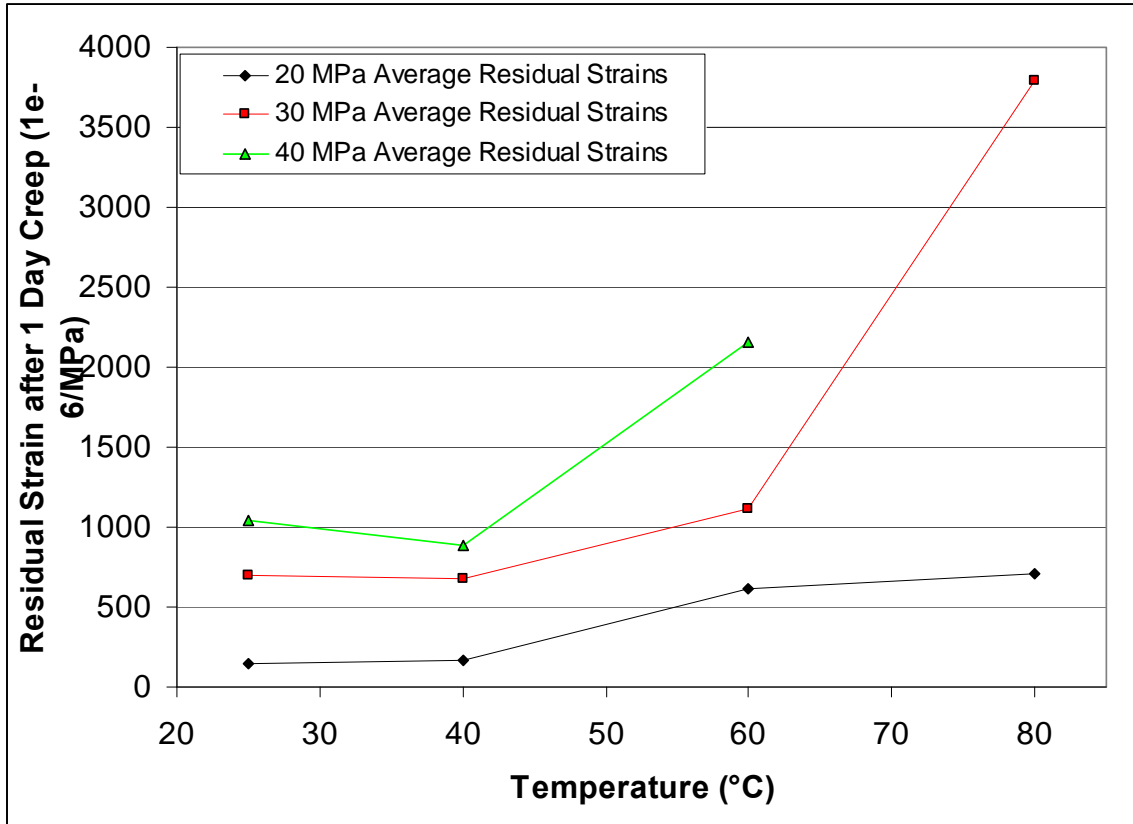
Figure 5.26: Residual strains after 1 day creep.

The micrographs of the material at 80 °C shown in Figure 5.27 contrasted with those taken at room temperature in Figure 4.5 would suggest that as temperature is increased, not only is there fibre matrix debonding and small transverse crack multiplication in the matrix, but bulk plastic deformation of the polymer matrix is extensive. Above the secondary glass transition, 60°C, bulk deformation of the matrix phase in the composite is dominant due to matrix softening. Deformation of the matrix phase triggers more fibre-matrix debonding which accelerates the progressive failure process as seen here. It suggests then that bulk plastic deformation of the matrix phase is a major contributor to residual strains measured in this work.

(a)

(b)
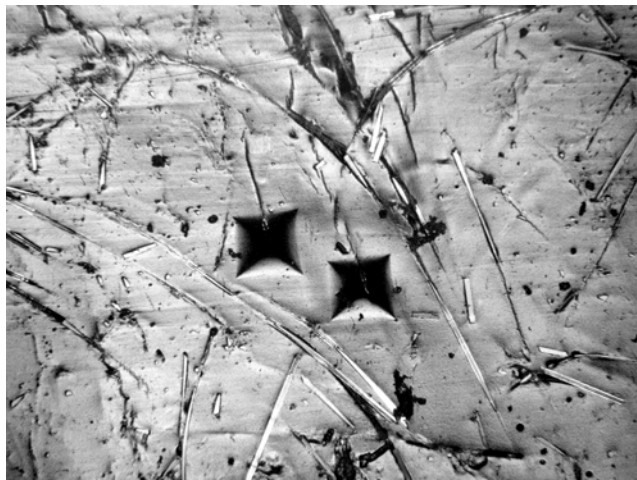
(c)

(d)

Figure 5.27: Material at (a) no load, creep for (b) 6 hrs, (c) 12 hrs, and (d) 15hrs at 21 MPa. [35]

5.4 Model Development

Although a long-term viscoelastic-viscoplastic model with temperature effects cannot confidently be developed with the present experimental data due to the relatively large material variability in this random GMT composite, the creep and recovery curves from high temperature tests can still be used to develop a simple model. It was shown in section 5.2 that the short-term data can still be used to show the applicability of TTS for long-term predictions at room temperature. This section will attempt to refine the short-term linear viscoelastic-viscoplastic model from section 4.4 to include the effects of temperature, noting that it will however not be able to predict long-term behaviour.

The short-term temperature data showed lower scatter and assumed to more accurately show the trends in viscoelastic behaviour. This is because the same preconditioned specimen was used for all experiments. Therefore, the data from this set of tests was used to modify the viscoelastic terms of the model presented in equation (47). From the parametric study of the introduced parameters g_0 and g_2 conducted in section 5.1, it was shown that the behaviour up to 60 °C for all three stress levels was identical and deviations only occurred above this temperature. From that study, it is difficult to determine a simple trend to describe the behaviour of all three stress levels since the changes in g_0 and g_2 are similar for both 30 and 40 MPa data. Therefore, the viscoelastic modeling with temperature effects was simplified and averages of the parameter values were taken for both g_0 and g_2. These average values were then curve fitted to attain R-square values of 0.98 and 0.94, respectively. Figure 5.28 shows the average values and the curve fits for each parameter that follow:

$$g_0(T) = 0.5758T^{0.1694} \tag{54}$$

$$g_2(T) = 0.7855e^{0.01T} \tag{55}$$

where T is measured in °C and is limited by the domain 25 °C $< T <$ 90 °C.
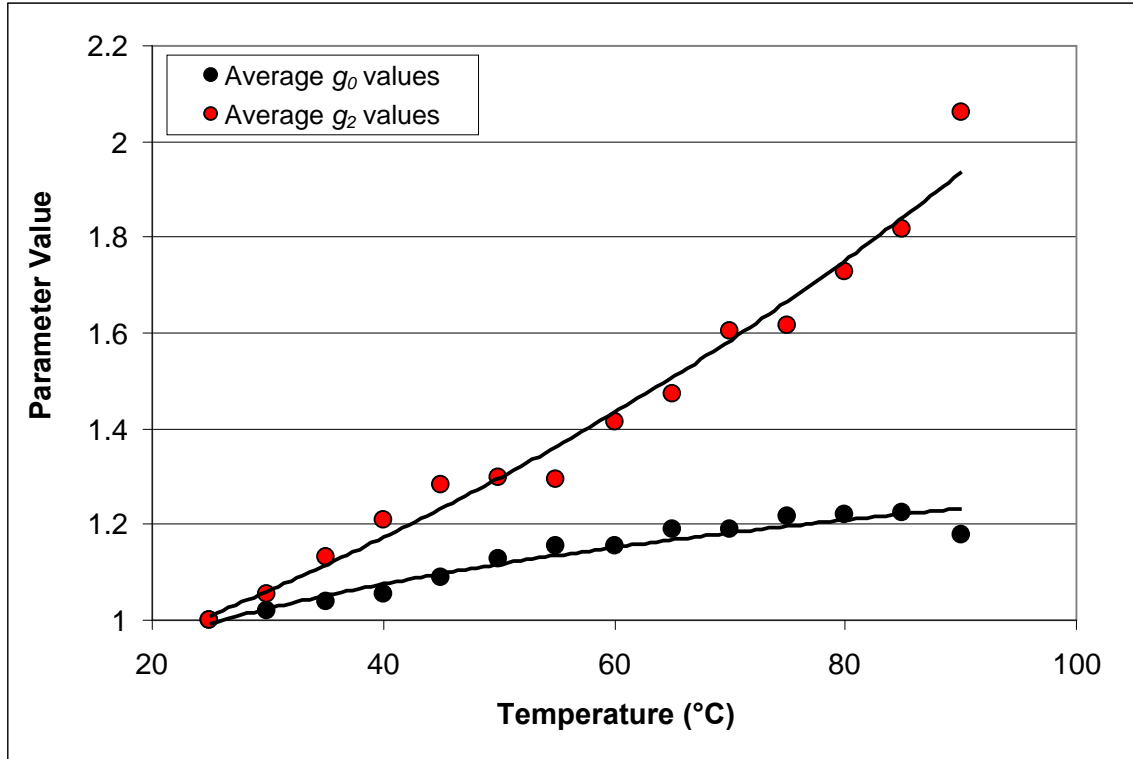
Figure 5.28: Parameter values to account for temperature effects in short-term viscoelastic model.

Since the only data available for modeling the temperature effects on viscoplastic strain development was the long-term temperature test data, this set of results was used to modify the Zapas-Crissman viscoplastic term to capture the behaviour and strains induced by the failure mechanisms examined earlier. The same data reduction method outlined in section 4.4 was used to isolate the viscoplastic strain from the total creep strain, and then the data was fitted to equation (28) to determine the viscoplastic parameters. This was conducted in multiple iterations to determine the stress and temperature dependence of the parameters A, m, and n in the model. During the first curve fitting using the least-squares method, all parameters were allowed to vary. From the results of the multiple curve fits, parameter m was found to be reasonably constant with changes in stress and temperature, having a standard deviation of approximately 3.1. Therefore, it was considered to be stress and temperature independent, meaning that the overall average value of 14.02 was used as the constant value of m. The parameter n was

fairly constant for all stresses as before, but showed significant variations with temperature. Consequently, *n* was treated as a stress independent, temperature dependent parameter. With a constant value for *m*, equation (28) was once again fitted to the viscoplastic strain data, resulting in *n* values shown in Figure 5.29.
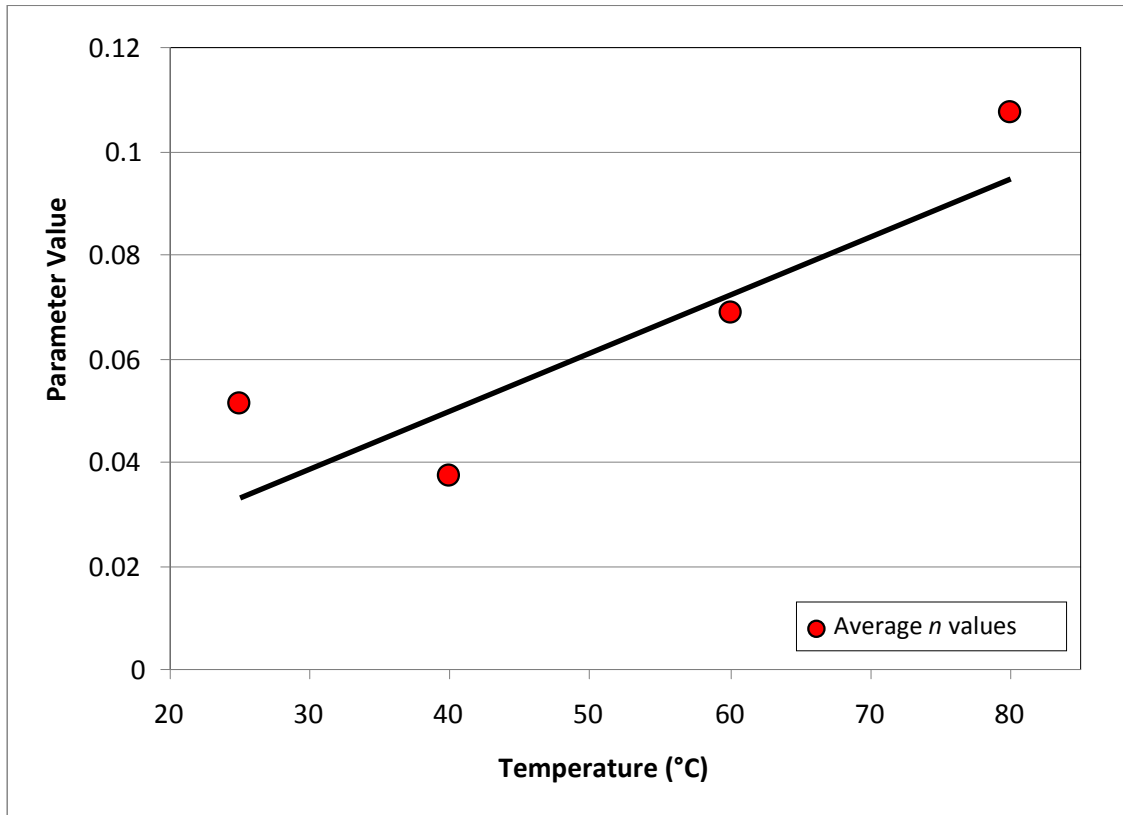
Figure 5.29: Values for the parameter *n* at various temperatures.

In an attempt to determine an equation for the development of parameter *n* in equation (28) with respect to temperature, the highest R-square values attained were below 0.8. This indicates that the temperature dependence of the model parameter is not clearly established by the long-term temperature data collected. Even with the collection of more data sets, the repeatability of viscoplastic damage accumulation data in the random GMT composite at high temperatures is questionable. As seen in the previous section, the addition of high temperature dramatically affects the occurrence of failure

mechanisms in the material, meaning that damage prediction in the material studied becomes even more problematic.

With such uncertain trends in parameter behaviour, it is difficult to accurately and meaningfully model the viscoplastic behaviour of the particular GMT composite with the Zapas-Crissman term. However, the development work was continued despite low R-square values, as there is potential value in outlining an approach to stress and temperature modeling of viscoplastic behaviour that can perhaps be applied to other materials with less variability.

After an equation to express the temperature dependence of n based on the linear regression seen in Figure 5.29 was established, these values along with the constant m value were used to, once again, fit the viscoplastic data using equation (28). The resulting values of parameter A are shown in Figure 5.30.
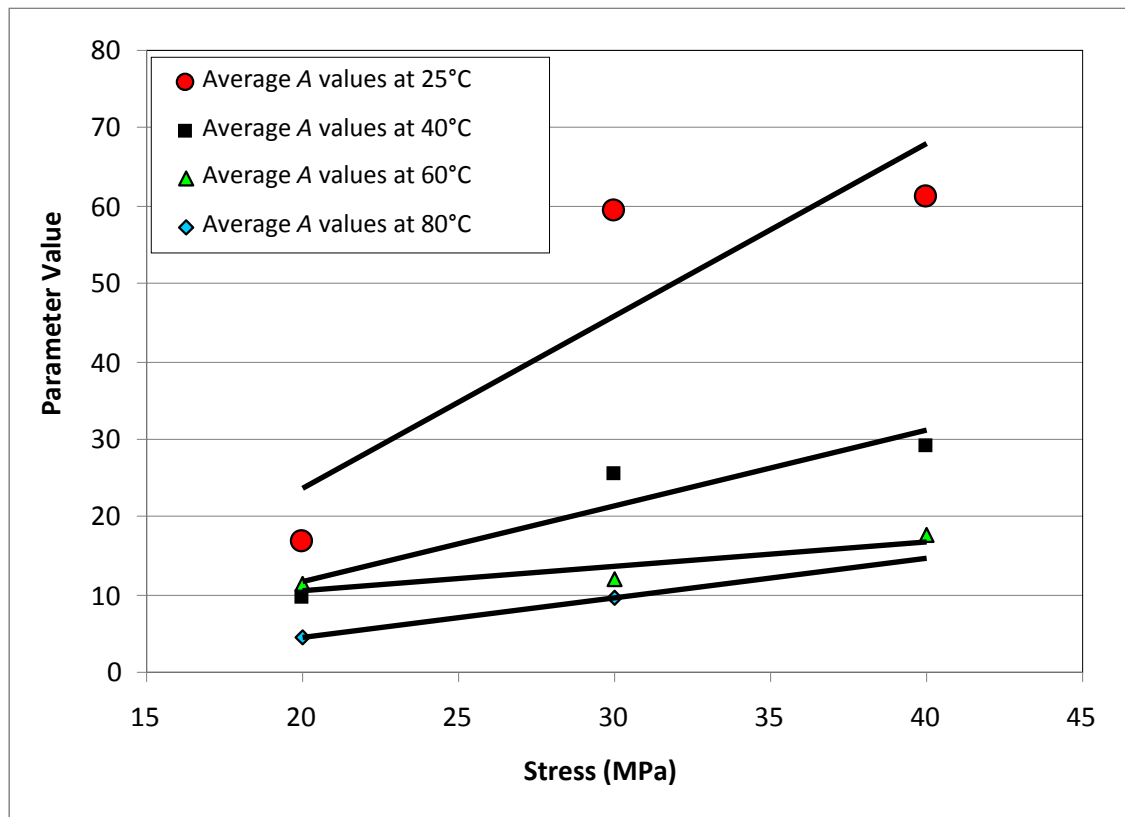
Figure 5.30: Values of the parameter *A* at various stresses and temperatures.

In order to model the stress and temperature dependence of model parameter *A*, regression analysis was used on each set of temperature data to determine behaviour with respect to stress. A linear regression was the simplest form to curve fit all the temperature data sets which resulted in high R-square values. Since the stress dependence of parameter *A* was found to be linear, the slopes and y-intercept of each linear curve fit were plotted with respect to temperature as shown in Figures 5.31 and 5.32.
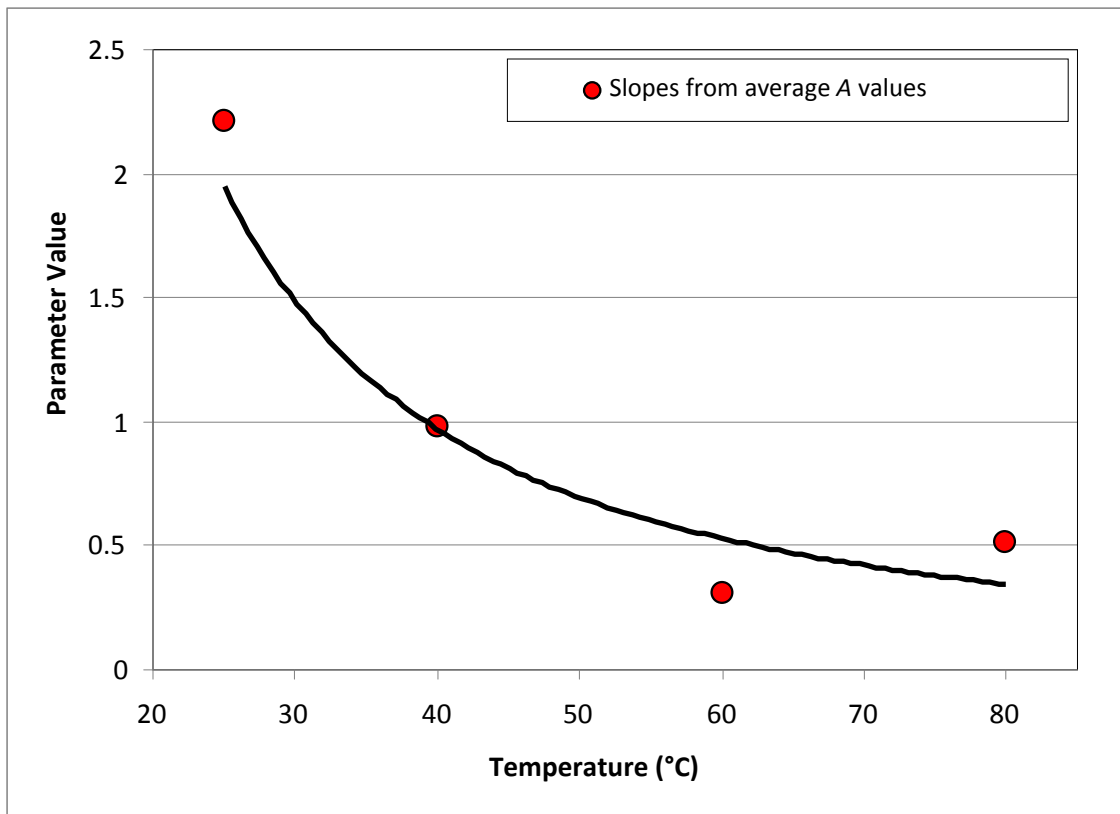
Figure 5.31: Slope from linear stress dependent behaviour of parameter *A* as functions of temperature.
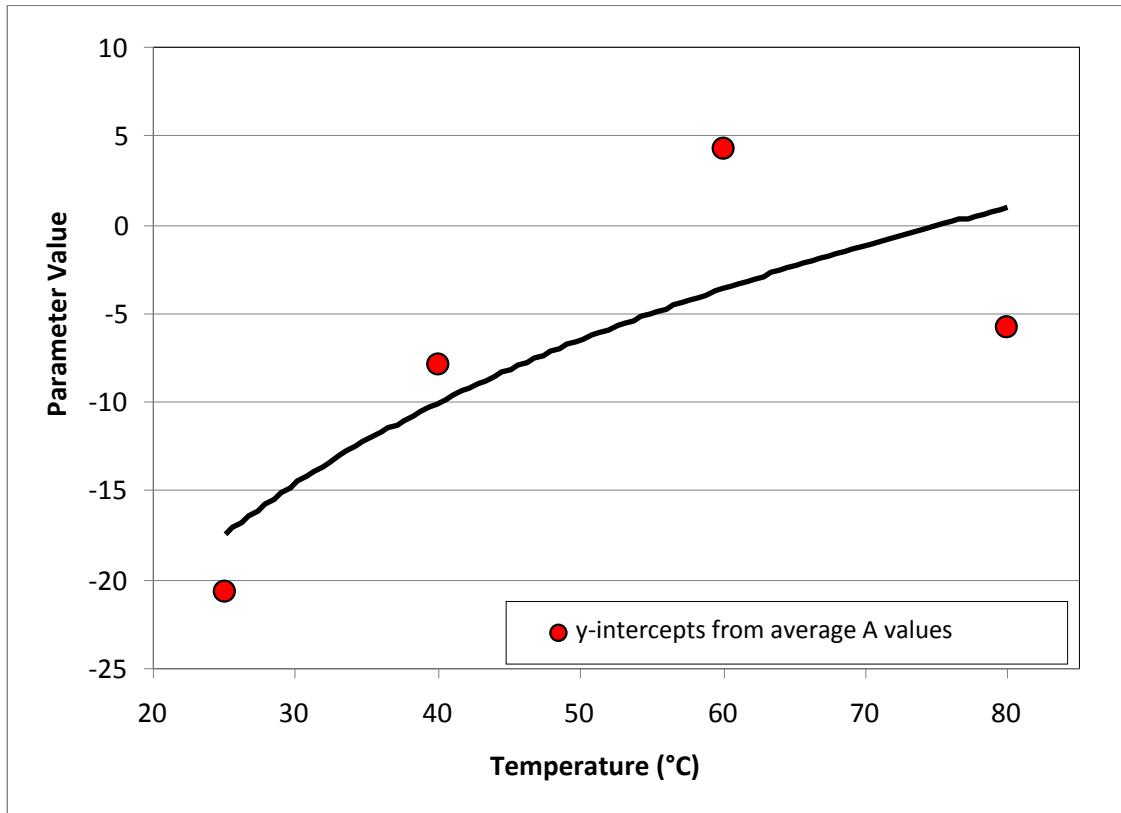
Figure 5.32: y-intercepts from linear stress dependent behaviour of parameter *A* as functions of temperature.

By combining the temperature dependent slope and y-intercepts that define the stress dependent behaviour of the parameter *A*, both effects were captured by the model. The predictions of viscoplastic strain after 1 day of creep based on the model estimates of *A*, *m*, and *n* are shown in Figure 5.33. While the model parameters determined have no physical meaning as they do not represent the experimental data collected with sufficient accuracy, especially at room temperature, the general trends in behaviour are illustrated by using the outlined procedure. The equations defining the parameters *A* and *n* used to create the model curves in the figure are included in Appendix D.
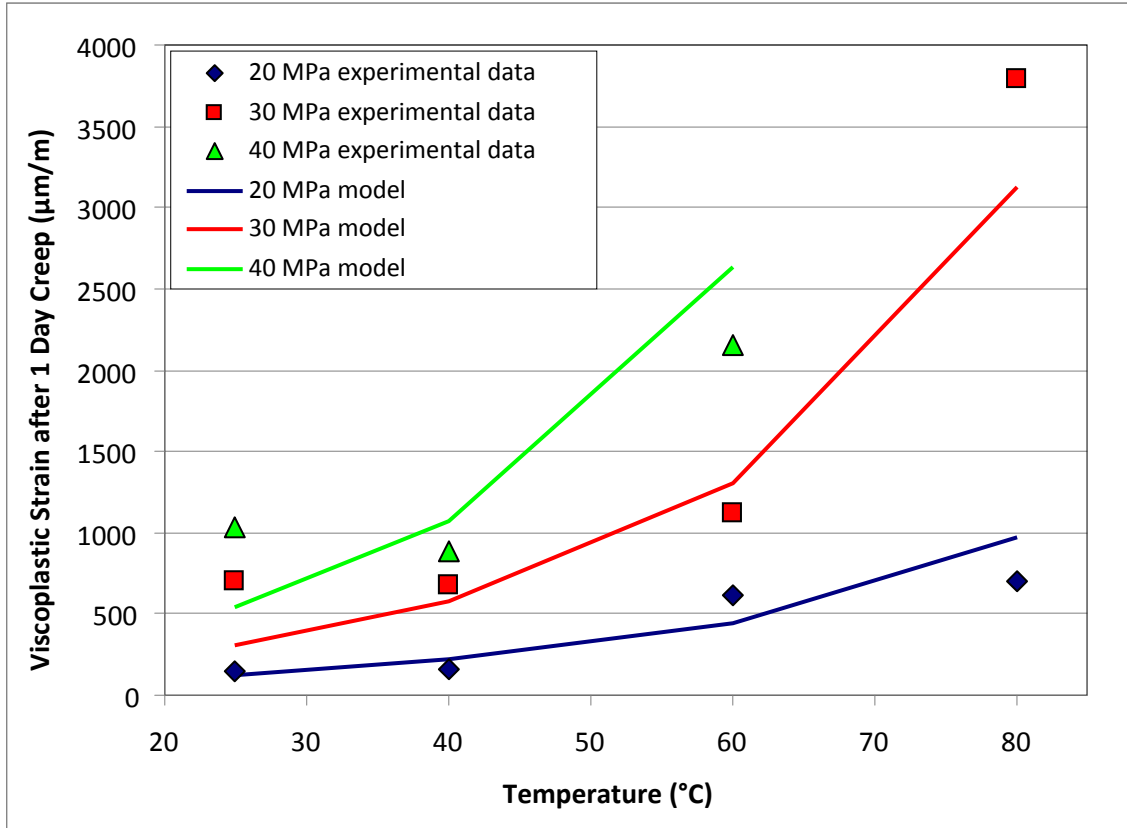
Figure 5.33: Viscoplastic strains after 1 day creep.

6.0 CONCLUSIONS

The present work on characterization and constitutive modeling of room temperature creep in random chopped fibre GMT composite has resulted in the following conclusions:

- Short-term creep experiments (30 minute creep followed by recovery) conducted at room temperature indicate that the chopped fibre GMT composite in this study was marginally nonlinear above 45 MPa and is therefore practically linear viscoelastic over the stress range of interest (20-50 MPa).

- Through long-term creep experiments (1 day creep followed by recovery) and microscopy, it was found that permanent damage develops in the material even at low stresses. As a result, a viscoelastic-viscoplastic model is required to accurately predict long-term creep behaviour.

- A constitutive model comprised of a linear viscoelastic model based on Boltzmann superposition and a 5-term Prony series, along with a Zapas-Crissman viscoplastic term can reasonably predict creep behaviour at room temperature. An associated scatter band of ±17% is necessary to account for the material property variability.

For the work on creep at elevated temperature, the following conclusions can be drawn:

- Variability in creep compliance increased with temperature by 3 - 7% on average over the temperature range studied. With this increased scatter, it is difficult to confidently and meaningfully model the long-term behaviour of the material using mathematical expressions that account for temperature effects.

- Changes in the viscoelastic behaviour of the material at temperatures above 60°C suggest that creep behaviour of the chopped fibre composite becomes strongly matrix dominated beyond the secondary glass transition.

- High temperatures cause bulk deformation of the polymer matrix, exacerbating fibre-matrix debonding and accelerating the progressive failure of the material. This also makes it extremely difficult to find trends for constitutive modeling of viscoplastic strains. Damage accumulation appears to be accelerated exponentially by temperature, and this acceleration is only compounded as the applied stress on the material is increased.

- Time-temperature superposition can be applied to the material studied, and the shift factors from 20 MPa creep data follow the WLF equation very well over the temperature range of 25 - 90°C.

REFERENCES

[1] L.A. Berglund and M.L. Ericson, "Glass mat reinforced polypropylene," in *Polypropylene: Structure, blends and composites*, vol. 3, J. Karger-Kocsis, Ed. London: Chapman & Hall, 1995, pp. 202-227.

[2] M. Megnis, J. Varna, D.H. Allen, and A. Holmberg, "Micromechanical modeling of viscoelastic response of GMT composite," *Journal of Composite Materials*, vol. 35, no. 10, pp.849-882, 2001.

[3] M. Ericson and L Berglund, "Deformation and fracture of glass-mat-reinforced polypropylene," *Composites Science and Technology*, vol. 43, pp. 269-281, 1991.

[4] I.M. Ward, *Mechanical Properties of Solid Polymers*. London: Wiley-Interscience, 1971.

[5] S.W. Park and R.A. Schapery, "Methods of interconversion between linear viscoelastic material functions. Part 1 – a numerical method based on Prony series," *International Journal of Solids and Structures*, vol. 36, pp. 1653-1675, 1999.

[6] N. Zhou, "Constitutive modeling of creep in a short fibre glass mat thermoplastic composite," M.A.Sc. thesis, University of Waterloo, Waterloo, ON, Canada, 2006.

[7] E. Ségard, S. Benmedakhene, A. Laksimi, and D. Laï, "Influence of the fibre-matrix interface on the behaviour of polypropylene reinforced by short glass fibres above the glass transition temperature," *Composite Science and Technology*, vol. 62, pp. 2029-2036, 2002.

[8] J. Lai and A. Bakker, "An integral constitutive equation for nonlinear plasto-viscoelastic behaviour of high-density polyethylene," *Polymer Engineering and Science*, vol. 35, no. 17, pp. 1339-1347, 1995.

[9] V.B. Gupta and J. Lahiri, "Non linear viscoelastic behaviour of polypropylene and glass reinforced polypropylene in creep," *Journal of Composite Materials*, vol. 14, pp. 286-296, 1980.

[10] S.P. Zaoutsos, G.C. Papanicolaou, and A.H. Cardon, "On the non-linear viscoelastic behaviour of polymer-matrix composites," *Composites Science and Technology*, vol. 58, pp. 883-889, 1998.

[11] E. Marklund, J. Varna, and L. Wallström, "Nonlinear viscoelasticity and viscoplasticity of flx/polypropylene composites," *Journal of Engineering Materials and Technology*, vol. 128, pp. 527-536, 2006.

[12] D.H. Allen, A. Holmberg, M. Ericson, L. Lans, N. Svensson, and S. Holmberg, "Modeling the viscoelastic response of GMT structural components," *Composites Science and Technology*, vol. 61, pp. 503-515, 2001.

[13] M.A. Zocher, S.E. Groves, and D.H. Allen, "A three-dimensional finite element formulation for thermoviscoelastic orthotropic media," *International Journal for Numerical Methods in Engineering*, vol. 40, pp. 2267-2288, 1997.

[14] J. Sorvari and M. Malinen, "On the direct estimation of creep and relaxation functions," *Mechanics of Time-Dependent Materials*, vol. 11, pp. 143-157, 2007.

[15] P. Dasappa, P. Lee-Sullivan, X. Xiao, and H.P. Foss, "Tensile creep of a long-fiber glass mat thermoplastic (GMT) composite Part II: Viscoelastic-Viscoplastic constitutive modeling," *Polymer Composites*, 2008, Accepted and in press.

[16] R.A. Schapery, "An engineering theory of nonlinear viscoelasticity with applications," *International Journal of Solids and Structures*, vol. 2, pp. 407-425, 1966.

[17] G.C. Papanicolaou, A.G. Xepapadaki, K. Karagounaki, and S.P. Zaoutsos, "Time and temperature effect on the linear-nonlinear viscoelastic transition threshold of a polymeric system," *Journal of Applied Polymer Science*, vol. 108, pp. 640-649, 2008.

[18] R.A. Schapery, "On the characterization of nonlinear viscoelastic materials," *Polymer Engineering and Science*, vol. 9, pp. 295-310, 1969.

[19] G.C. Papanicolaou, S.P. Zaoutsos, and A.H. Cardon, "Further development of a data reduction method for the nonlinear viscoelastic characterization of FRPs," *Composites: Part A*, vol. 30, pp. 839-848, 1999.

[20] A. Pasricha, M.E. Tuttle, A.F. Emery, "Time-dependent response of IM7/5260 composites subjected to cyclic thermo-mechanical loading," *Composites Science and Technology*, vol. 55, pp. 49-56, 1995.

[21] D. Peretz and Y. Weitsman, "Nonlinear viscoelastic Characterization of FM-73 Adhesive," *Journal of Rheology*, vol. 26, no. 3, pp. 245-261, 1982.

[22] D.J. Pooler and L.V. Smith, "Nonlinear viscoelastic response of a wood-plastic composite including temperature effects," *Journal of Thermoplastic Composite Materials*, vol. 17, pp. 427-445, 2004.

[23] Y.C. Lou and R.A. Schapery, "Viscoelastic characterization of a nonlinear fibre-reinforced plastic," *Journal of Composite Materials*, vol. 5, pp. 208-234, 1971.

[24] J. Kolařík and A. Pegoretti, "Proposal of the Boltzmann-like superposition principle for nonlinear tensile creep of thermoplastics," *Polymer Testing*, vol. 27, pp. 596-606, 2008.

[25] A.D. Drozdov and A.L. Kalamkarov, "A constitutive model for nonlinear viscoelastic behavior of polymers," *Polymer Engineering and Science*, vol. 36, no. 14, pp. 1907-1919, 1997.

[26] M.S. Green and A.V. Tobolsky, "A new approach to the theory of relaxing polymeric media," *Journal of Chemical Physics*, vol. 14, pp. 80-92, 1946.

[27] A.D. Drozdov, "A model of adaptive links in finite viscoelasticity," *Mechanics Research Communications*, vol. 24, no. 2, pp 161-166, 1997.

[28] A.D. Drozdov, "A constitutive model in finite thermoviscoelasticity based on the concept of transient networks," *Acta Mechanica*, vol. 133, pp. 13-37, 1999.

[29] A.D. Drozdov, "A model for the non-linear viscoelastic response and physical aging in glassy polymers," *Computations and Theoretical Polymer Science*, vol. 9, pp. 73-87, 1999.

[30] A.D. Drozdov and R.K. Gupta, "Non-linear viscoelasticity and viscoplasticity of isotactic polypropylene," *International Journal of Engineering Science*, vol. 41, pp. 2335-2361, 2003.

[31] M.E. Tuttle, A. Pasricha, A.F. Emery, "The nonlinear viscoelastic-viscoplastic behaviour of IM7/5260 composites subjected to cyclic loading," *Journal of Composite Materials*, vol. 29, pp. 2025-2046, 1995.

[32] J. Hugo, M. Sova, and J. Čižinský, "Creep and creep damage of glass fibre reinforced polypropylene," *Composite Structures*, vol. 24, pp. 233-244, 1993.

[33] J. Lindhagen and L. Berglund, " Microscopial damage mechanisms in glass fibre reinforced polypropylene," *Journal of Applied Polymer Science*, vol. 69, pp. 1319-1327, 1998.

[34] E. Ségard, S. Benmedakhene, A. Laksimi, and D. Laï, "Damage analysis and the fibre-matrix effect in polypropylene reinforced by short glass fibres above glass transition temperature," *Composite Structures*, vol. 60, pp. 67-72, 2003.

[35] A. Law, "Creep deformation and thermal aging of random glass-mat polypropylene composite," M.A.Sc. thesis, University of Waterloo, Waterloo, ON, Canada, 2007.

[36] X.R. Xiao, C.C. Hiel, and A.H. Cardon, "Characterization and modeling of nonlinear viscoelastic response of PEEK resin and PEEK composites," *Composites Engineering*, vol. 4, no. 7, pp. 681-702, 1994.

[37] L.O. Nordin and J. Varna, "Nonlinear viscoplastic and nonlinear viscoelastic material model for paper fibre composites in compression," *Composites: Part A*, vol. 37, pp. 344-355, 2006.

[38] L.J. Zapas and J.M. Crissman, "Creep and recovery behaviour of ultra-high molecular weight polyethylene in the region of small uniaxial deformations," *Polymer*, vol. 25, pp. 57-62, 1984.

[39] R.A. Schapery, "Nonlinear viscoelastic and viscoplastic constitutive equations based on thermodynamics," *Mechanics of Time-Dependent Materials*, vol. 1, pp. 209-240, 1997.

[40] R. A. Schapery, "Nonlinear viscoelastic and viscoplastic constitutive equations with growing damage," *International Journal of Fracture*, vol. 97, pp. 33-66, 1999.

[41] D. Peretz and Y. Weitsman, "The Nonlinear Thermoviscoelastic Characterizations of FM-73 Adhesives," *Journal of Rheology*, vol. 27, iss. 2, pp. 97-114, 1983.

[42] H. Leaderman, "Textile materials and the time factor: I. Mechanical behaviour of textile fibres and plastics," *Textile Research Journal*, vol. 11, pp. 171-193, 1941.

[43] H. Leaderman, *Elastic and Creep Properties of Filamentous Materials and Other High Polymers*. Washington: The Textile Foundation, 1943.

[44] M.L. Williams, R.F. Landel, and J.D. Ferry, "The temperature dependence of relaxation mechanisms in amorphous polymers and other glass-forming liquids," *Journal of the American Chemical Society*, vol. 77, pp. 3701-3707, 1955.

[45] J.D. Ferry, *Viscoelastic Properties of Polymers*. New York: John Wiley & Sons, Inc., 1961

[46] L.C.E. Struik, "Mechanical and physical ageing of semicrystalline polymers: 1," *Polymer*, vol. 28, no. 9, pp. 1521-1533, 1987.

[47] L.C.E. Struik, "Mechanical behaviour and physical ageing of semicrystalline polymers: 2," *Polymer*, vol. 28, no. 9, pp. 1534-1542, 1987.

[48] L.C.E. Struik, "Mechanical behaviour and physical ageing of semi-crystalline polymers: 3. Prediction of long-term creep from short time tests," *Polymer*, vol. 30, no. 5, pp.799-814, 1989.

[49] L.C.E. Struik, "Mechanical behaviour and physical ageing of semi-crystalline polymers: 4," *Polymer*, vol. 30, no. 5, pp.815-830, 1989.

[50] D. Dean, A. Miyase, and P.H. Geil, "The interaction of creep and physical aging in a semicrystalline thermoplastic matrix composite above T_g," *Journal of Thermoplastic Composite Materials*, vol. 5, pp.136-151, 1992.

[51] E.J. Barbero and K.J. Ford, "Equivalent time temperature model for physical aging and temperature effects on polymer creep and relaxation," *Journal of Engineering Materials and Technology*, vol. 126, pp. 413-419, 2004.

[52] K. Banik, J. Karger-Kocsis, and T. Abraham, "Flexural creep of all-polypropylene composites: model analysis," *Polymer Engineering and Science*, vol. 48, no. 5, pp. 941-948, 2008.

[53] K.Y. Tshai, E.M.A. Harkin-Jones, P.J. Martin, and G.H. Menary, "Modeling of the behaviour of semi-crystalline polypropylene at elevated strain rate and temperature," in *Proceedings of the Society of Plastics Engineers 61st Annual Technical Conference*, vol. 1, 2003, pp. 785-790.

[54] J. Lai and A. Bakker, "Non-linear creep and recovery behaviour of high-density polyethylene," *Scripta Metallurgica et Materialia*, vol. 28, pp. 1447-1452, 1993.

[55] J.Lai and A. Bakker, "Analysis of the non-linear creep of high-density polyethylene," *Polymer*, vol. 36, no. 1, pp. 93-99, 1995.

[56] H.F. Brinson, D.H. Morris, and Y.T. Yeow, "A new experimental method for the accelerated characterization of composite materials," in *Proceedings of the 6th International Conference on Experimental Stress Analysis*, 1978, pp. 395-400.

[57] H.F. Brinson and D.A. Dillard, "The prediction of long-term viscoelastic properties of fibre reinforced plastics," in *Proceedings of the 4th International Conference on Composite Materials*, 1982, pp. 795-801.

[58] M.E. Tuttle and H.F. Brinson, "Prediction of the long-term creep compliance of general composite laminates," *Experimental Mechanics*, vol. 26, no. 1, pp. 89-102, 1986.

[59] X. Xiao, "Studies of the viscoelastic behaviour of a thermoplastic resin composite," *Composites Science and Technology*, vol. 34, pp. 163-182, 1989.

[60] N.J. Lee and J. Jang, "The effect of fibre content on the mechanical properties of glass fibre mat/polypropylene composites," *Composites: Part A*, vol. 30, pp. 815-822, 1999.

[61] J.L. Thomason, "The influence of fibre length and concentration on the properties of glass fibre reinforced polypropylene: 7. interface strength and fibre strain in injection moulded long fibre PP at high fibre content," *Composites: Part A*, vol. 38, pp. 210-216, 2007.

[62] V.K. Stokes, "Random glass mat reinforced thermoplastic composites. Part I: phenomenology of tensile modulus variations," *Polymer Composites*, vol. 11, no. 1, pp. 32-44, 1990.

[63] W.C. Bushko and V.K. Stokes, "Random glass mat reinforced thermoplastic composites. Part VII: a statistical approach to strength," *Polymer Composites*, vol. 15, no. 5, pp. 359-366, 1994.

[64] G.D. Tomkinson-Walles, "Performance of random glass mat reinforced thermoplastics," *Journal of Thermoplastic Composite Materials*, vol. 1, pp. 94-106, 1988.

[65] R.D. Donoghue, P.W.M. Peters, and G. Marci, "The influence of mechanical conditioning on the viscoelastic behaviour of short-fibre glass reinforced epoxy resin (GRP)," *Composites Science and Technology*, vol. 44, pp. 43-55, 1992.

[66] J.M. Crissman and L.J. Zapas, "On the mechanical preconditioning of ultrahigh-molecular-weight polyethylene at small uniaxial deformations," *Journal of Polymer Science: Polymer Physics Edition*, vol. 23, pp. 2599-2610, 1985.

[67] C. Hiel, A.H. Cardon, and H.F. Brinson, "The nonlinear viscoelastic response of resin matrix composite laminates," College of Engineering, Virginia Polytechnic Institute and State University, Blacksburg, Virginia, Tech. Rep. VPI-E-83-6, 1983.

[68] P. Dasappa, J. Mui, and P. Lee-Sullivan, GM Technical Report CRDPJ311196 - #7, August 2008.

[69] K.P. Menard, *Dynamic Mechanical Analysis: A Practical Introduction*. USA: CRC Press LLC, 1999.

[70] ASTM D2990-01, Standard test method for tensile, compressive and flexural creep and creep rupture of plastics, *American Society of Testing Materials*, Philadelphia, United States.

[71] ASTM D638M-93, Standard test method for tensile properties of plastics, *American Society of Testing Materials*, Philadelphia, United States.

[72] P. Dasappa, "Constitutive modelling of creep in a long fibre random glass mat thermoplastic composite," GM Progress Report, University of Waterloo, Waterloo, ON, Canada, 2006.

[73] D. Houston, E. Hagerman, K. Willson, G. Luckey, and J. Henshaw, "Test Procedure to Evaluate Structural Composites Subjected to Sustained Loading," $ACCM - T - 03$, July 2000.

[74] S. Vleeshouwers, A.M. Jamieson, and R. Simha, "Effect of physical agin on tensile stress relaxation and tensile creep of cured EPON 828/epoxy adhesives in the linear viscoelastic region," *Polymer Engineering and Science*, vol. 29, iss. 10, pp. 662-670, 1989.

[75] Y. Guo and R.D. Bradshaw, "Isothermal physical aging characterization of polyether-ether-ketone (PEEK) and polyphenylene sulphide (PPS) films by creep and stress relaxation," *Mechanics of Time-Dependent Materials*, vol. 11, pp. 61-89, 2007.

[76] T. Ariyama, Y. Mori, and K. Kaneko, "Tensile properties and stress relaxation of polypropylene at elevated temperatures," *Polymer Engineering and Science*, vol. 37, no. 1, pp.81-90, 1997.

APPENDIX A: MATERIAL DATA SHEET

QUADRANT PLASTIC COMPOSITES

Product Data Sheet

D100 F40 F1

D100 F40 F1 is a chopped fiber glass mat reinforced PP laminate with randomly oriented glass fibers. This product provides good flow properties, a very homogeneous fiber distribution and higher heat stabilization. It is commonly used for structural applications, like front-ends, seat back structures, door modules, battery trays, underbody shields and IP structures.

Properties		Standard	SI Units		Engl. Units	
Physical Properties						
Laminate Thickness*		Internal	4.8	mm	0.189	in
Area Weight*		Internal	5.8	kg/m^2	1.188	lb/ft^2
Fiber Content**		ISO 1172	40	%	40	%
Density (Laminate)*		ISO 1183	1.21	g/cm^3	0.0437	lb/in^3
Density (Molded)**		ISO 1183	1.22	g/cm^3	0.0441	lb/in^3
Mechanical Properties						
Tensile Strength		ISO 527 / EN 13677	85	MPa	12329	psi
Tensile Elongation at Break		ISO 527 / EN 13677	2.5	%	2.5	%
Tensile Modulus		ISO 527 / EN 13677	5000	MPa	725	ksi
Flexural Strength		ISO 178 / EN 13677	140	MPa	20307	psi
Flexural Modulus		ISO 178 / EN 13677	5000	MPa	725	ksi
Impact Strength -	IZOD (4.0mm)	ISO 180/A	78	kJ/m^2	37	ft*lb/in^2
	IZOD (3.2mm)	ASTM D256 E	786	J/m	15	ft*lb(wt)/in
	Charpy (4.0mm)	ISO 179-1/2fn	85	kJ/m^2	40	ft*lb/in^2
Multiaxial Impact (4.0mm)						
Max. Load		ASTM D-3763	3423	N	770	lb(wt)
Energy @ Max. Load			17	J	13	ft*lb
Energy @ Failure			31	J	23	ft*lb
Max. Load		ISO 6603-2	5739	N	1290	lb(wt)
Energy @ Max. Load			16	J	12	ft*lb
Energy @ Failure			39	J	29	ft*lb
Processing Properties						
Molding Shrinkage		ISO 2577	0.2 - 0.3	%	0.2 - 0.3	%
Special Properties						
Heat Deflection Temperature		ISO 75-2	155	°C	311	°F
Coefficient of Thermal Expansion		EN ISO 11403-2	15 - 25	10^{-6}/K	15 - 25	10^{-6}/K
Burning Rate		ISO 3795 / FMVSS302	<10	mm/min	<0.4	in/min

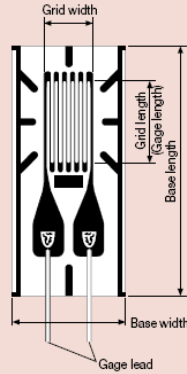1) = measured in longitudinal direction
2) = measured in transverse direction

* = Property was determined on the laminate
** = Property was determined on flat molded plaques

www.quadrantcomposites.com

Lenzburg, 04. August 2004

APPENDIX B: EXPERIMENTAL EQUIPMENT

Gages for General Stress Measurement

KFG

● Gage Factor	Approx. 2.1
● Applicable Linear Expansion Coefficients	5, 11, 16, 23, 27
● Self-temperature-compensation Range	10 to 100°C

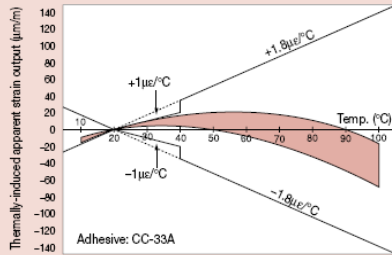**Applicable Adhesives and Operating Temperature Ranges**

CC-33A: −196 to 120°C
CC-35: −30 to 120°C
EP-34B: −55 to 150°C
PC-6: −196 to 150°C

Grid width
Grid length (Gage length)
Base length
Base width
Gage lead

■General-purpose Foil Strain Gages

The KFG gages use polyimide resin for the base approximately 13μm thick, ensuring excellent flexibility. Besides indoor measurement, the outstanding moisture resistance lets them effectively perform outdoor measurement. Unless directly exposed to waterdrops, no coating treatment is required.

- Various lengths and patterns are available to cope with multiple applications.
- Excellent moisture resistance.
- The thin gage base provides less resiliency, and thus ensures excellent workability and easy bonding to curved surfaces.
- Compensated temperature range is as wide as 10 to 100°C and thermal effect in a range of 20 to 40°C is as small as ±1με/°C.
- Strain limit at room temperatures is approximately 5% and fatigue life is 1.2×10^7 times (uniaxial gages), making them suitable for material tests.
- The resistance, gage factor and leadwire cable are labeled.
- Delivered in an airtight package.
- Characteristic values are expressed in accordance with the OIML International Recommendation No. 62.
- Immediate delivery is ensured.

■Typical characteristic curve of thermally-induced apparent strain with KFG gage

Thermally-induced apparent strain output (μm/m)
+1.8με/°C
+1με/°C
Temp. (°C)
−1με/°C
−1.8με/°C
Adhesive: CC-33A

KFG Gages ●Uniaxial 120Ω

Pattern	Leadwire Cable – Type and Shape	Operating Temp. Range	Leadwire Length	Model
KFG-30-120-C1-11 **16** **23** **27**	Vinyl-coated flat 3-wire cable L-7 (L-10 for 6m or longer)	−10 to 80°C	1m	KFG-30-120-C1-11 L1M3R
			3m	KFG-30-120-C1-11 L3M3R
			5m	KFG-30-120-C1-11 L5M3R
	Vinyl-coated flat 2-wire cable L-6 (L-9 for 6m or longer)	−10 to 80°C	1m	KFG-30-120-C1-11 L1M2R
			3m	KFG-30-120-C1-11 L3M2R
			5m	KFG-30-120-C1-11 L5M2R
	Middle-temperature 3-wire cable L-12	−100 to 150°C	1m	KFG-30-120-C1-11 R1M3
			3m	KFG-30-120-C1-11 R3M3
			5m	KFG-30-120-C1-11 R5M3
	Middle-temperature 2-wire cable L-11	−100 to 150°C	1m	KFG-30-120-C1-11 R1M2
			3m	KFG-30-120-C1-11 R3M2
			5m	KFG-30-120-C1-11 R5M2
	3 polyester-coated copper wires 30cm 50cm·1m	−196 to 150°C	30cm	KFG-30-120-C1-11 N30C3
			50cm	KFG-30-120-C1-11 N50C3
			1m	KFG-30-120-C1-11 N1M3
	2 polyester-coated copper wires 30cm 50cm·1m	−196 to 150°C	30cm	KFG-30-120-C1-11 N30C2
			50cm	KFG-30-120-C1-11 N50C2
			1m	KFG-30-120-C1-11 N1M2
	Silver-clad copper wires	−196 to 150°C	25mm	KFG-30-120-C1-11

Uniaxial
- Base Size 37 x 5.2 mm
- Gage Length 30 mm
- Gage Resistance 120Ω
- Pieces per Pack 10

Compatible adhesive & Operational temperature
CN：−20〜＋80℃
P-2：−20〜＋80℃   EB-2：−20〜＋80℃

GENERAL USE

Gauge pattern	Type	Gauge size		Backing		Resistance in Ω
		L	W	L	W	
		L : length		W : width (Unit : mm)		
	FLA-6-1000-11 -17 -23	6	4.6	13.5	7.0	1000
FLA-10	Single-element					
	FLA-10-11 -17 -23	10	2.5	16.7	5.0	120
FLA-30	FLA-30-11 -17 -23	30	2.0	36.1	5.1	120
FLK-1	FLK-1-11 -17 -23	1	0.7	4.5	1.4	120
FLK-2	FLK-type with narrow gauge width					
	FLK-2-11 -17 -23	2	0.9	5.5	1.5	120
FLK-6	FLK-6-11 -17 -23	6	1.0	11.2	2.2	120
FLK-10	FLK-10-11 -17 -23	10	1.6	16.2	3.8	120

F L A - 1 - 11   Materials for S-T-C
Gauge length
—11   Mild steel
—17   Stainless steel
—23   Aluminium

Each package contains 10 gauges.

Strain Gage Adhesive

OTHER ACCESSORIES USED IN AN M-BOND AE-10 INSTALLATION:

- CSM Degreaser or GC-6 Isopropyl Alcohol
- Silicon-Carbide Paper
- M-Prep Conditioner A
- M-Prep Neutralizer 5A
- GSP-1 Gauze Sponges
- CSP-1 Cotton Applicators
- PCT-2M Gage Installation Tape
- HSC Spring Clamp
- GT-14 Pressure Pads and Backup Plates

DESCRIPTION

Two-component, 100%-solids epoxy system for general-purpose stress analysis. Transparent, medium viscosity. Cure time as low as six hours at +75°F [+24°C] may be used. Elevated-temperature postcure is recommended for maximum stability, and/or tests above room temperature.

Highly resistant to moisture and most chemicals, particularly when postcured. For maximum elongation, bonding surface must be roughened. Cryogenic applications require very thin gluelines.

CHARACTERISTICS

Operating Temperature Range:
Long Term: –320° to +200°F [–195° to +95°C].

Elongation Capabilities:
1% at –320°F [–195°C];
6% to 10% at +75°F [+24°C];
15% at +200°F [+95°C].

Shelf Life:
12 months at +75°F [+24°C]; 18 months at +20°F [–7°C]. If crystals form in resin jar, heat to +120°F [+50°C] for 30 minutes. Cool before mixing.

Pot Life:
15 to 20 minutes at +75°F [+24°C]. Can be extended by cooling jar or by spreading adhesive on clean aluminum plate.

Clamping Pressure:
5 to 20 psi [35 to 140 kN/m^2].

Cure Requirements:
Preferred Room-Temperature Cure: 24-48 hours at +75°F [+24°C].
Recommended Postcure: 2 hours at 25°F [15°C] above maximum operating temperature.
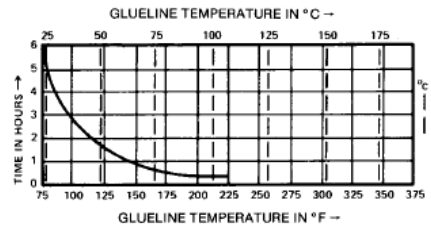
PACKAGING

Kit:
6 mixing jars [10 g ea] Resin
1 bottle [15 ml] Curing Agent 10
6 calibrated pipettes
6 stirring rods

Bulk:
200 g Resin
40 g Curing Agent 10
3 calibrated pipettes

References: Instruction Bulletin B-137, "Strain Gage Applications with M-Bond AE-10, AE-15, and GA-2 Adhesive Systems", included in each kit.

Strain Gage Adhesive

OTHER ACCESSORIES USED IN AN M-BOND 300 INSTALLATION:

- CSM Degreaser or GC-6 Isopropyl Alcohol
- Silicon-Carbide Paper
- M-Prep Conditioner A
- M-Prep Neutralizer 5A
- GSP-1 Gauze Sponges
- CSP-1 Cotton Applicators
- PCT-2M Gage Installation Tape
- HSC Spring Clamp
- GT-14 Pressure Pads and Backup Plates

DESCRIPTION

Special-purpose, two-component polyester adhesive. Not recommended as a general-purpose strain gage adhesive, but useful when a low-temperature-curing adhesive is required. While possessing the high shear strength required of a strain gage adhesive, peel strength and solvent sensitivity are relatively poor. Should not be used for impact strain measurements, or with solvent-thinned protective coatings.

CHARACTERISTICS

Operating Temperature Range:
Long Term: –40° to +300°F [–40° to +150°C].

Elongation Capabilities:
1% to 2% at +75°F [+24°C].

Shelf Life:
4 months at +75°F [+24°C].

Pot Life:
15 to 20 minutes at +40°F [+5°C]; 5 to 8 minutes at +75°F [+24°C].

Clamping Pressure:
5 to 20 psi [35 to 140 kN/m^2].

Cure Requirements:
24 hours at +40°F [+5°C];
18 hours at +60°F [+15°C];
12 hours at +75°F [+24°C].

PACKAGING

Kit:
6 mixing jars [10 g ea] Resin
6 calibrated pipettes
1 bottle [6 g] Catalyst
6 stirring rods

References: Instruction Bulletin B-133, "Strain Gage Installations with M-Bond 300 Adhesive", included in each kit.

Precision Miniature Load Cells
Model 31 and 34

WELDED STAINLESS

RUGGED, SMALL SIZE

TENSION/COMPRESSION

Model 31
(Tension/Compression)

Model 34
(Tension/Compression)

Models 31 and 34, Precision Miniature load cells measure both tension and compression load forces of 50 grams to 10,000 lb. These models are our highest accuracy, rugged miniature load cells. Model 31's welded, stainless steel construction is designed to eliminate or reduce to a minimum, the effects of off-axis loads. (The internal construction assures excellent long term stability for ranges 1000 grams and above.) A modification permits this model to be completely welded for underwater applications. The Model 31 tension/compression load cell has male threads while the Model 34 tension/compression load cell has female threaded load attachments. High accuracies of 0.15-0.25% full scale are achieved. Each bonded strain gage unit is built of welded 17-4 PH stainless steel for additional ruggedness. All load cells that have ranges 10 lb. have a small electrical zero balance circuit board which is in the lead wire (approximately 1"x .087" thick). This balance board does not have to be the same temperature as the transducer. Applications include cable tension and electromechanical parts testing.

Dimensions (inches)

Model 31 (Order Code AL311)

Available Ranges*	T Thread	D"	H"	C"	F"	A"	B"
50; 150; 250 500; g.	#6-32 UNC	1.00	0.75	0.25	0.11	0.50	0.38
1,000 g.; 5; 10 lb.	#6-32 UNC	0.75	0.45	0.25	0.05	0.31	0.19
25; 50; 100 lb.	#10-32 UNF	1.00	0.52	0.25	0.03	0.50	0.25
250; 500; 1,000 lb.	1/4-28 UNF	1.00	0.52	0.38	0.03	0.50	0.25
2,000; 3,000 lb.	3/8-24 UNF	1.00	0.72	0.50	0.03	0.50	0.38
4,000; 5,000 lb.	1/2-20 UNF	1.25	0.94	0.63	0.03	0.50	0.38
7,500; 10,000 lb.	3/4-16 UNF	1.38	1.10	0.88	0.03	0.50	0.38

* Stocked ranges are in bold face print.
Notes: Model 31 load cells ≤250 grams have overload stops. For custom cells without overload stops consult SENSOTEC.
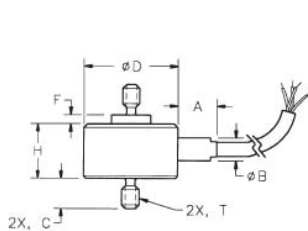
Model 31 Male Threads
(Tension/Compression)
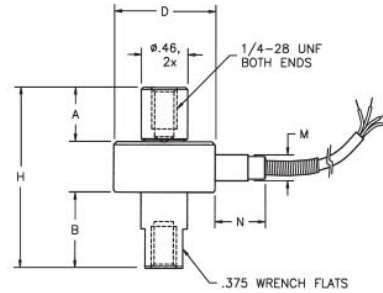
Model 34 Female Threads
(Tension/Compression)

Model 34 (Order Code AL312)

Available Ranges	D"	H"	A"	B"	M"	N"
50; 150; 250; 500 g.	1.00	1.75	0.52	0.52	0.38	0.50
1,000 g.; 5; 10 lb.	0.75	1.75	0.60	0.72	0.19	0.31
25; 50; 100 lb.	1.00	1.75	0.52	0.72	0.25	0.50
250; 500; 1,000 lb.	1.00	2.00	0.75	0.75	0.25	0.50

LO-18

122

APPENDIX C: ANOVA RESULTS

Anova of Compliance Data

The GLM Procedure

Class Level Information

Class	Levels	Values
Stress	8	20 22.5 25 30 35 40 45 50

Number of Observations Read	40
Number of Observations Used	40

Dependent Variable: Inst_Comp

Source	DF	Sum of Squares	Mean Square	F Value	Pr > F
Model	7	3163.396033	451.913719	2.56	0.0328
Error	32	5655.576432	176.736764		
Corrected Total	39	8818.972465			

R-Square	Coeff Var	Root MSE	Inst_Comp Mean
0.358703	7.498245	13.29424	177.2980

Source	DF	Type I SS	Mean Square	F Value	Pr > F
Stress	7	3163.396033	451.913719	2.56	0.0328

Source	DF	Type III SS	Mean Square	F Value	Pr > F
Stress	7	3163.396033	451.913719	2.56	0.0328

Tukey's Studentized Range (HSD) Test for Inst_Comp

NOTE: This test controls the Type I experimentwise error rate, but it generally has a higher Type II error rate than REGWQ.

```
              Alpha                                  0.05
              Error Degrees of Freedom                 32
              Error Mean Square                   176.7368
              Critical Value of Studentized Range  4.58107
              Minimum Significant Difference        27.236


         Means with the same letter are not significantly different.


              Tukey Grouping        Mean      N    Stress


                          A       191.253     5     50
                          A
                   B      A       188.895     5     45
                   B      A
                   B      A       181.473     5     40
                   B      A
                   B      A       177.554     5     35
                   B      A
                   B      A       172.616     5     25
                   B      A
                   B      A       172.417     5     22.5
                   B      A
                   B      A       171.067     5     30
                   B
                   B              163.107     5     20



                        Anova of 1Day Compliance Data


                             The GLM Procedure


                          Class Level Information


                   Class        Levels    Values


                   Stress          4     20 30 40 50



              Number of Observations Read          20
              Number of Observations Used          20



Dependent Variable: Day_Comp


                             Sum of
      Source               DF     Squares     Mean Square    F Value    Pr > F


                               124
```

```
Model                     3    3264.858371    1088.286124      8.73    0.0012

Error                    16    1994.617314     124.663582

Corrected Total          19    5259.475685
```

```
            R-Square    Coeff Var    Root MSE    Day_Comp Mean

            0.620757    5.992288     11.16528         186.3276
```

Source	DF	Type I SS	Mean Square	F Value	Pr > F
Stress	3	3264.858371	1088.286124	8.73	0.0012

Source	DF	Type III SS	Mean Square	F Value	Pr > F
Stress	3	3264.858371	1088.286124	8.73	0.0012

Tukey's Studentized Range (HSD) Test for Day_Comp

NOTE: This test controls the Type I experimentwise error rate.

```
    Alpha                                      0.05
    Error Degrees of Freedom                     16
    Error Mean Square                        124.6636
    Critical Value of Studentized Range      4.04609
```

Comparisons significant at the 0.05 level are indicated by ***.

Stress Comparison	Difference Between Means	Simultaneous 95% Confidence Limits		
30 - 50	9.365	-9.078	27.808	
30 - 40	14.820	-5.800	35.439	
30 - 20	36.229	15.609	56.849	***
50 - 30	-9.365	-27.808	9.078	
50 - 40	5.454	-15.165	26.074	
50 - 20	26.864	6.244	47.484	***
40 - 30	-14.820	-35.439	5.800	

```
40 - 50       -5.454    -26.074   15.165
40 - 20       21.409     -1.179   43.997
20 - 30      -36.229    -56.849  -15.609  ***
20 - 50      -26.864    -47.484   -6.244  ***
20 - 40      -21.409    -43.997    1.179
```

APPENDIX D: VISCOPLASTIC PARAMETER ESTIMATION

$y = 0.0011x + 0.0087$
$R^2 = 0.7806$

$y = 2.213x - 20.631$
$R^2 = 0.7799$

$y = 0.9753x - 7.9198$
$R^2 = 0.888$

$y = 0.3124x + 4.2118$
$R^2 = 0.8239$

$y = 0.514x - 5.75$
$R^2 = 1$